University of Nevada, Reno

Asymmetrical transmembrane potential in intracellular organelles of adrenal chromaffin cells exposed to nanosecond electric pulses

A thesis submitted in partial fulfillment of the
requirements for the degree of Master of Science in
Electrical Engineering

by

Guillermo Jose Aramendia Zabaleta

Dr. Indira Chatterjee/Thesis Advisor
Dr. Gale L Craviso/Thesis Co-Advisor

August 2017

University of
Nevada
Reno

THE GRADUATE SCHOOL

We recommend that the thesis
prepared under our supervision by

Guillermo Jose Aramendia Zabaleta

Entitled

Asymmetrical transmembrane potential in intracellular organelles of adrenal chromaffin cells exposed to nanosecond electric pulses

be accepted in partial fulfillment of the
requirements for the degree of

MASTER OF SCIENCE

Indira Chatterjee, Ph. D., Advisor

Gale L. Craviso, Ph. D., Co-Advisor

Josette El Zaklit, Ph. D., Committee Member

Ji Hwan Yoon, Ph. D., Committee Member

M. Sami Fadali, Ph. D., Committee Member

Normand LeBlanc, Ph. D., Graduate School Representative

David W. Zeh, Ph. D., Dean, Graduate School

August 2017

Abstract

In our research on exploring the effects of 5 ns, high intensity electric pulses on neurosecretory adrenal chromaffin cells, cell modeling has played an important role in understanding and explaining the experimental results. Externally applied nanosecond-duration electric pulses (NEPs) can affect cells by creating nanopores in the cell and intracellular organelle membranes, making these membranes permeable to certain ions.

A chromaffin cell contains, at a minimum, 7000 secretory granules plus other organelles such as mitochondria and the endoplasmic reticulum. In all the biological cell models constructed in the literature, there is no evidence of asymmetrical Transmembrane Potential (TMP) distribution in the intracellular membranes. However, these models do not include a realistic number of intracellular organelles. The goal of this research was to construct a more realistic cell model that incorporates a large number of secretory granules in the cytosol. To this end, a beta-version of the real-valued unstructured mesh Finite Element Method (FEM) electro-quasi-static module in Sim4life (SPEAG, Switzerland) has been used to model a chromaffin cell in which 1000 secretory granules are included in the cytosol. The model is, we believe, the most detailed geometrical cell model developed. It includes a spherical chromaffin cell (radius 8 μm), nucleus (radius 2.5 μm) located off-center, 500 granules (radius 200 nm) randomly located within a distance of 2 μm from the surface of the nucleus, and additional 500 granules randomly located in the remaining region of the cytosol. Cell and granule membrane thickness was set to 5 nm and nuclear membrane thickness to 10 nm. Dielectric properties of all constituents of the model were obtained from the literature or measured. Because the FEM Low Frequency solver is a quasi-static solver and not capable of accepting a time-varying pulse as input, all computations have been performed at single frequencies in the range DC to 60 MHz, sampled from the Fourier spectrum of the actual 5 ns pulse used in experiments. Electric field and TMP distributions have been computed in the cell model as a function of frequency, granule radius, and orientation of the applied

E-field.

Results show that granules located in the vicinity of the equatorial side of the nucleus had a higher TMP magnitude than the rest of the granules. In contrast, granules located in the vicinity of the poles of the nucleus had a lower TMP magnitude. The TMP distribution in the granules was strongly dependent on their location with respect to the nucleus and could exhibit asymmetries. Clearly, the nucleus had an influence on the TMP of the surrounding granules and the region of influence extended to a radial distance of 2 μm from the nucleus.

Creating a realistic model of a chromaffin cell is fundamental in order to estimate the TMP and electric field in a chromaffin cell. Such knowledge is important for understanding the impact of NEPs on the modulation of hormone secretion.

Acknowledgments

First thanks to my advisor Dr. Chatterjee and my co-advisor Dr. Craviso for helping me with my thesis and thank you very much for your dedication and consideration during the elaboration of this thesis. Without your help I would have never been able to finish this thesis.

To all the people in the laboratory group: Dr. Yoon, Dr. El Zaklit, Robert, Aaron and Lisha. Merci beaucoup Josette pour tout ton aide!!

Ich mchte mich bei Herr Dr. Kuster bedanken, da er mich an der ITIS Foundation angenommen hat, und Esra und Manuel, fr ihre Hilfe mit diesem Projekt. Herzlichen Dank Brynn, dass Du mir VTK Library beigebracht hast, und fr die Implementierung der multidomain Mesher. Eskerrik asko Odei y tambien muchas gracias a ti Hazael por haberme enseñ–ado a programar en VTK.

Diese Erfahrung in der Schweiz um dieses Projekt weiterzufhren, wre nicht mglich gewesen ohne das Stipendium das ich vom Eidgenssisches Departement fr auswrtige Angelegenheiten (EDA) bekommen habe. Thank you very much Dr. Chatterjee for recommending me for the ThinkSwiss Scholarship and Dr. Kuster for accepting me at the ITIS Foundation.

Thank you to Will Haines and Patrick Blumm for an amazing summer in Switzerland. Jon ez means ez, gracias por adoptarme durante 3 meses!

I would like to acknowledge the Air Force Office of Scientific Research (AFOSR Grant FA9550-14-1-0018) for providing funding for this thesis.

To my friends in Reno and in Donosti that has always supported me, muchas gracias a todos! Kriti thanks for all your help.

A mi familia con especial cariño por haberme apoyado en estos tres años.

Eskerrik asko guztioi,

Contents

List of Tables

List of Figures

CHAPTER 1

Introduction

Biological cells are sensitive to external high intensity nanosecond electric pulses (NEPs) that can be used to modify their behavior and function [1, 2]. This manipulation of cell behavior and function is based on the ability of NEPs to create nanopores in the cell membrane [3] and in the membranes of intracellular organelles.This phenomenon is known as electroporation wherein the dielectric properties of the cell membrane and intracellular organelles are affected [4–7]. For example, the formation of nanopores can make membranes permeable to certain ions such as Na^+ and Ca^{2+} [5, 7]. The potential for novel clinical applications of NEPs based on their membrane permeablizing effects has opened a new field of research such as studies investigating the modulation of hormone secretion [5, 8–10].

In order to study the phenomenon of electroporation due to NEPs, both theoretical and experimental approaches have been used [11]. For example, patch clamp eletrophysiological has been used to study membrane permeabilization [3, 5]. Because the size of a biological cell is in the range of micrometers and hence it is not possible to make E-field measurements in the experimental setup, theoretical approaches are needed. In this regard, theoretical models can be used to predict the values of the transmembrane potential (TMP) [12]. The project described in this thesis is based on numerical models of adrenal chromaffin cells, i.e. the author did not perform any experiments and therefore only certain theoretical aspects of electroporation will be discussed.

This project complements patch clamp and fluorescence imaging experiments on chromaffin cells that are ongoing in our laboratory [5,8–10]. The research also builds upon 2-D numerical models [13] in order to have a better understanding of the effects of NEPs on chromaffin cells, specifically on intracellular organelles such as secretory granules and the endoplasmic reticulum.

To the best of our knowledge, the cell model presented in this thesis is the most detailed model created. In this model, the cell membrane, the nuclear membrane and the membranes of 1000 secretory granules were successfully implemented in the software package Sim4life (SPEAG, Switzerland).

In the following section, the state-of-the-art in numerical modeling of biological cells will be described and the geometrical limitations of these models will be discussed as it relates to this project.

1.1 Brief description of the state-of-the-art in numerical modeling of biological cells

Several models of biological cells have been created by various researchers in order to help understand the effects of NEPs on biological cells. The first numerical studies were based on the equivalent circuit of a biological cell [14]. These studies were limited due to their inability to account for non-linearities of processes and changes in cell membrane properties due to pore formation. Advances in computer technology permitted the development of theoretical and numerical approaches for modeling the dynamics of the effects of NEPs on biological cells, i.e. pore formation [6, 12, 15, 16].

The main challenge in modeling a biological cell exposed to NEPs is to account for the effects of pores formed in the membranes. In most biological cells, the cell membrane and the membranes of intracellular organelles are a single layer that have a thickness of 5 nm (except for the nucleus and the mitochrondria which typically have a double membrane). In numerical modeling of a biological cell and its intracellular components including the membranes, generating a geometrical mesh with such small dimensions can be problematic due to the large number of meshcells required (this is further explained in Section 3.3).

A model developed by Smith et al. [6] is based on a 2-D equivalent circuit model of a biological cell. The geometry is generated with a custom Matlab script and the electric potential is computed with the circuit modeling software Berkeley SPICE (Linear Technology

Corporation, USA) [6, 17]. This model has a 5 nm cell membrane thickness and includes a nucleus and a spherical intracellular organelle with membrane thicknesses of 5 nm. The goal of this model was to show that NEPs affected both the intracellular membranes and the cell membrane. When biological cells were exposed to NEPs, in experimental studies the formation of nanopores has been inferred [5, 7]. In the model developed by Smith et al. [6] in which the cell was exposed to multiple types of pulses (Figure 1.2), first the cell membrane is porated, then the nuclear membrane is porated and finally the organelle is porated. In Chapter 8, the importance of these results for this thesis will be discussed.

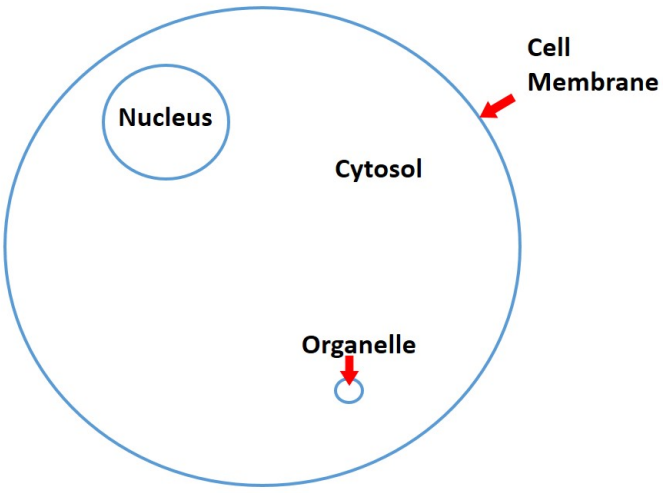

Figure 1.1: Model developed by Smith et al. [6]

In another electroporation model developed by Retlej et al. [12], a 3-D model of a biological cell with 5 liposomes and a nucleus has been created in COMSOL Multiphysics (Stockholm, Sweden). The goal of this work was to investigate the parameters that would cause electroporation of the liposomes but not result in significant electroporation of the cell membrane or the nuclear membrane. One of the parameters that was varied in the model was the size of the liposomes. The results showed that all the liposomes porated equally regardless of their location and that only the larger liposomes could be subject to selective electroporation that is no electroporation of the cell membrane or nuclear membrane. However,

for the small liposome model, the temporal order in which the membranes porate is the same as in the model developed by Smith et al. [6]. First the cell membrane is porated followed by the nuclear membrane and then the liposome membranes.

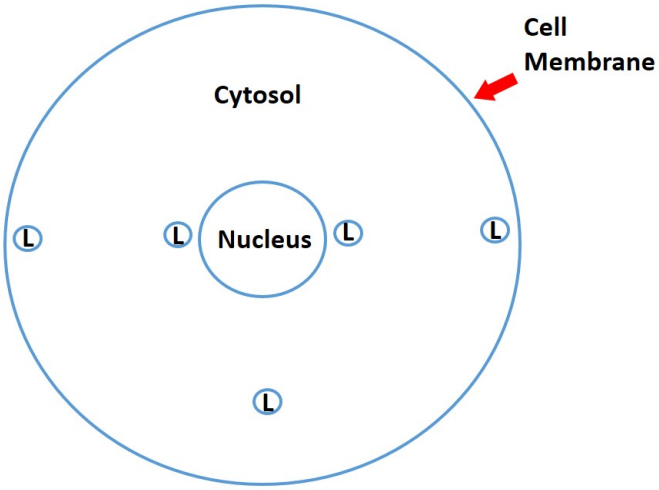

Figure 1.2: Model developed by Retlej et al. [12]. L stands for liposome

The cell models developed by Retlej et al. [12] and Smith et al. [6] both incorporate the model of poration developed by DeBruin and Krassowska [18]. This poration model describes the formation of aqueous pores with a constant radius as a function of the TMP. Gowrishankar et al. [1] and Saulis et al. [19] suggest from experimental data that NEPs create pores that do not grow in radius. As a consequence, the model of DeBruin and Krassowska [18] is a good approximation for modeling electroporation in biological cells exposed to NEPs. Although the cell models developed so far have had good success in helping to understand the effects of NEPs on biological cells, they have certain limitations in terms of modeling a large number of intracellular organelles that could contribute to the inhomogenities in the E-field.

In this thesis, a more realistic model of a adrenal chromaffin cell than previously generated in this laboratory has been developed. The goal is to study the TMP of the membranes and E-field distribution within the cytosol of bovine adrenal chromaffin cells that are being used

in our laboratory for investigating the effects of nanosecond duration high intensity NEPs.

1.2 Previous experiments and cell modeling in chromaffin cells exposed to NEPs

In our laboratory, experimentation coupled with numerical modeling has been employed to understand the effects of 5 ns pulses on adrenal chromaffin cells (the system used for pulse delivery is detailed in Chapter 4). Experimentally it was determined that at an E-field amplitude of 5 MVm, only the cell membrane is permeabilized; higher E-field amplitudes (8 MV/m) are required to porate the endoplasmic reticulum and cause Ca^{2+} release. A cell model in which the intracellular geometry included strutures representing a nucleus, endoplasmic reticulum and a secretory granule helped with explaining this difference. In addition, the cell model further suggested that even higher E-field amplitudes (22 MV/m) are required to porate secretory granules [13]. A localized 2-D model of a chromaffin cell was developed in which 13 spherical structures representing secretory granules were placed in a cluster next to a single larger spherical structure representing the endoplasmic reticulum (Figure 1.3). The goal was to investigate NEP porating effects when a larger number of intracellular organelles were present.

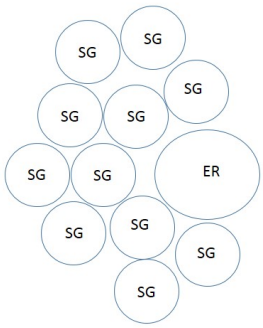

Figure 1.3: 2D Geometry modeled [10] to determine the effects of the presence of granules on the TMP of the endoplasmic reticulum

In this model there was no evidence that the granules affected the TMP of the endoplasmic reticulum. However, the model showed slight differences in the E-field threshold for porating the granules [13] . This latter result suggests that the presence of the granules could cause inhomogenities in the E-

eld distribution within the cytosol. Since this model included only 13 granules (a chromaffin cell has on average 10,000 granules per cell [20] , a more realistic model of a chromaffin cell comprising a much larger number of granules needs to be developed to further investigate E-field inhomogeinities.

1.3 Basis of a simple model for a biological cell

As stated previously, the mechanisms for stimulating adrenal chromaffin cells exposed to NEPs that are 5-6 ns in duration are being explored in our laboratoryIn our laboratory [8,9]. The overall goal is to understand the mechanisms that cause the release of catecholamines and to identify intracellular effects [8, 9].

To advance our understanding the effect of NEPs on chromaffin cells, a simple 1-D model with the most relevant parts of the exposure system used in our laboratory for cell stimulation has been created in Python. In Python the equivalent circuit for the exposure system is modeled and for each part of the exposure system the electric potential is computed. This model is based on the equivalent circuit of each component of the exposure system and includes: the pulse generator, the electrodes (that deliver the NEP to the cell), the external medium, the cell membrane (a nonconducting lipid bilayer) and the cytosol (the conductive media inside the cell). The electrodes deliver the NEP that is generated from the a pulse generator to the cells. Our laboratory uses a Balanced Salt Solution (BSS) as the external medium in which the cells are exposed to NEPs [8, 9]. In Figure 1.4 a schematic of the equivalent circuit for the cell stimulation exposure system is shown.

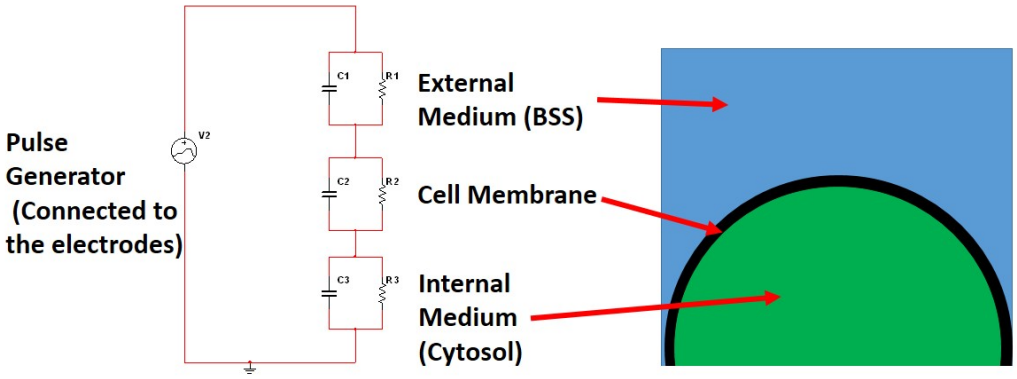

Figure 1.4: A simplified equivalent circuit of the exposure system used in our laboratory [8,9] for stimulating chromaffin cells. The pulse generator and the electrodes are modeled as a voltage source. The external medium (BSS), the cell membrane and the cytosol (the internal medium) are represented by three sets of resistors and capacitors in parallel.

The 5 ns pulse generator is connected to the electrodes that deliver the pulse into a dish of chromaffin cells that are bathed in BSS. The pulse generator and the electrodes are represented in the circuit as a voltage source. The BSS, the cytosol and the cell membrane are modeled as three series connected sets of a resistor and a capacitor connected in parallel (Figure 1.4). The potential difference between the interior and the exterior of the cell (i.e. across the cell membrane) is known as the TMP. When the applied voltage is increased, the electric potential across all the components in the circuit increases but not uniformly. The TMP will increase much more in the cell membrane (C2 and R2 in the circuit shown in Figure 1.4) than across the other components (C1, R1, C3, R3 in the circuit shown in Figure 1.4) due to its high impedance (Section 8.7). However, once the TMP reaches a threshold voltage value, known as the threshold for reversible electrical breakdown [21], pores start forming within the cell membrane making it more conductive. In some cases the conductivity can increase by an order of seven. For example, for a mammalian cell membrane, the value of the conductivity increases from $8.3 \cdot 10^{-10}$ S/m by 7 orders of magnitude when the cell

membrane is fully electroporated [10].

This simplistic model can help us understand the dynamics of pore formation. However, the geometry in this model is extremely simple and therefore and more realistic model is required in order to have accurate results.

1.4 Questions to be addressed in this research

In order to understand better the effects of NEPs on chromaffin cells, a realistic model of a chromaffin cell has been created and analyzed in Sim4life. Sim4life is an EM (electromagnetic) software package that has the ability to create complex geometries and numerically compute EM quantities such as E-field and electric potential. The quantities to be addressed with the model of a chromaffin cell are: 1. The TMP of the granules and 2. the E-field within the cytosol.

In Sim4life, the Stationary Currents solver is based on the Finite Element Method (FEM) and the high frequency solver is based on the Finite-Difference Time-Domain (FDTD) technique [22,23]. Three detailed realistic models of a chromaffin cell including an off-center nucleus, 1000 randomly distributed granules, the cell membrane and membranes of the nucleus and granules have been created in Sim4life. In Plattner et al. [20] shows a electronmicrograph of a chromaffin cell. Chromaffin cells have, on average, approximately 10,000 secretory granules that store catecholomies and other bioactive substances [20,24,25].

All granules have a non-conductive membrane of thickness 5 nm and the cell membrane also has a thickness of 5 nm. The nucleus has a double membrane consisting of two layers each of thickness of 5 nm, which in the geometric model is represented as a single layer of thickness 10 nm due to certain geometry restrictions in the Sim4life mesher (detailed discussion in Section 7). To our knowledge, this is the first realistic model of a chromaffin cell that has been developed and studied under exposure to a high intensity E-field. The goal of this project is to study the TMP across the chromaffin cell plasma membrane and intracellular organelles to evaluate the impact of applied NEPs. Due to limitations of Sim4life (Chapter

5), the formation of pores in real time cannot be included in the simulations. However, since all the membranes porate within a few nanoseconds, poration has been considered as an instantaneous phenomenon and the formation of pores and their effect on the TMP and E-field distributions have also been studied (Section 8.7).

In Chapter 2, the frequency spectrum of the NEP used in the exposure system in our laboratory [5, 8–10] will be described. In Chapter 3, the numerical methods to solve EM problems such as the FDTD and the Low Frequency quasi-static method (LF) are briefly described. In Chapter 4, the inability of the FDTD method to properly model the cell membrane of a biological cell is discussed. In Chapter 5, the LF FEM of Sim4life is presented. This EM software package has the unique ability to model a layer of 5 nm thickness in 3-D using the thin layer feature of Sim4life that will be shown to be an excellent tool for modeling the membranes of biological cells. In Chapter 6, the results for the TMP obtained using the model of a chromaffin cell developed in Sim4life and based on the thin layer feature, are compared to those obtained using Schwan's well-known equation [14] and the model developed by Kotnik and Miklavcic [26]. In this chapter, certain limitations of the LF FEM solver will also be discussed. In Chapter 7, the process of developing three geometries of a chromaffin cell with 1000 randomly distributed granules and an off-center nucleus inside a chromaffin cell is described. In Chapter 8, the geometries developed in Chapter 7 are exposed to an E-field of 5 MV/m at different frequencies and the TMP results for the cell, nuclear and granule membranes are presented. Also, the E-field distributions within the chromaffin cell are presented. In Chapter 9, the results shown in Chapter 8 are discussed. The conclusions about the results are presented in Chapter 10. In Chapter 11, suggestions are made for future work that can potentially improve the cell models presented in this thesis.

CHAPTER 2

Frequency Spectrum of Nanosecond pulses

2.1 Introduction

In this section the characteristics of the NEP used in our laboratory [8, 9] will be discussed. The main parameters for a NEP are: the shape, the amplitude, the duration and the rise/fall time. Advances in circuit technology have permitted the development of nanosecond (ns) pulse generators [27]. When exposing cells to a NEP using a pulse generator, the pulse duration is of the order of nanoseconds and the magnitude of the E-field at the location of the cells can reach MV/m [17, 27]. These pulses do not cause thermal effects on the cells because the energy delievered to the cells is approximately in the tens of Joules [2, 28] and does not cause a physiologically relevant increase in temperature.

2.2 Frequency content of the pulse

The Stationary Currents module in Sim4life will be used for the computations in this thesis. This module is a low frequency solver that can only process single frequencies, i.e. it cannot process signals in the time domain. For this reason, this project will be based on the study of single frequencies that constitute the frequency spectrum of the NEPs used in experiments in our laboratory. (Section 3.3). The Fourier Transform (FT) of a signal in the time domain decomposes the signal into a sum of sinusoidal functions in the frequency domain [29].

A Matlab script has been written to obtain the FT of the pulse used in our laboratory [5, 8–10]. In order to validate the Matlab script, Parseval's theorem (Eq 1) was tested [29], i.e. the square of the energy of the signal in both the frequency and time domain must be equal (Eq 1). The pulse in the time domain (x(t)) and the transformed pulse in the frequency

domain (X(f)) had an energy of 1.3 mJ.

$$\int |x(t)|^2 dt = \sum |X(f)|^2 \tag{1}$$

The signal output from the NEP generator (Transient Plasma Systems) used in our laboratory is recorded by an oscilloscope (Tektronics, TDS 3012C) at a sampling rate of 0.2 ns. In Figure 2.1, the average of 10 pulse traces is displayed [5, 10]. The rise time is defined as the time required for a pulse to rise from 10 percent to 90 percent of its peak value. The rise time of the pulse in Figure 2.1 is 6 ns. The width (defined at the half amplitude points of the pulse) of the averaged trace in Figure 2.1 is 5.5 ns; the duration range for a pulse is between 5.2 ns and 6 ns.

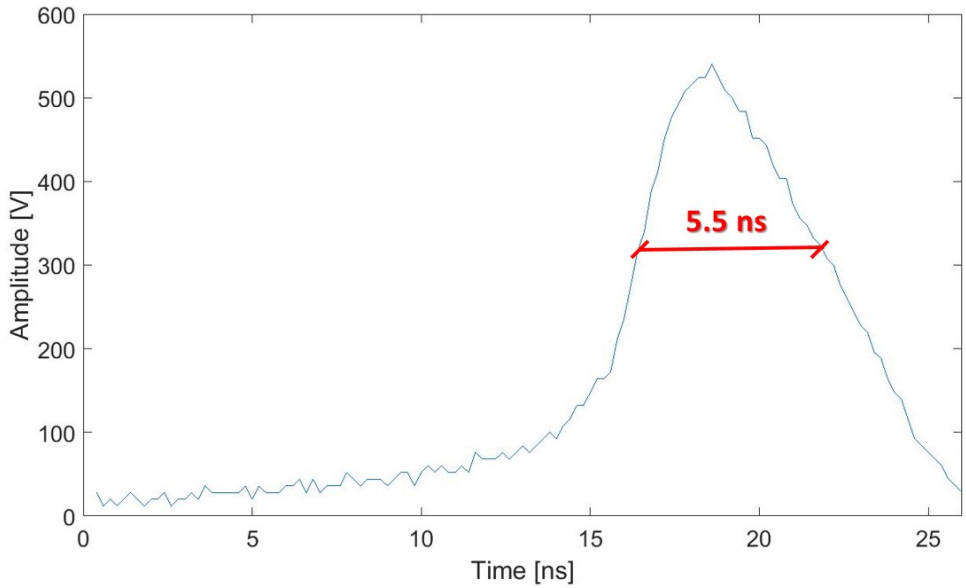

Figure 2.1: Average of ten pulse traces recorded in the exposure system used in our laboratory. The rise time of the pulse is 6 ns, the average pulse duration is 5.5 ns. Pulse amplitude = 500 V.

In order to obtain an accurate FT of the pulse, the trace shown in Figure 2.1 must be interpolated to obtain a sufficient number of samples since the number of samples acquired by the oscilloscope is small.

After running the Matlab script, the FT of the pulse trace shown in Figure 2.1 was obtained and is displayed in Figure 2.2.

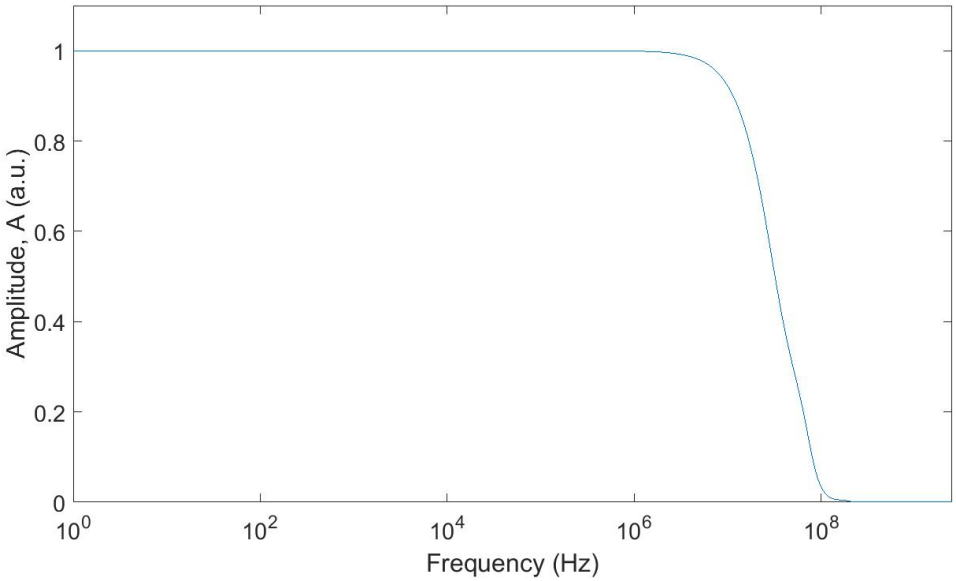

Figure 2.2: FT of the pulse used on our laboratory (Figure 2.1). This graph represents the amplitude of the FT in the frequency domain. 90% of the energy is below 66 MHz. a.u.= arbitrary units

The FT of the pulse used in our laboratory shows that most of the energy content, (90%) is contained in frequencies below 66 MHz [5,10]. This result is similar to that of Schoenbach et al. [2], who used a similar pulse (Gaussian pulse) and have shown that 90% of the energy was contained in frequencies below 60 MHz.

In conclusion, in this section the frequency content of the NEP used in our laboratory [8,9] has been computed. Ninety percent of the energy is concentrated between DC and 66 MHz. The shortest wavelength (λ) at 66 MHz (f) and in BSS ($\varepsilon_r = 80$) can be calculated as

$$\lambda = \frac{c}{f\sqrt{\varepsilon_r}} = 0.59\ m \tag{2}$$

where c is the speed of light. The dimensions of the exposure system are in the micrometer range. Therefore it can be assumed that EM fields are quasistatic in the experimental setup (up to 1 GHz) and therefore a quasi-static approximation to compute EM fields would be

acceptable (Chapter 4). In the following chapter, a brief description on the method of functioning of high frequency solvers (Section 1.1) and low frequency solvers in Section 3.3 will be discussed.

CHAPTER 3

Numerical methods for solving EM problems

3.1 Introduction

Recent advances in computer technology have enabled the development of a wide variety of powerful EM software packages. These software packages can compute the Electric (E)-field, Magnetic (H)-field, current, voltage and other EM quantities by solving Maxwell's equations for a specified source and geometry [22, 30]. The user can create a geometry, input the electrical and magnetic properties of each material in the geometry, define an excitation source and compute the distribution of the EM fields in the space within and surrounding the geometry.

There are many numerical methods used to solve Maxwell's equations. For each method, the software designers have developed a program called "solver" which is a key feature of all EM packages because it computes the solution to Maxwell's equations. Solvers can be divided into two categories: High Frequency (HF) solvers and Low Frequency (LF) solvers [31]. The solver used in a particular problem is based on the frequency of the input signal and the electrical and magnetic properties of the materials that constitute the geometry. Furthermore, solvers can also be classified based on the numerical technique used to solve Maxwell's equations. There are three popular techniques: the Finite-Difference Time-Domain (FDTD) method, the Finite Element method (FEM) and the Method of Moments (MoM). In this project, software packages based on both the FDTD and the FEM techniques are used and a brief description of each will be given.

3.2 Brief introduction to specific considerations in the Finite-Difference Time-Domain technique

This numerical method was first proposed by Kane S. Yee in 1966 [31–33] and is a solution to Maxwell's equations (Eqs 3 to 6)

$$\nabla \cdot \vec{D} = \rho \tag{3}$$

$$\nabla \cdot \vec{B} = 0 \tag{4}$$

$$\nabla \times \vec{E} = -\frac{\partial \vec{B}}{\partial t} \tag{5}$$

$$\nabla \times \vec{H} = \frac{\partial \vec{D}}{\partial t} + \vec{J} \tag{6}$$

where $\vec{E}$ is the E-field intensity, $\vec{D}$ is the electric flux density, $\vec{B}$ is the magnetic flux density, $\vec{H}$ is the H-field intensity, $\vec{J}$ is the current density, ε_o is the dielectric permittivity of free space, μ_o is the magnetic permeability of free space and ρ is the charge density.

Maxwell's equations can be complemented by the continuity equation which is essentially the law of conservation of charge:

$$\nabla \cdot \vec{J} = \frac{\partial \rho}{\partial t} \tag{7}$$

The FDTD technique is ideal for high frequency applications such as at microwave and radio frequencies and even in some optical applications [33]. The FDTD technique is not adequate for low frequency problems in which the signal does not propagate within the computational domain (Section 2.2). The computational domain is the region where the numerical simulation will be performed and is composed of the geometry and its surroundings. The size of the computational domain must be carefully chosen in order to avoid any undesired reflections from the edges of the computational domain (Section 6.5).

The FDTD method can compute the EM quantities of any object exposed to EM fields, if the EM properties of the materials involved are known. All materials are characterized by

their complex permittivity (Eq 8).

$$\widehat{\varepsilon} = \varepsilon_r \varepsilon_o + \frac{\sigma}{j\omega} \tag{8}$$

where σ is the electrical conductivity, $\omega = 2\pi \times frequency$ is the angular frequency, ε_o is the dielectric permittivity of free space and ε_r is the relative dielectric permittivity of the material.

Advances in Computer Aided Design (CAD) programs have enabled the accurate creation of complex geometries in 3-D. These geometries can be imported from the CAD program into the EM software package or in some cases the EM software package includes the basic tools to create the desired geometry. The geometry must be appropriately discretized and the discretization process divides the geometry into meshcells (Section 4.2). Once the geometry has been created and discretized, the excitation signal or source must be defined. Sources are inserted into the model as regular 3-D objects and are used to excite EM fields outside and inside the geometry. Once the desired object has been defined, the material that surrounds the object needs to be specified. By default, in most EM software packages this is usually air or free space. The surrounding material delimits the computational domain, i.e. it determines where Eqs 3 to 6 will be solved. Furthermore, the Boundary Conditions (BCs) in the computational domain must be defined. The BCs specify the solution for Maxwell's equations at the edges of the computational domain (Section 6.5).

3.2.1 Courant Stability Condition

When using the FDTD technique, the Courant Stability Condition (CSC) must be met in order to ensure numerical stability of the solution. Numerical stability is an important factor for the accuracy of the computed fields because it determines the numerical errors introduced into the solution [22, 30, 33]. The CSC is given by Eq 9 and determines the minimum time step (Δt) for a stable simulation. The time step Δt is defined as the incremental change in

time for which Maxwell's equations are being solved (Figure 3.1).

$$\Delta t = \frac{c}{\sqrt{\frac{1}{\Delta x^2} + \frac{1}{\Delta y^2} + \frac{1}{\Delta z^2}}} \tag{9}$$

where c is the speed of light and Δx, Δy, Δz are the dimensions of the smallest meshcells in the x, y and z directions respectively. A meshcell is defined as the geometrical unit that discretizes the geometry created by the user. These meshcells are generated by the mesher, a specific part of the EM software package, that discretizes the geometry. In each meshcell the E and H fields are computed (Section 4.2).

As an example, a sinusoidal input signal is sampled at a rate determined by the time step Δt, i.e. the signal will be sampled every Δt (Figure 3.1). For every sample of the signal, the solver will solve Maxwell's equations for the entire computational domain; these time samples are called iterations.

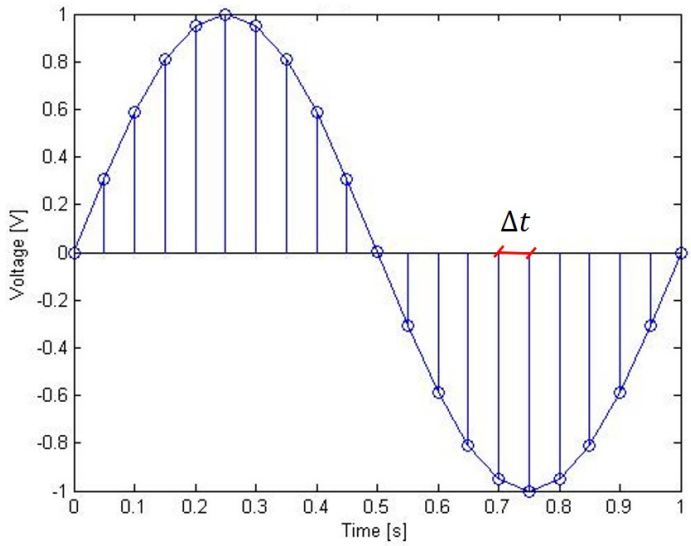

Figure 3.1: Sampling of a sinusoidal input signal. Each time step is represented by a circle. Every point is considered an iteration and the time difference between these points is Δt.

The number of iterations can be calculated as shown in Eq 10. If a meshcell dimension is small compared to the chosen computational domain, the time step will be small, the

number of iterations will increase and as a consequence the computational time will increase as shown in (Eq 9).

$$Number\ of\ iterations = \frac{Total\ duration\ of\ the\ input\ signal}{Time\ Step\ (\Delta t)} \tag{10}$$

A large number of iterations can cause prohibitively long simulation times. In section 4.3, it will be shown that the CSC for a 5 nm meshcell will make the simulation impossible within a reasonable amount of time.

3.3 Low Frequency (LF) Solver

A LF solver is a simpler version of high frequency solvers where Maxwell's equations (Eqs 3 to 6) are solved in the frequency domain [33]. Solving Maxwell's equations in the frequency domain does not allow the solvers to perform computations of EM fields as a function of time. Therefore, LF solvers can only take DC sources as input and can be used when the EM fields are static within the computational domain [32]. However, the EM properties can be modeled in the frequency domain if the term $\omega\varepsilon$ is chosen instead of (Section 3.3.1).

Another simplification in the LF solver is that the H-field is decoupled from the E-field (explained in [22]). To describe how Maxwell's equations can be solved in the frequency domain, (Eqs 3 to 6) can be rewritten in the frequency domain as:

$$\nabla \cdot \vec{D} = \rho \tag{11}$$

$$\nabla \cdot \vec{B} = 0 \tag{12}$$

$$\nabla \times \vec{E} = -j\omega\vec{B} \tag{13}$$

$$\nabla \times \vec{H} = j\omega\vec{D} + \vec{J} \tag{14}$$

where $\vec{E}$ is the E-field intensity, $\vec{D}$ is the displacement current density, $\vec{B}$ is the magnetic

flux density, $\vec{H}$ is the magnetic field intensity, $\vec{J}$ is the current density and ρ is the charge density. Furthermore, the continuity equation (Eq 7) can be written in the frequency domain as

$$\nabla \cdot \vec{J} = -j\omega\rho \tag{15}$$

3.3.1 Electro quasi-static Solvers

LF solvers are based on the electro quasi-static approximation where the temporal change of magnetic flux is neglected [33]. Furthermore, in a LF simulation, the materials in the computational domain must fulfill the condition $\omega^2\widehat{\varepsilon}\mu d^2 << 1$ where d is the maximum length of the computational domain. This condition ensures that waves do not propagate within the computational domain, i.e. the EM fields are quasi-static.

In quasi-static solvers, Maxwell's equations are solved in the frequency domain and for a single frequency. Futhermore, the E-field can be calculated as $\nabla V = \vec{E}$. In addition in quasi-static solvers, the E-field is assumed to be decoupled from the H-field and Eqs 12-13 can be reduced to Eq 16 [22]

$$\nabla \cdot \widehat{\varepsilon}\nabla V = 0 \tag{16}$$

where V is the electric potential to compute and $\widehat{\varepsilon}$ is the complex permittivity of the materials.

Therefore, the E-field is only dependent on the potential V. The excitation is provided by the Boundary Conditions (BC) and two types of BCs can be distinguished: Dirichlet's and Neumann's BC. In an ordinary or partial differential equation (DE), Dirichlet's BC establishes the solution of the DE along the boundary of the computational domain; in EM simulations Dirichlet's BC specifies the voltage on the boundary of the computational domain. The Neumann BC, on the other hand, specifies the solution to the derivative of the DE along the boundary of the computational domain. In EM simulations, the Neumann's BC specifies the charge on the boundary of the computational domain. When the Neumann

BC is set to zero Coulomb, the boundary is equivalent to an insulating boundary.

The Stationary Current solver in Sim4life is based on the FEM technique and can handle only real quantities, i.e. it can only accept one part of the complex dielectric permittivity as input (Eq 8), i.e. either $\omega\varepsilon$ or σ [22]. Therefore, depending on the properties of the materials and the frequency involved, the imaginary part or the real part of the complex permittivity will be chosen as input. If $\sigma >> \omega\varepsilon$ then it can be assumed that the conduction current dominates the displacement current. Therefore, the electrical conductivity (σ) term is used for all the materials in the computational domain and the Stationary Current solver only computes the conduction current; the equation solved is given by:

$$\nabla \cdot \sigma \nabla V = 0 \tag{17}$$

where σ is the electrical conductivity of the materials and V is the electric potential. When $\sigma << \omega\varepsilon$ i.e. the displacement current dominates over the conduction current Eq 17 can be written as:

$$\nabla \cdot \varepsilon\omega \nabla V = 0 \tag{18}$$

where V is the electric potential and $\varepsilon\omega$ is the EM property of the materials material (frequency dependent)For a chromaffin cell, the value of the conductivity of the cell membrane is $8.3 \cdot 10^{-10}$ S/m and the ε_r is 5.5 [10, 34]. Above a certain frequency the term $\omega\varepsilon$ will be larger in magnitude than σ. In this project, only for the membranes (cell membrane and internal organelle membranes) the displacement current prevails over the conduction current. For the membranes of a chromaffin cell, the term $\omega\varepsilon$ is greater than σ above 10 Hz. Therefore, during the simulations, for frequencies up to 10 Hz the of σ will be used for the membranes in Eq 17 (which equals to $8.3 \cdot 10^{-10}$ S/m). For frequencies above 10 Hz, the value of $\omega\varepsilon$ will be used in Eq 18, which will increase as frequency increases.

In this chapter a brief introduction to the high frequency and low frequency solvers has

been given. High frequency solvers can take signals in the time domain as input while low frequency solvers can only take single frequency input signals. Due to the non-linear dynamics of the membranes (i.e. the formation of pores in the membranes) and because the NEP is a time domain signal the solver of choice would be the high frequency solver. However, as will be seen in Chapter 4, high frequency solvers are not capable of computing the E-field in a cell model.

CHAPTER 4

Homogeneity of the E-field in the vicinity of a chromaffin cell in the exposure system and limitations of the FDTD method in modeling a chromaffin cell

4.1 Introduction

A geometric model of the experimental setup used in our laboratory for exposing chromaffin cells to high intensity NEPs has been created using the Finite-Difference Time-Domain (FDTD) software package SEMCAD 14.8 (SPEAG, Zurich, Switzerland) to compute the detailed distribution of the E-field in the vicinity of the electrodes used to deliver a NEP and at the location of a chromaffin cell placed centrally between the electrodes [5]. SEMCAD 14.8 is an EM software package that has the ability to create complex geometries and compute EM quantities such as E-field and electric potential within these geometries.

The experimental setup consists of two tungsten rod electrodes separated by 100 μm at the tips (Figure 4.1). One of the electrodes acts as the excitation source and the other acts as ground. A chromaffin cell is located centrally in the gap between the electrodes and 40 μm below the electrodes tips (Figure 4.1). The goal of these numerical simulations is to compute the induced TMP and the detailed distribution of the E-field at the location of the cell.

In order to create an accurate model of the exposure setup, the dimensions of the electrodes and the chromaffin cell must be accurately modeled. This experimental setup is a complex multi-scalar study case in which the dimensions of the exposure setup range from centimeters to decimeters and the chromaffin cell dimensions range from nanometers to micrometers.

In Section 4.2, the procedure to create the geometric model with SEMCAD will be explained. Also, in this section the homogeneity of the E-field within the region containing the cell will be discussed. In Section 4.3, it will be shown that the range of dimensions involved (decimeters to nanometers) will not permit the SEMCAD mesher to create an appropriate mesh for the simulation.

4.2 Determination of the E-field distribution in the experimental setup

In the experiments conducted in our laboratory [8, 9], chromaffin cells are exposed to high amplitude (5 MV/m) 5 ns duration pulses (Figure 2.1). The FDTD method has been proven to be one of the most effective numerical methods for modeling the effects of an applied signal in the time domain. An accurate geometry of the experimental setup was generated (Figure 4.1) with the CAD tools in SEMCAD [5].

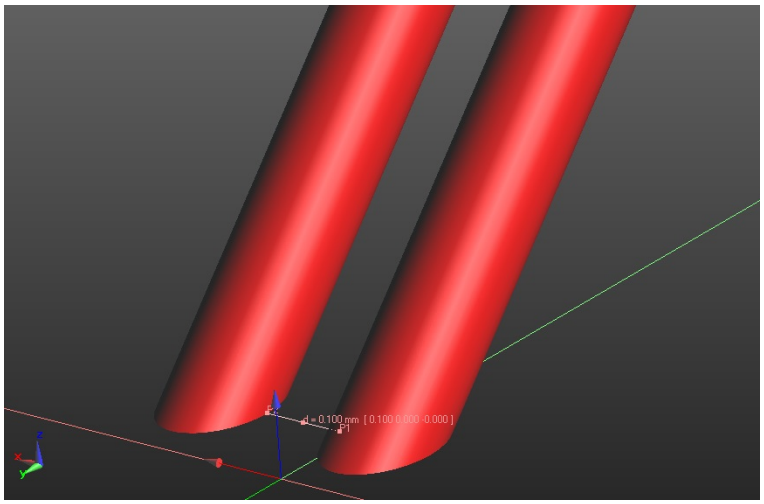

Figure 4.1: Geometry of the experimental setup with two tungsten electrodes. This geometry has been adapted from [5].

After generating the geometry, the EM properties of each material must be assigned. The conductivity of tungsten is $6.8 \cdot 10^6$ S/m, making this material a good conductor and therefore acceptable for the Perfect Electric Conductor approximation. This approximation

speeds up the SEMCAD solver's convergence. The chromaffin cell is bathed in a dielectric liquid, which in our experiments is BSS. The BSS dielectric permittivity is $\varepsilon = 5.5\ F/m$ and the conductivity is $\sigma = 1.3\ S/m$ [10, 34].

The next step is to discretize the geometry into meshcells. The mesher is a specific tool for helping the user discretize the geometry by specifying the size of the meshcells. A meshcell (or voxel) is the minimum unit comprising the geometry. An example of a discretized geometry built in SEMCAD 14.8 is shown in Figure 4.2. A small meshcell size refines the precision of the geometry, but also increases the number of meshcells and as a consequence the computational time will increase (Section 3.2.1). Therefore, the size of the meshcell needs to be carefully chosen in order to obtain both an accurate geometrical resolution and an acceptable simulation time.

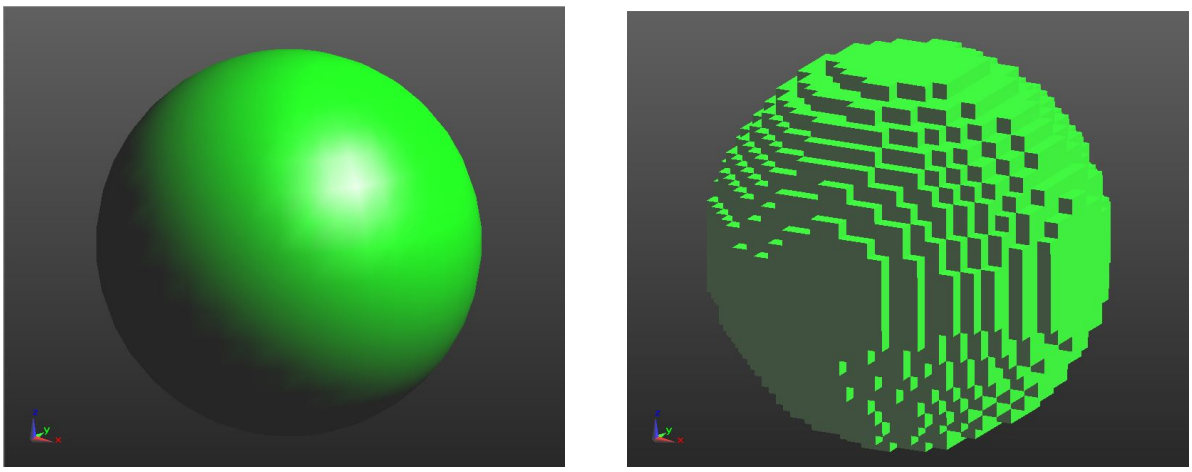

(a) Geometry of a sphere with a radius of 8 μm. This geometry can be created using the CAD tools in SEMCAD 14.8

(b) Discretization of the 8 μm sphere using hexahedral meshcells. The edge length of every hexahedron was set to 0.5 μm.

Figure 4.2: Example of discretization of a sphere using hexahedrons as meshcells

Initially, the experimental setup was modeled with SEMCAD 14.8 and a rectilinear mesh was used. A rectilinear or structured mesh is based on the discretization of the geometry into hexahedrons (Figure 4.3).

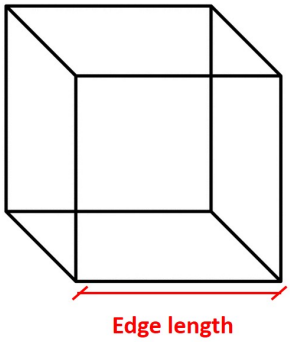

Figure 4.3: Hexahedron with the same edge length in all three directions

The electrode geometry in Figure 4.4 is discretized. Each meshcell (or in this case hexahedron) has an edge length of 0.2 mm and a total number of meshcells equal to 1.56 million.

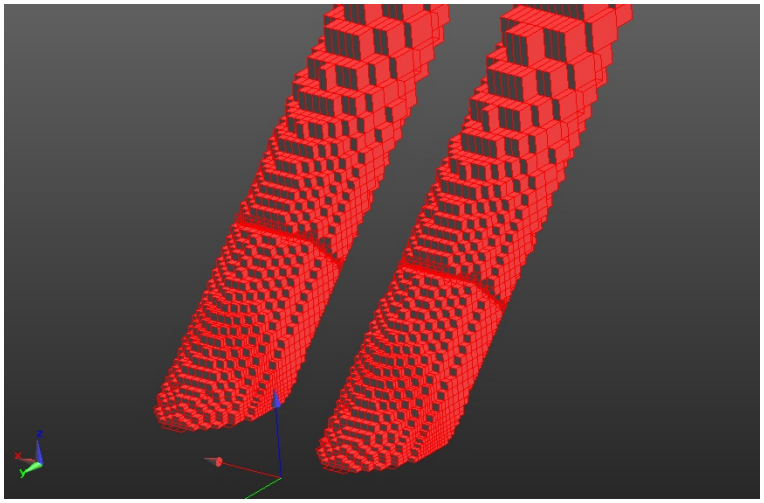

Figure 4.4: Discretization into meshcells of Figure 4.1 into hexahedrons. The meshcell size is 0.2 μm

After the meshcells were generated, the simulation to compute the E-field distribution was run. The obtained E-field was homogeneous at the location of the chromaffin cell to within 10%. In a similar exposure system simulation, Yoon et al. [5] the computed E-field was homogenous to within 6 % . In biological experiments, this level of homogeneity is acceptable [35, 36].

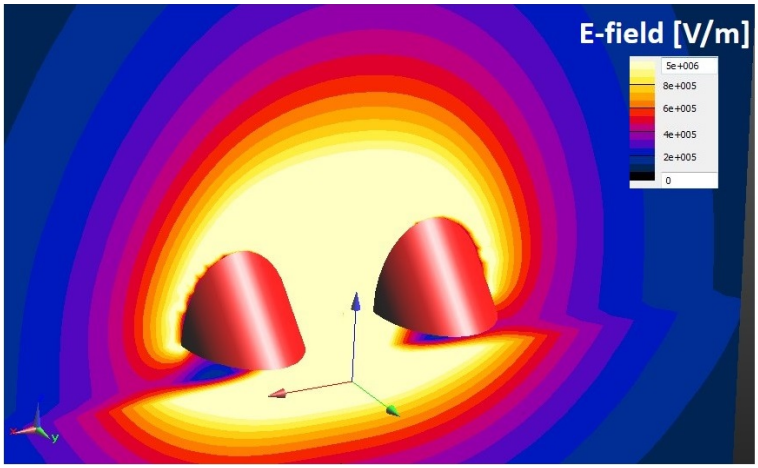

Figure 4.5: Results for the E-field distribution in the vicinity of the rod electrodes. The E-field at the location of the chromaffin cell is homogeneous to within 10%

4.3 Non-suitability of the FDTD technique for creating a realistic model of a chromaffin cell

The next step is to properly model the chromaffin cell placed between the tungsten rod electrodes in the geometry of the exposure setup shown in the previous section. A chromaffin cell is modeled as a sphere of radius 8 μm.

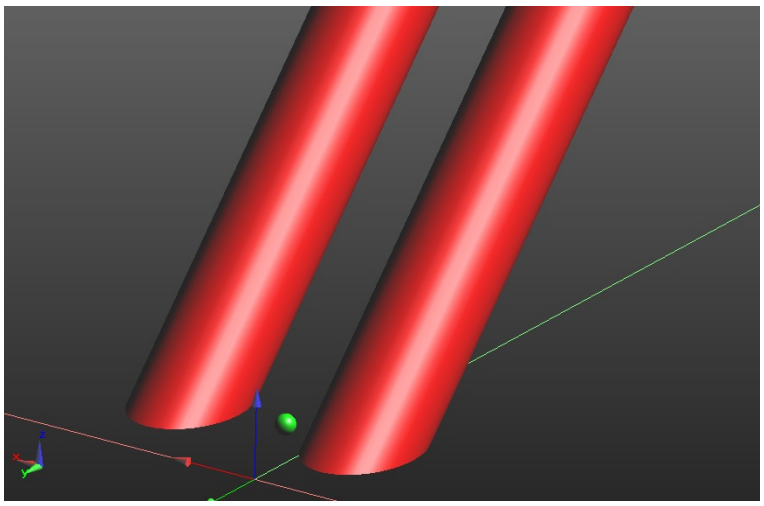

Figure 4.6: The chromaffin cell (represented as a green sphere with a 8 μm radius) is placed on the glass bottom dish (not shown) and the electrode tips are centrally positioned 40 μm above the cell.

The geometry was discretized into meshcells of dimensions 0.2 μm. In Figure 4.7 the generated meshcells for the rod electrodes and the chromaffin cell are displayed. In this type of discretization the geometrical refinement of the chromaffin cell is too coarse to accurately represent the features of the cell including the membranes.

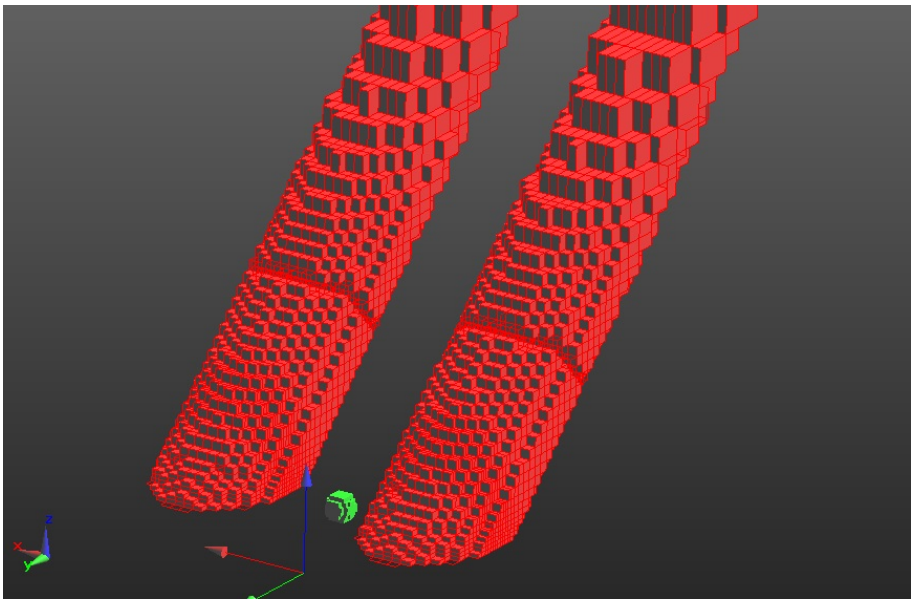

Figure 4.7: View of the discretization of the experimental setup with a cell placed centrally and 40 μm below the tip of the electrodes.

The thickness of the cell membrane is 5 nm which requires a very fine geometrical refinement and discretizing such a thin layer is not possible with a structured mesh in SEMCAD. The main impediments are the memory required to run this simulation (20 GigaCells), along with the extremely small time step as determined by the Courant stability condition (Chapter 3). In order to meet the Courant stability condition with a 5 nm meshcell size, the time step must be 10^{-17} s. As a result, the required time for such a simulation would be approximately 1 year, making it prohibitively long. Due to these impediments, none of the attempts to properly model the cell membrane of a chromaffin cell with a rectilinear mesh were successful. As a result, another method with an infinitesimally thin layer representing the cell membrane was tested. The thin resistive sheet (TRS) is a feature in SEMCAD 14.8 that can model very thin conductive layers without actually discretizing the layer [30].

This feature is derived from plane wave theory where in the TRS algorithm determines the reflection and transmission coefficients at the interface of two media [32]. As stated before, the TRS algorithm would be ideal to represent the cell membrane, but this algorithm is only valid for good conductors and not for dielectric materials such as the cell membrane. Therefore, a different technique had to be explored and is described in Chapter 5.

CHAPTER 5

Creation of a model in Sim4life with the LF FEM solver

5.1 Introduction

In the previous chapter, the difficulty of modeling cellular membranes with the FDTD technique was highlighted. The E-field generated by the exposure system in our laboratory was determined to be homogeneous to within 10% at the location of the chromaffin cell. In Section 2.2 it was shown that the EM fields are quasi-static. Also it was shown that 90% of the energy is below 66 MHz in which EM fields do not propagate and the E-field is homogeneous in the location of the cell. Therefore, using a LF solver is a good approximation to compute the E-field. In this chapter the procedure to create a realistic model of a chromaffin cell with a 5 nm cell membrane in the LF FEM solver of Sim4life will be explained.

This chapter is divided into three sections. In Section 5.2, the configuration of the LF FEM solver of Sim4life will be discussed. A geometry to generate an E-field will be discussed. In Section 5.3, the EM properties of the thin layer feature of Sim4life will be discussed. Also it will be shown that the thin layer feature of Sim4life will be a key element for modeling the membranes of a chromaffin cell and its organelles. In Section 5.4, a model for a chromaffin cell with a cell membrane created in Sim4life will be discussed. Also, the limitations of the chromaffin cell model created in Sim4life (based on the thin layer feature of Sim4life) will be discussed.

5.2 Configuration of the Stationary Currents Low Frequency solver in Sim4life

The LF FEM solver of Sim4life is a real-valued unstructured mesh FEM electro quasi-static solver developed at SPEAG (Zurich, Switzerland) [23]. An unstructured mesh is composed

of tetrahedra. The usage of the Sim4life software will be described including certain aspects that will be described: 1. Creation of the model, 2. Mesh generation and 3. Setup of the excitation source.

5.2.1 Creating a geometric model in Sim4life

The Sim4life interface offers the user the ability to create solids of regular shape such as spheres, cubes and cylinders. Furthermore, these solids can be combined with Boolean operations to create complex geometries. For users experienced in programming, Sim4life offers a script developer console called Scripter (Figure 5.1) where the user can write a Python script and generate a complex geometry. In this project, a Python script was written in order to create a geometry of a chromaffin cell with 1000 granules within the cell cytosol (Chapter 7).

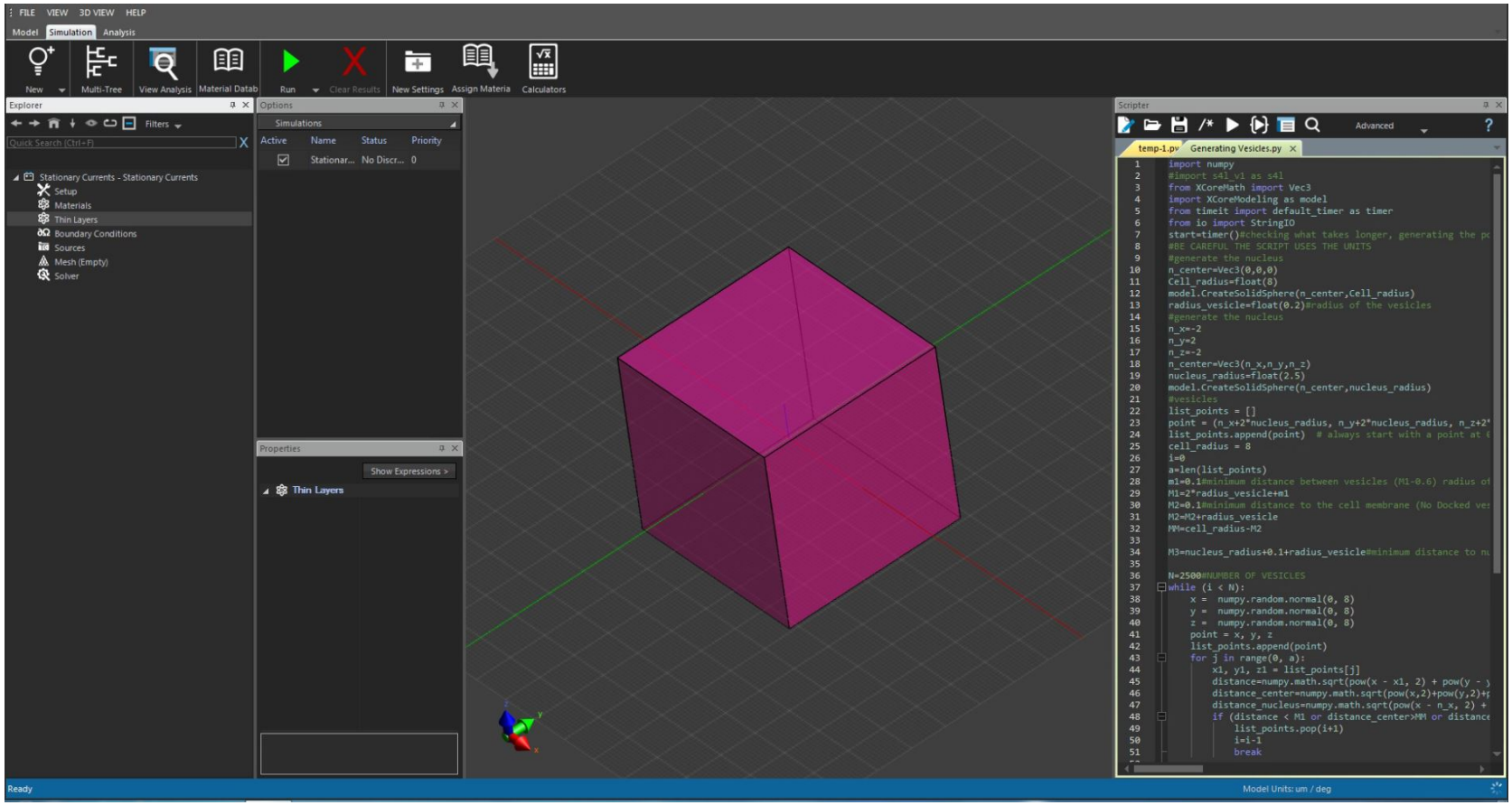

Figure 5.1: View of the interface offered by Sim4life; scripter tab is displayed on the right side

5.2.2 Mesh generation

A multidomain mesher based on the method suggested by Si and Shewchuk [37] was incorporated by B. Lloyd (SPEAG, Zrich, Switzerland) into Sim4life. This mesher discretizes the geometry into a first order tetrahedral mesh [23]. The mesh must be carefully designed in order to accelerate the computations in a simulation. For example, all the triangles on any surface must have six connection points in order to favor the convergence of the solver. The mesh can be easily modified with the tool *Remesh*. This tool allows the user to manually mesh all the surfaces in the geometry (Figure 5.2).

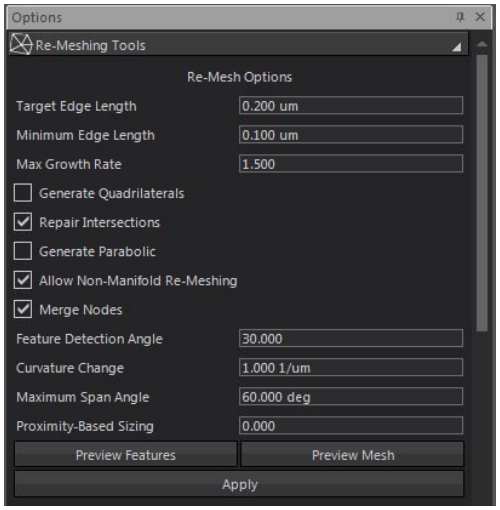

Figure 5.2: Tool for remeshing the surfaces in the computational domain

By unclicking *Generate Quadrilaterals* and *Generate Parabolic*, all the surfaces will be remeshed with triangles. When using multiple kinds of triangles such as isosceles and right triangles, the mesh in Figure 5.3 is obtained for a sphere. In Figure 5.3 it can be seen that the top node of the sphere (located at the pole) is connected to 40 neighboring nodes. This high number of connections will increase the computational time when determining the electric potential at this node. For the project described in this thesis, 1000 granules will be placed inside the chromaffin cell (Chapter 7) and therefore the mesh must be optimized to favor the fastest convergence of the solver. Therefore, all spheres included in the geometry

of the chromaffin cell will be remeshed with triangles that are close to equilateral in order to obtain 6 connections per node and speed up the convergence of the solver (Figure 5.4).

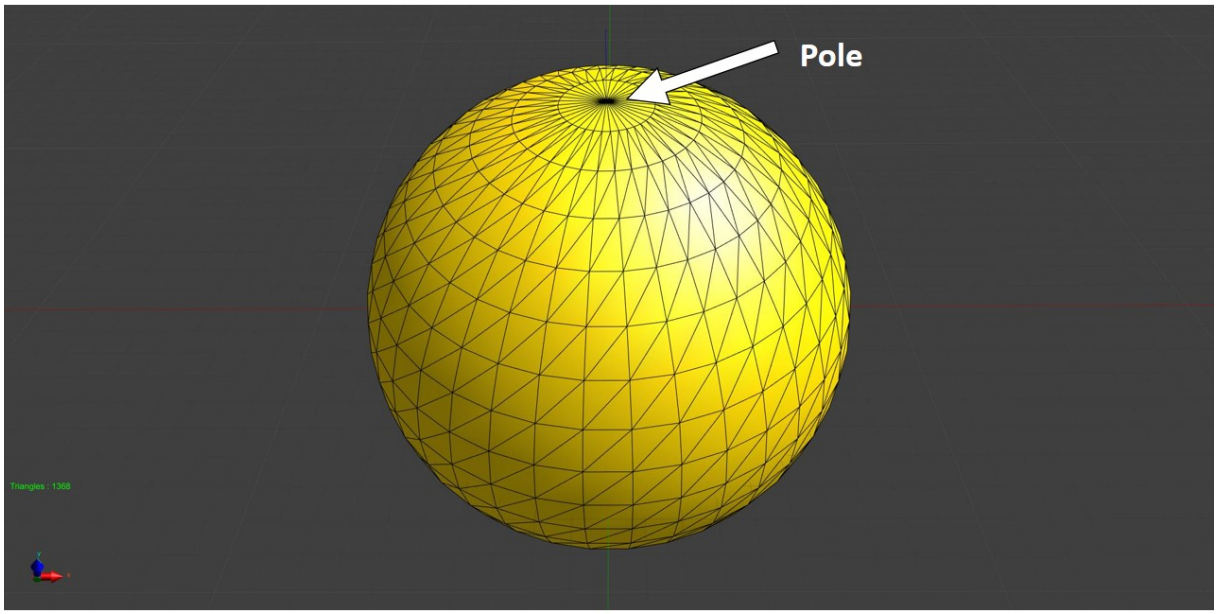

Figure 5.3: Sphere with a mesh based on right and isosceles (at the pole) triangles.

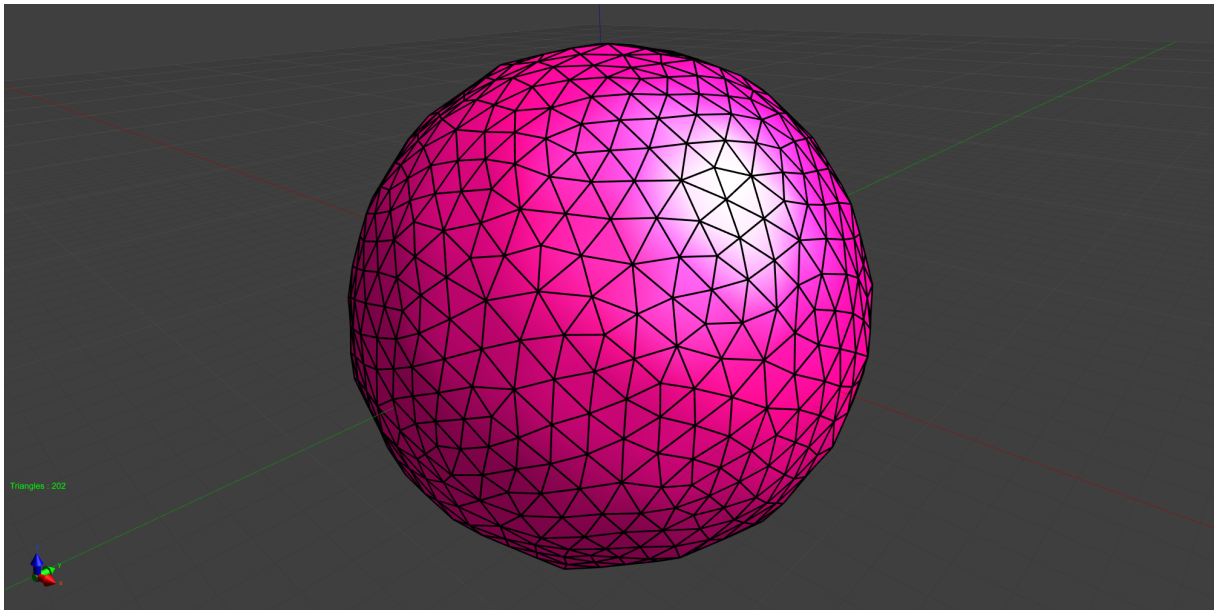

Figure 5.4: Sphere with a mesh based on triangles that are close to equilateral.

The next step is to generate the 3-D mesh using the multidomain mesher. This mesher

permits the user to determine the target and minimum edge length of the tetrahedra (Figure 5.5). When generating a tetrahedral mesh, the target edge length refers to the desired length for each meshcell; each meshcell will be different and therefore a minimum edge length needs to be specified in the mesher.

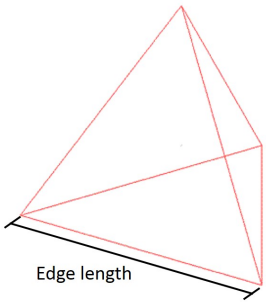

Figure 5.5: Tetrahedron with the same edge length

Based on these parameters, the number of tetrahedra in the mesh will vary. In Figure 5.6 the configuration tab for the 3-D mesher in Sim4life is shown.

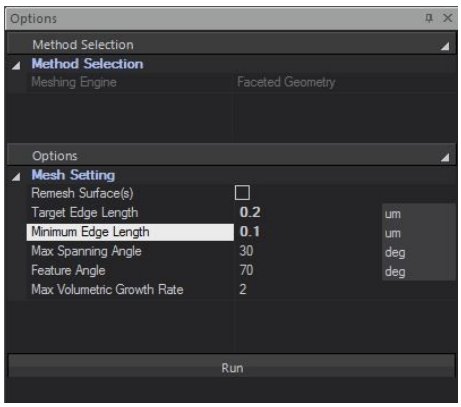

Figure 5.6: Configuration tab in the 3-D Mesher

Once the mesh has been generated, the "Create Patch" tool can be useful for selecting a surface on the computational domain (such as the boundary) and to create an interface between two objects in the computational domain. For example, with the "Create Patch" tool and thin layer feature, a conductive material in the computational domain can be covered

by an electrically insulating thin layer. In the case of a biological cell two conductive media (the external medium and the cytosol content) are separated by a non conductive thin layer, i.e. the cell membrane.

5.2.3 Configuration of the Boundary Conditions

In LF solvers, multiple procedures exist to define an excitation source. For this project, the geometry that will be used is a cube with the same edge length (Figure 5.7). In Section 4.3 with FDTD simulations that included the experimental setup of the rod electrodes used in our laboratory [**?**, 8, 9], the E-field in the vicinity of the chromaffin cell was homogeneous. The most suitable computational domain to generate a homogeneous E-field is a rectangle?? (Figure 5.7) in which two planar electrodes are placed on opposite faces being the distance between the electrodes much smaller than the side of the electrodes. The planar electrodes are defined as Dirichlet BCs (Figure 5.7). One of the faces is set to ground (i.e. 0 V) and the opposite face is set to a specific voltage in order to generate the desired E-field in the space between the faces and can be calculated as:

$$E = \frac{V}{d} \tag{19}$$

where V is the applied voltage between the electrodes and d is the distance between the electrodes (Figure 5.7). The computational domain used in the Sim4life simulations is a cube and therefore there could be some fringing effect which can be mediated by increasing the convergence factor of the solver (Section 5.2.5). In Section 6.5, it will be shown, that when a chromaffin cell is placed between the plates, there must be a minimum distance between the plates in order to obtain an accurate result for the TMP. In the experiments being carried out in our laboratory [8–10], the E-field in the exposure system has a typical value of 5 MV/m at the location of the chromaffin cells. Therefore, in all the Sim4life simulations the voltage applied to the electrodes will be chosen to create an E-field of 5 MV/m.

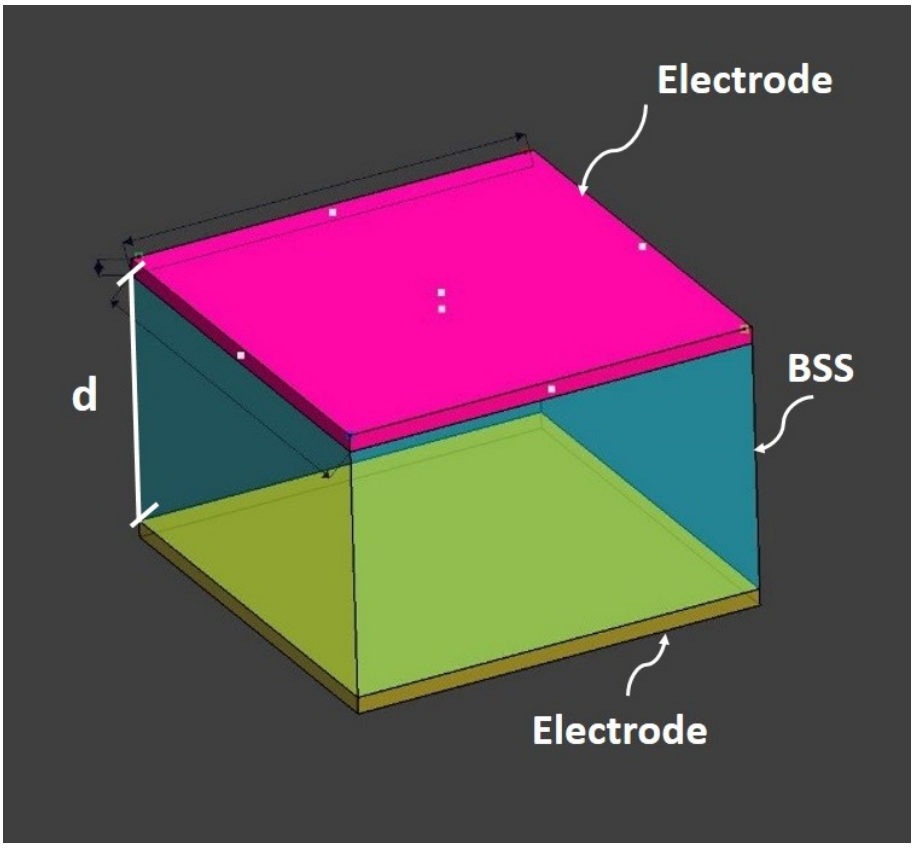

Figure 5.7: This computational domain represents two planar electrodes that generate a uniform E-field in the space between them. For better clarity, the electrodes are shown with exaggerated thickness; the plates are represented in pink and yellow and the dielectric material in turquoise. The distance of separation between the electrodes is d.

In order to select one of the faces, the user needs to use the Select Patch tool. With this tool any face of the computational domain can be selected in order to create a Boundary Condition.

5.2.4 EM properties of materials

Under the simulation tab, in the materials section (Figure 5.1), the EM properties of all the materials in the computational domain can be assigned. The LF FEM solver is a real-valued solver and therefore only one part of the complex permittivity can be input, i.e. either the term σ or $\omega\varepsilon$ can be input into the solver (Section 3.3). The thin layer section is located below the materials section, (Figure 5.1). In this tab, the user can assign to the patches

earlier defined, a thickness and dielectric property (σ or $\omega\varepsilon$). This will create a layer around the patch with the user-defined thickness and dielectric property. The thickness of the thin layer feature can range from nanometers to meters.

5.2.5 Convergence factor

The LF FEM solver computes Eq 20 for the whole geometry. Supposing that $\sigma >> \omega\varepsilon$, Eq 20 is solved at all mesh nodes of the geometry:

$$\nabla \cdot \sigma \nabla V = 0 \tag{20}$$

where σ is the electrical conductivity and V is the electric potential. If $\sigma << \omega\varepsilon$ then the Eq 21 is solved

$$\nabla \cdot \omega\varepsilon \nabla V = 0 \tag{21}$$

Assuming that Eq 20 is used, Eq 20 can be rewritten as a linear system:

$$Ax = b \tag{22}$$

where A represents coefficient matrix which can be obtained from the geometry, the unknown x represents electric potential and b represents the electric charge [31, 38, 39]. The exact solution of x cannot be found and therefore the solver computes an approximate solution (x_{approx}). The solution error can be defined as $\|x_{approx} - x\|$. Since the exact solution of x cannot be computed, the solver goes through an iterative solution process. This process consists of evaluating the residual error that is defined by $\|Ax_{approx} - b\|$ where for convenience b_{approx} is defined as $Ax_{approx} = b_{approx}$ [38, 40]. When performing an iterative analysis of the residual error, the relative residual error can be defined as

$$Relative\ residual\ error\ = \frac{\|b_{approx} - b\|}{\|b\|} \tag{23}$$

Eq 23 computes the difference between b_{approx} and b.

To obtain a homogeneous E-field in the region between the electrodes where the cell is placed, it was found that the relative residual error had to be 10^{10} (Section 5.3.1).

5.3 The thin layer feature

The thin layer algorithm is a novel feature in Sim4life that permits the user to model very thin layers of thickness of the order of nanometers and unlike in SEMCAD this feature can be implemented for both dielectric materials and conductors. The user can enter the EM properties of the material and the thickness of the layer. Again, only one part of the complex permittivity can be input, i.e. either σ or $\omega\varepsilon$. For this project, the thin layer feature was used to model the cell membrane, the nuclear membrane and the membrane of the granules. In Section 5.3.2 the accuracy of modeling a membrane using the thin layer feature will be discussed.

5.3.1 Accuracy of the LF FEM solver in Sim4life

The first step in the computations was to test the accuracy of the LF FEM solver in Sim4life with a geometry based on the thin layer feature (Figure 5.7). In this geometry a thin layer is inserted between two homogeneous materials and a voltage is applied between opposite faces. As shown in Figure 5.8, the computational domain is split into three sections. Two sections of thickness d_{BSS} are composed of BSS with an electrical conductivity of $\sigma = 1$ S/m and the other section is composed of a thin layer of 1 μm thickness and an electrical conductivity of 10^{-1} S/m. The thin layer is indicated by the turquoise region and is located centrally between the two other materials (BSS) indicated in blue (Figure 5.8) with a conductivity of 1 S/m and dimensions 20 x 20 x 9.5 μm.

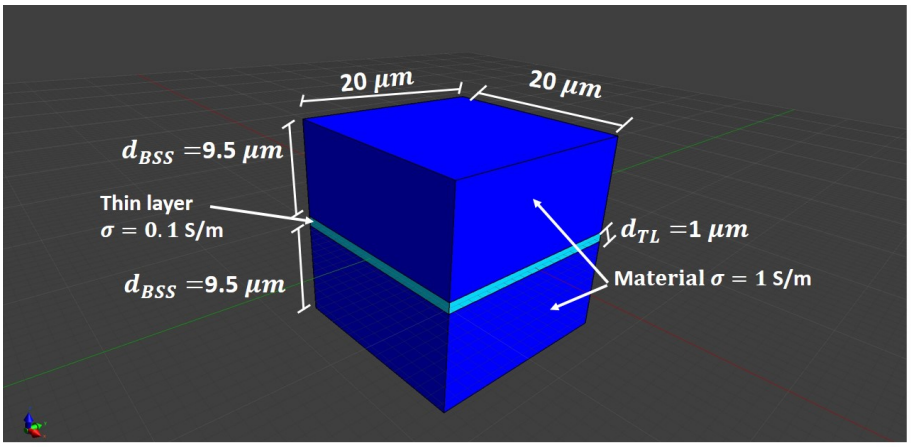

Figure 5.8: Proposed geometry to test the thin layer algorithm. The dimensions for the geometry are shown.

Once the geometry has been generated in Sim4life, the simulation to compute the electric potential and the E-field needs to be configured: first the mesh needs to be generated (Table 5.1) and then the source excitation and the EM properties of the materials need to be input. In an unstructured mesh, the size of the tetrahedra will vary and therefore the target edge length (the desired length of the tetrahedra) and the minimum target edge length (the minimum size of the tetrahedron) must be defined (Section 5.2.2).

Table 5.1: Settings for the tetrahedral mesh in the simulation. The surface mesh refers to the remeshing of the surfaces in the computational domain and 3-D mesher refers to the multidomain mesher (Section 5.2.2).

Surface Mesh		**3-D Mesher**		**Number of mehscells in millions**
Target Edge Length [μm]	Minimum Edge Length [μm]	Target Edge Length [μm]	Minimum Edge Length [μm]	
0.2	0.1	0.2	0.1	1.3

In the test geometry for the thin layer of Sim4life, at the interface between the thin layer and the BSS, the current density is continuous [27] and is given by

$$\sigma_{BSS} E_{tang-BSS} = \sigma_{TL} E_{tang-TL} \tag{24}$$

where $E_{tang-BSS}$ is the magnitude of the E-field in the BSS, $E_{tang-TL}$ is the magnitude of the E-field in the thin layer, σ_{BSS} is the electrical conductivity of the BSS and σ_{TL} is the conductivity of the thin layer. In electrostatics, Eq 24 can be developed into

$$\sigma_{BSS} \frac{\Delta V_{BSS}}{d_{BSS}} = \sigma_{TL} \frac{\Delta V_{TL}}{d_{TL}} \tag{25}$$

where ΔV_{BSS} is the voltage across the BSS, ΔV_{TL} is the voltage across the thin layer, d_{BSS} is the thickness of the BSS and d_{TL} is the thickness of the thin layer. In order to extract the results for the potential distribution from Sim4life, a program called Paraview (Los Alamos National Laboratory) was used. With Paraview, the results from Sim4life can be visualized and multiple post processing tools can be used. In Paraview the potential in the entire computational domain can be processed (Figure 5.9). Furthermore, Paraview can plot the potential distribution within a specific region of the geometry (Figure 5.10).

For this project, the electric potential along the Z-axis of the results in Figure 5.9 is extracted using Paraview. The white dot at the top of the cube in Figure 5.9 indicates the top of the Z-axis. The line goes all the way down to the bottom of the cube parallel to the Z-axis (dashed). The electric potential along the Z-axis is shown in Figure 5.10.

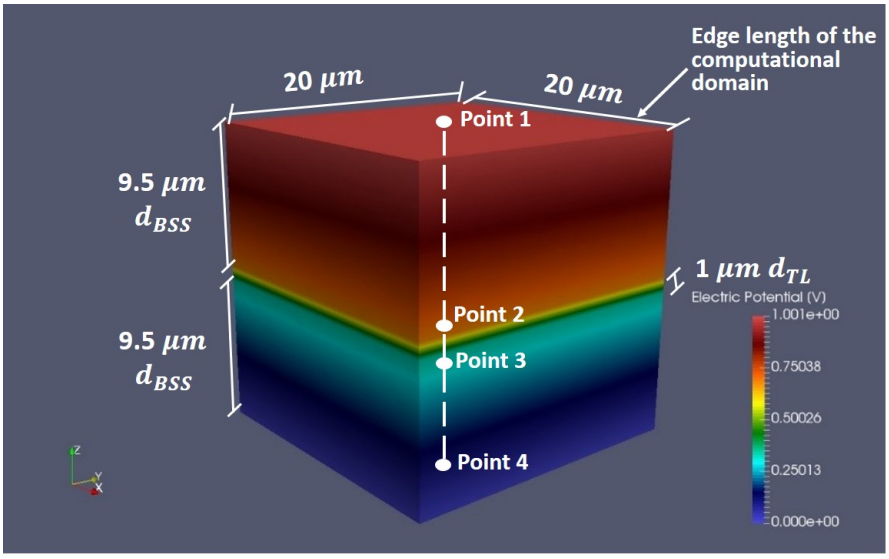

Figure 5.9: Results for the electric potential distribution in the geometry shown in Figure 5.8. The thickness of the thin layer is 1 μm and the thickness of the BSS regions are 9.5 μm. The dashed line indicates the line along which the potential is extracted using Paraview.

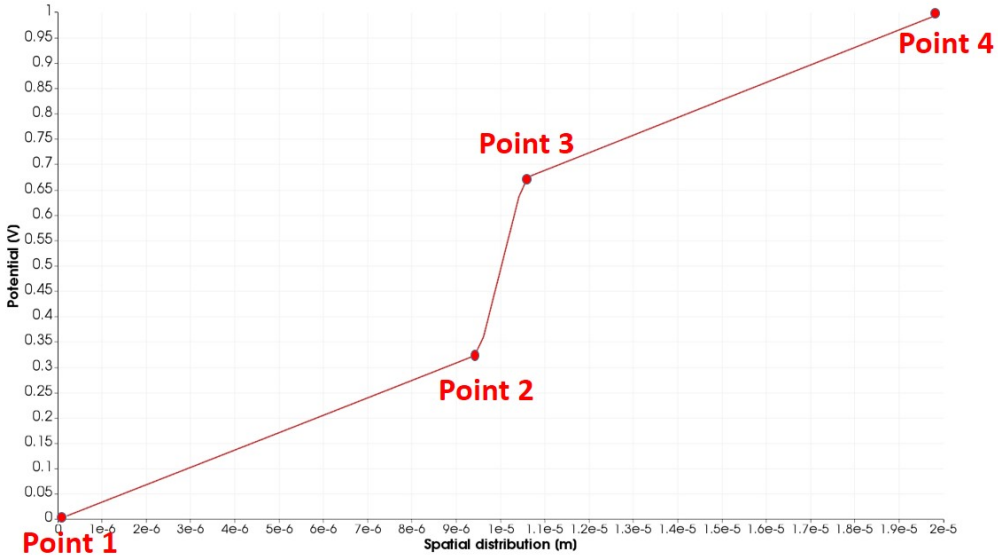

Figure 5.10: Potential along the dashed line centered in the cube as in Figure 5.9.

These results obtained From Sim4life must be verified with Eq 24. From Figure 5.10, the total potential across the cube in Figure 5.8 is 1 V and the potential difference across the thin layer is 0.35 V (Table 5.2).

Table 5.2: Potential at different points in Figure 5.10

Point	**Electric Potential [V]**
1	0
2	0.33
3	0.67
4	1

Now that the potential distribution in the geometry is known, Eq 25 will be solved

$$\sigma_{thinlayer}\frac{\Delta V_{thinlayer}}{d_{thinlayer}} = \sigma_{BSS}\frac{\Delta V_{BSS}}{d_{BSS}} \tag{26}$$

Substituting the values of $\sigma_{thinlayer} = 0.1\ S/m, \Delta V_{thinlayer} = 0.34\ V, d_{thinlayer} = 1\ \mu m$ on the left side of the Eq 26 and $\sigma_{BSS} = 1\ S/m, \Delta V_{BSS} = 0.66\ V, d_{BSS} = 19\ \mu m$ on the right side of the Eq 26, the following results are obtained:

$$0.1S/m\frac{0.34V}{1\mu m} = 1S/m\frac{0.66V}{19\mu m}\ ;\ 3.4\cdot 10^4 A/m^2 = 3.47\cdot 10^4 A/m^2 \tag{27}$$

where both sides of the equation agree to within 0.1%. This proves that the thin layer feature of Sim4life generates accurate results for the potential distribution.

Another result that can be extracted from Sim4life is the E-field. In the geometry in Figure 5.9, a much higher E-field is expected across the membrane than in the BSS (Figure 5.11).

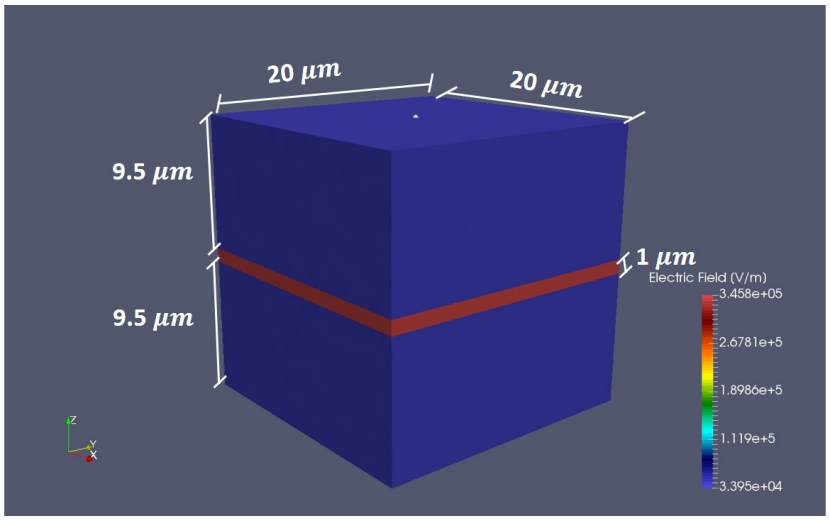

Figure 5.11: Electric field distribution for the geometry in Figure 5.9

In Figure 5.11 it can be seen that the E-field in the thin layer is 10 times higher than the BSS. In conclusion, the thin layer feature of Sim4life can model very thin structures with only a small error introduced.

5.3.2 Equivalent Circuit for the test geometry of the thin layer

The 3-D geometry proposed in Figure 5.9 can be simplified into a 1-D geometry because the current density is being forced through the thin layer. This statement can be supported because the Neumann BC (0 Coulomb i.e. electrically insulating) does not allow any current through the boundaries.

The equivalent circuit for the geometry in Figure 5.9 consists of three resistors in series that represent each material and a voltage source that represents the voltage applied across the planar electrodes (top and bottom faces). For this geometry, the values of the resistors can be calculated with the well known equation given by:

$$R = \frac{1}{\sigma}\frac{L}{A} \tag{28}$$

where σ is the electrical conductivity of the material, L is the thickness in the Z direction of the material and A is the area of the upper face of the computational domain. The area

for all the materials is 400 μm^2. The geometry in Figure 5.9 is represented as a voltage divider circuit (Figure 5.12) and simulated in Multisim (National Instruments, USA). The resultant voltages of the circuit at the same locations as in Figure 5.9 are shown.

Table 5.3: Geometrical parameters for the BSS and thin layer and their equivalent resistance values calculated using Eq 28.

Materials	**L** (μm)	$\sigma(S/m)$	**R** ($k\Omega$)
Thin layer	1	0.1	25
BSS	9.5	1	23.75

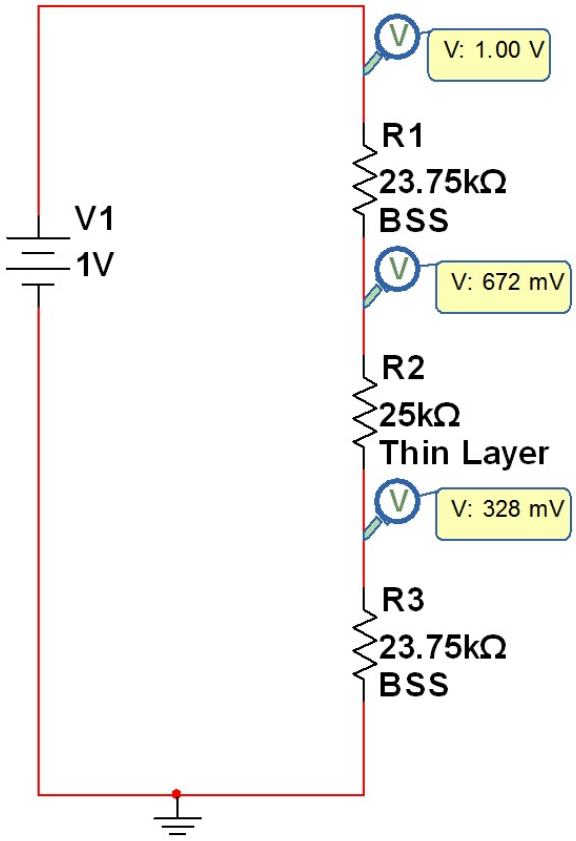

Figure 5.12: Equivalent 1-D circuit for the 3-D geometry (Figure 5.9) simulated using Multisim. The computed voltages are shown for every node.

A comparison of the potentials across the three layers in Figure 5.9 (Table 5.2) and those

computed using the equivalent circuit (Figure 5.12) is shown in Table 5.4.

Table 5.4: Comparison of the potentials obtained from the 1-D equivalent circuit and the 3-D geometry generated in Sim4life 5.9

Point/Material	**1-D Equivalent Circuit**	**3-D Geometry in Sim4life**
1/External Medium (BSS)	0	0
2/Cell Membrane	0.33	0.328
3/Cell Internal Medium	0.67	0.672
4/Cell Internal Medium	1	1

It is seen that the results agree to within 0.6%. In this section it was shown that the computations using the thin layer feature in LF FEM solver of Sim4life computations at DC and create a very small error.

5.4 Discussion of equivalent circuit models for biological cells

To understand the effect of external E-fields on biological cells, many equivalent circuit models have been developed by various researchers [11, 27, 36]. In all these models, an equivalent circuit (similar to the one presented in Figure 5.12) in which the external medium, the cell membrane that is an electrically insulating bilipid layer and the internal medium (cytosol) can be represented by a capacitor and resistor in parallel (Figure 5.13).

In Figure 5.13 an equivalent 1-D circuit for a biological cell consisting of the external medium, the cell membrane and the internal medium is shown. As in most circuits in the literature, in this circuit each material is represented by a resistor and capacitor connected in parallel. The capacitors account for the displacement current and a resistor account for the conduction current. In [11], the computational software (Spice) that was used was capable of processing a time-varying signal (like a pulse) and therefore both currents (conduction and displacement) could be taken into account. The main goal of this model was to determine the TMP across the cell membrane and the electric potential distribution in the cytosol.

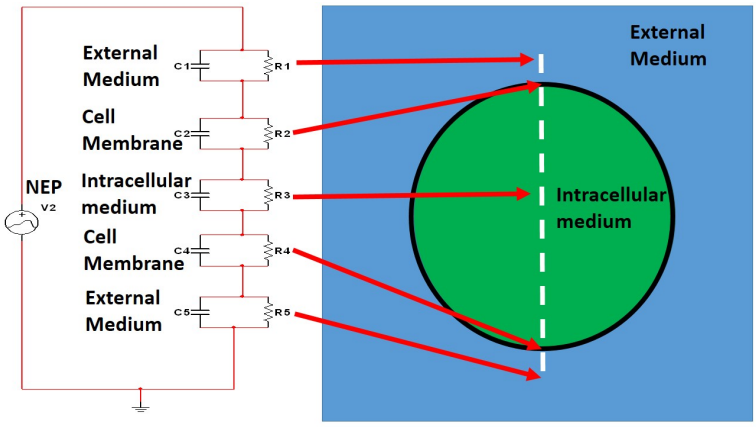

Figure 5.13: Equivalent circuit for a biological cell. The circuit is composed of resistors and capacitors. The resistors account for the conduction current and the capacitors for the displacement current.

The difference between the models in Figure 5.12 and 5.13 is clear; the model in Figure 5.13 can compute displacement currents while the model in Figure 5.12 cannot. The EM LF Stationary Current Solver computes quasi-static fields, i.e. it can only process DC voltages and low frequencies. When applying a pure DC voltage to the circuit in Figure 5.13, there will be no current going through the capacitors due to the high impedance. In other words, the capacitors behave as open circuits. Therefore, for applied DC voltages, all current will be flowing through the resistors and as a consequence the circuit in Figure 5.13 can be reduced to a purely resistive circuit (such as the circuit in Figure 5.12) since all the capacitors will be acting as open circuits. Due to this limitation, the Stationary Currents solver of Sim4life is only valid for models of a biological cell at DC and low frequencies. In the following chapter, the accuracy of the solver will be tested at different frequencies.

CHAPTER 6

Validation of Sim4life for simple biological cell models

6.1 Introduction

In the previous chapter it was shown that the thin layer feature of Sim4life is an excellent tool for meshing a biological membrane with a thickness of the order of nanometers. A cell model with a cell membrane and nuclear membrane based on the thin layer feature was developed in Sim4life and in this section the validation process for this model in Sim4life will be described. The validation will be based on the comparison of the TMP results obtained in Sim4life with two well accepted cell models: Schwan's equation [14] and Kotnik and Miklavcic [26]. Schwan [14] an equivalent circuit of a biological cell is described and the TMP for the cell membrane is computed. In Kotnik and Miklavcic [26], from Laplace's equation, an analytical expression for the TMP of a biological cell with nucleus has been developed.

For the validation process, two cell models were created in Sim4life: 1. A spherical cell with a cell membrane and 2. A cell with a cell membrane that includes an organelle with a membrane. The validation was performed in the following order: 1. The spatial distribution of the cell membrane TMP was computed with Schwan's equation [14] and compared to results from Sim4life and 2. An analysis of the membrane TMP in the frequency domain will be performed with Schwan's model [14] as well as the model presented by Kotnik and Miklavcic in [26] and compared with the results in Sim4life. For the frequency study, the TMP of the membranes will be compared at the pole where the TMP is maximum [14]. In both models, the excitation source is a sinusoid. In Sim4life, frequency is not an input; however, the EM properties of the materials that are input into the software simulate different frequencies (Section 6.5). In addition, in this section the impact of the computational domain

size on the cell and nuclear membrane TMP obtained in Sim4life will be discussed. At the end of this chapter, the limitations of the LF FEM electro quasi-static solver of Sim4life will be discussed.

6.2 Discussion of the geometry, mesh and homogeneity of the E-field

The exposure system used in our laboratory [8,9] creates a homogenous E-field at the location of the chromaffin cell has been shown using FDTD simulations (Section 4) [5]. In order to generate a homogeneous E-field in Sim4life, it was decided that the most suitable geometry for the computational domain would be a cube (Section 5.2) [36]. The computational domain is a cube that will represent the 100 μm gap between the rod electrodes. The cube is filled with BSS and the chromaffin cell (represented by a sphere) is centrally placed within the cube (Figure 6.1). The geometry in Figure 6.1 simulates the homogeneous 5 MV/m E-field to which the chromaffin cell is exposed by the rod electrodes in the experimental set up in our laboratory [8, 9]. The optimal dimensions of the cube will be discussed in Section 6.5. The geometry in Figure 6.1 was created in Sim4life and the mesh settings are tabulated in Table 6.1

Table 6.1: Mesh settings for the simulation with a chromaffin cell within a cube (as the computational domain) with dimensions 100 x 100 x 100 μm

Surface Mesh		**3-D Mesher**		**Number of mehscells in millions**
Target Edge Length [μm]	Minimum Edge Length [μm]	Target Edge Length [μm]	Minimum Edge Length [μm]	
0.2	0.1	0.2	0.1	1.3

In order to generate a homogeneous E-field, the upper face of the cube normal to the Z direction is set to the Dirichlet BC with a fixed voltage value. The voltage will depend on the desired E-field can be calculated from Eq 19. On the opposite face of the excitation

source, there will be another Dirichlet BC set to 0 V (i.e. this face will act as the ground). The remaining faces are set to Neumann BCs with zero charge (electrically insulating i.e. no current goes through the boundaries).

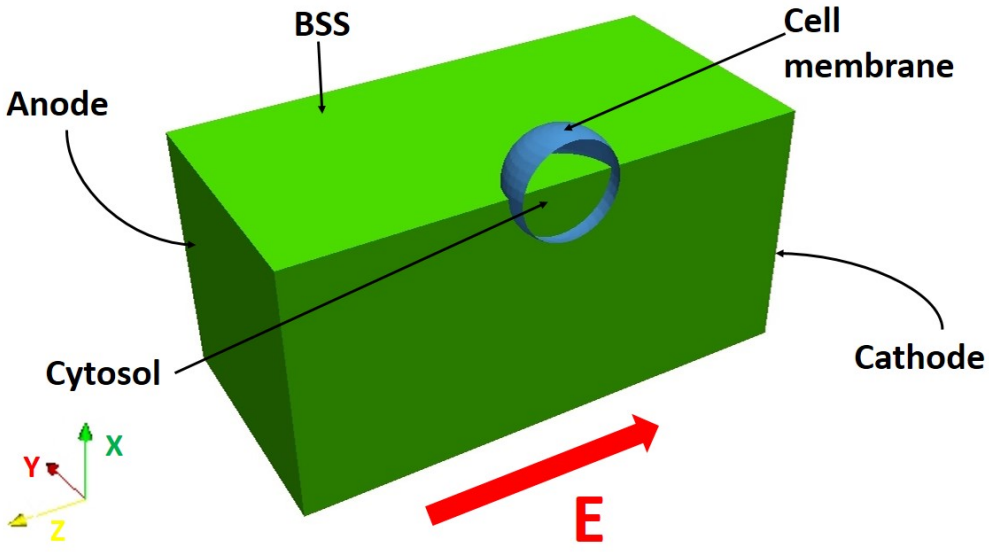

Figure 6.1: Representation of the planar electrodes (in order to generate a homogeneous field) and the direction of the E-field. The dimensions of the cube and the applied voltage must satisfy Eq 19 in order to obtain a 5 MV/m E-field.

To generate a 5 MV/m E-field the voltage at the upper face is set to 500 V. In the middle of the cube, a 8 μm radius sphere represents a chromaffin cell which is surrounded by a membrane of thickness 5 nm. In this simulation, the dielectric properties for a chromaffin cell are used (Table 6.2).

Table 6.2: EM properties for the simulation [34]

Material	**Conductivity [S/m]**	**Relative Permittivity**
BSS	1.3	80
Cytosol	0.5	80
Cell Membrane	$8.3 \cdot 10^{-10}$	5.5

6.3 Validation of the spatial distribution of the TMP of the cell membrane obtained from Sim4life with results from Schwan's Equation at DC

Schwan's equation will be used to evaluate the TMP at different locations of the membrane. Schwan's equation calculates the TMP for a cell with a radius R exposed to an external E-field.

$$\Delta\Phi = \frac{3}{2}\, E\ R\ cos(\theta) \tag{29}$$

where theta (θ) represents the angle measured from the center of the cell with respect to the direction of the E-field (Figure 6.2). In order to solve and plot the TMP a script in Matlab was written.

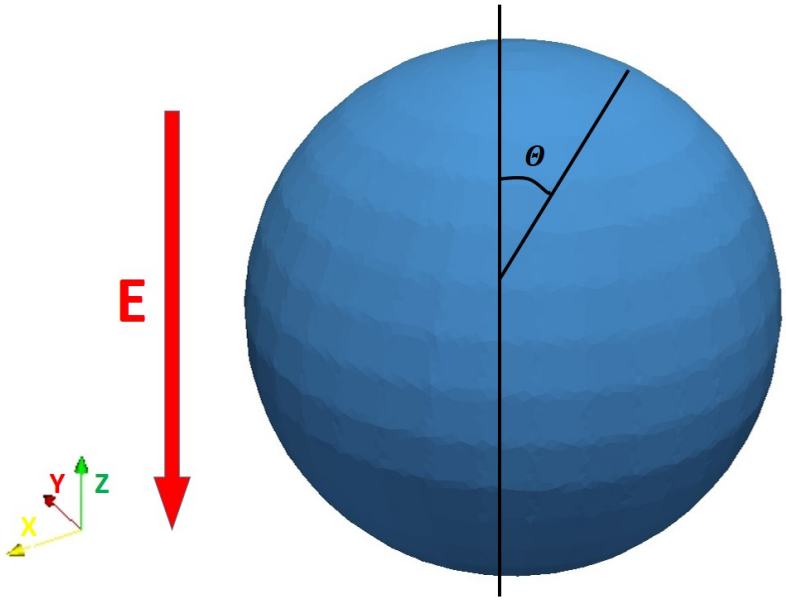

Figure 6.2: The cell is placed suspended within the BSS and placed centrally. The direction of the E-field is parallel to the Z direction. Theta (θ) is the angle measured from the center of the cell with respect to the direction of the E-field.

To compare the TMP results obtained using Schwan's equation (Eq 29) and Sim4life, the computational domain size for the simulations in Sim4life was set to 100 μm. As stated

in Section 5.2, a cube with the same edge length as the computational domain was chosen because it generates a homogeneous E-field. The distance between the planar electrodes was set to 100 μm because in the experimental setup of our laboratory [5,8,9] the space between the rod electrodes is 100 μm. In Figure 6.3, the results from Sim4life for the distribution of the TMP in the XZ plane and Schwan's equation 29 are shown. Figure 6.4 the TMP of the cell membrane is plotted vs theta (Figure 6.2).

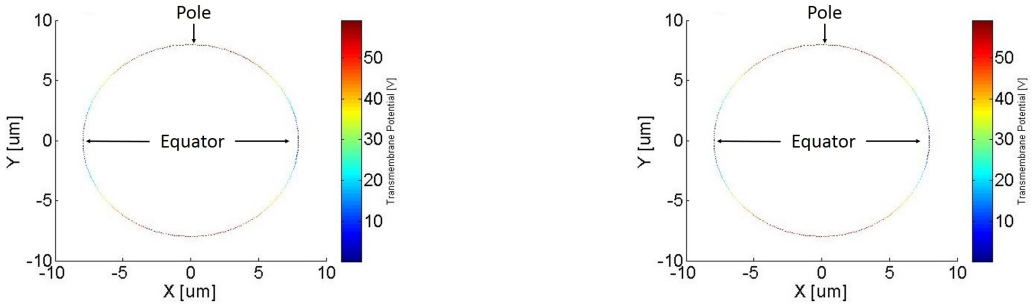

(a) Results for the spatial distribution of the TMP from Sim4life

(b) Results for the spatial distribution of the TMP from Schwna's Equation

Figure 6.3: Comparison of the spatial distribution of the TMP obtained using Sim4life (left figure) and Schwan's equation (right figure). The values for the TMP were compared and to within less than 1%

The poles are located at 0 and 180 degrees (where the TMP is maximum) and the equator at 90 degrees (where the TMP is minimum); from Eq 29 at the poles (0 and 180 degrees) the absolute value of the cosine function is maximum. At the equator (90 degrees), the value of the cosine function is 0. As can be seen the results shown in Figure 6.3 results are symmetric with respect to the Y axis. For quantitative comparison, from Figure 6.4 it is clear that the error is below 1%.

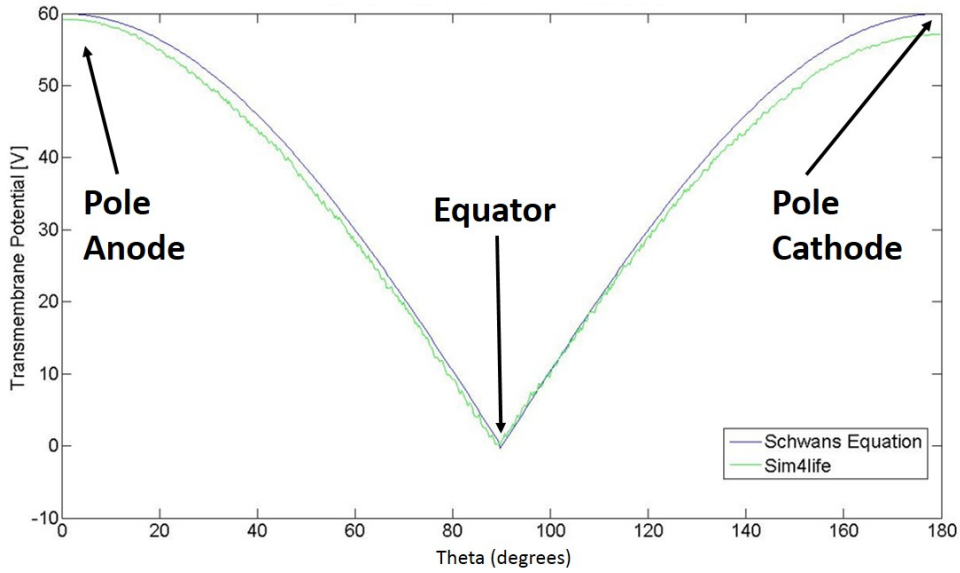

Figure 6.4: TMP vs θ; only half of the cell is represented. The equator is located at 90 degrees and the TMP is minimum. The poles are located at 0 and 180 degrees and the TMP is maximum.

The results of the spatial distribution of the cell membrane TMP agree to within 1% with the results from Schwan's equation (Eq 29). The results obtained from Sim4life are therefore satisfactory and the validation will be continued. In the next section, a nucleus will be introduced into the model in Sim4life to check whether an internal organelle can influence the TMP of the cell membrane. The results are compared to those in Kotnik and Miklavcic [26].

6.4 Effect of the nucleus on the cell membrane

In this section, the effects produced by a nucleus (placed of the center of the cell) on the TMP of the cell membrane will be evaluated. The TMP of the cell membrane will be compared with Schwan's equation [14] as well as that obtained from the model developed by Kotnik and Miklavcic [26]. Schwan's model [14] can only compute the TMP on the cell membrane. The model described by Kotnik and Miklavcic [26] includes a nucleus placed concentric all in the cell in which both the nucleus and the cell have a membrane. Two cell geometries

are generated in Sim4life: one with a nucleus and another without a nucleus. As stated in Section 6.2 the size of the computational domain for the Sim4life simulations is a cube with an edge length of 100 μm. In all models, the EM properties for a chromaffin cell are used [10, 34]. The values for the conductivity used in the simulation are shown in Table 6.2. In the simulations performed in Sim4life with a computational domain 100 μm in dimensions, the applied voltage is set to 500 V in order to generate a homogeneous E-field of 5 MV/m. The results for the cell membrane TMP are shown in Table 6.3

Table 6.3: Results for the TMP obtained using Sim4life (without and with the model), Schwan's model [14] and the Kotnik and Miklavcic [26] model.

	TMP at the pole of the cell membrane (V)	
	Model Without Nucleus	**Model With Nucleus**
Sim4life	59.95	59.95
Schwan	60	N/A
Kotnik and Miklavcic	N/A	60

From Table 6.3, it can be seen that the presence of the nucleus does not affect the TMP of the cell membrane. Also the cell membrane TMP obtained from the models is to within 0.1%. Therefore, from these results it can be concluded that a concentric nucleus does not affect the TMP of the cell membrane. So far, all the TMP computations were performed at DC. In the next section, the TMP of both the cell membrane and the nuclear membrane will be evaluated in the frequency domain. In addition, the size of the computational domain required to lower the required computational resources will be discussed.

6.5 Minimization of the computational domain without altering the accuracy of the TMP in the frequency domain

In this section the TMP of the cell membrane and the nuclear membrane obtained from Sim4life will be compared with the results obtained from the cell model developed by Kotnik

and Miklavcic [26]. In addition, the cell membrane TMP will be compared with that obtained from the cell model developed by Schwan et al. [14]. Furthermore, multiple geometries with different computational domain sizes will be generated in Sim4life to study the effects of the computational domain size on both the nuclear and cell membrane TMP.

The gap between the rod electrodes in the experimental setup used in our laboratory [5, 8, 9] is 100 μm and this has been the computational domain dimensions for the previous simulations in Sim4life. A simulation with a computational domain of 100 μm edge length requires a larger amount of computer resources (such as RAM) than a simulation with a smaller computational domain. However, a small computational domain could lead to inaccurate TMP results due to inhomogenities in the E-field. Therefore, results using multiple computational domain sizes will be compared in order to determine the smallest computational domain size that will compute TMPs of the nucleus and cell membrane to a high degree of accuracy (Figure 6.5).

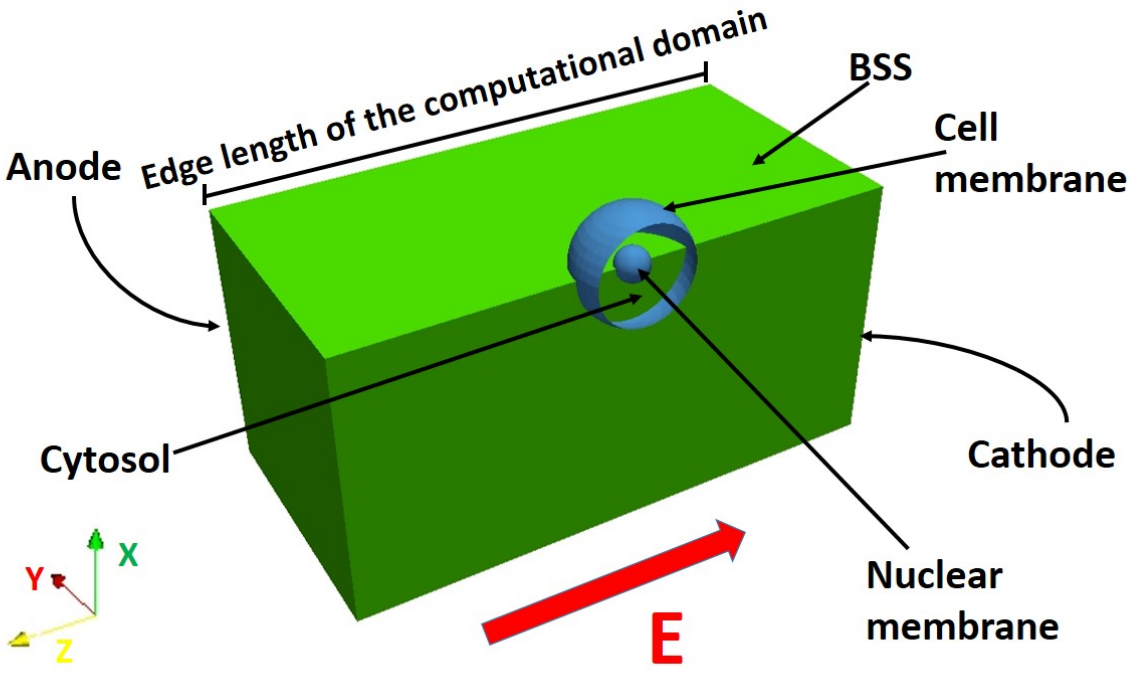

Figure 6.5: View of the overall geometries of the cell, nucleus, BSS and planar electrodes in the Sim4life simulations. The computational domain is filled with BSS, the surface of the outer sphere represents the cell membrane (8 μm radius) and surface of the inner sphere represents the nuclear membrane (2.5 μm radius)which is concentric to the cell. Four simulations with different edge lengths for the computational domain were created in Sim4life. The size of the computational domain for each simulation is tabulated in Table 6.5. It should be noted that the axis have been rotated.

The influence of the computational domain size in the TMP study will be studied in the frequency domain. In the cell model developed by Kotnik and Miklavcic [26], an analytical solution for the TMP at the poles of the nucleus and at the poles of the cell membrane is described. The results obtained from the model of Kotnik and Miklavcic [26] will be compared with the four simulations in Sim4life at the pole of the nuclear and cell membrane (Figure 6.6).

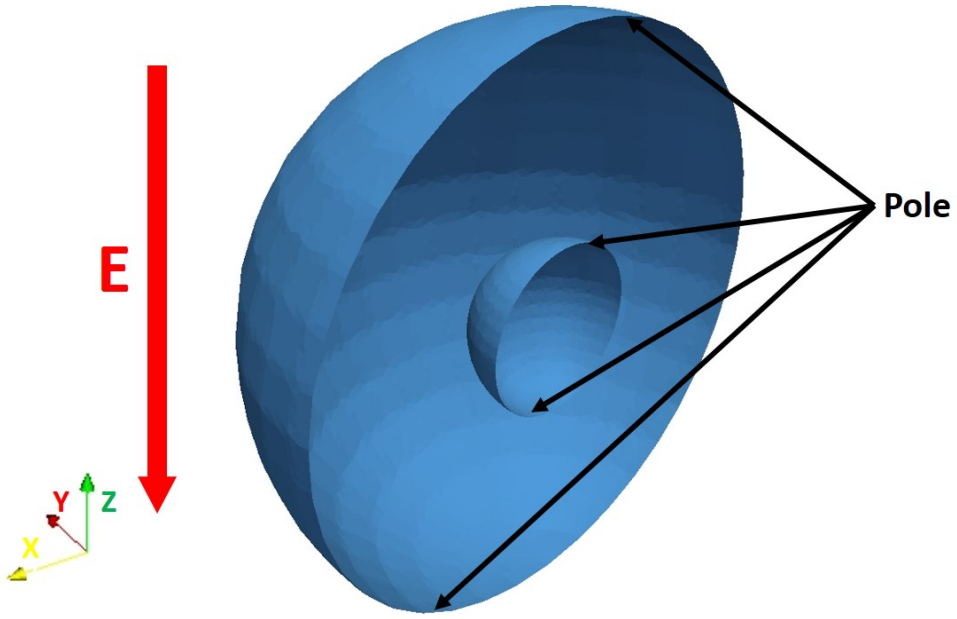

Figure 6.6: View of the inside of the cell. At the center of the cell a nucleus has been placed concentrically . The radius of the cell is 10 μm and the radius of the nucleus is 3 μm. The E-field is parallel to the Z axis.

For this study, the dielectric properties and the cell dimensions specified in the model of Kotnik and Miklavcic [26] are used. The dielectric properties of the cell and nucleus are tabulated in Table 6.4.

Table 6.4: EM properties used for the validation process. These are the default values for the EM properties used in the model developed by Kotnik and Miklavcic [26]

Material	**Epsilon [F/m]**	**Conductivity [S/m]**
External Medium	$6.4 \cdot 10^{-10}$	1.2
Cellular Internal Medium	$6.4 \cdot 10^{-10}$	0.3
Nuclear Internal Medium	$6.4 \cdot 10^{-10}$	0.3
Cell Membrane	$4.4 \cdot 10^{-11}$	$3 \cdot 10^{-7}$
Nuclear Membrane	$4.4 \cdot 10^{-11}$	$3 \cdot 10^{-7}$

The radius of the cell is 10 μm and the radius of the nucleus is 3 μm. The thickness of the nuclear and cell membranes is 5 nm. The applied E-field is 50 KV/m.

In the LF FEM solver in Sim4life, the frequency is not an input. In order to carry out an analysis in the frequency domain in Sim4life, the dominant part of the complex permittivity (Eq 8) must be selected as an input. From DC to 50 Hz the electrical conductivity term (σ) prevails and therefore the (σ) term will be assigned to the dielectric properties of the membranes. Above 50 Hz the term $\varepsilon\omega$ prevails and therefore the ($\varepsilon\omega$) term will be assigned to the dielectric property of the membranes.

The nucleus is spherically concentric to the sphere representing the cell, i.e. the nucleus is placed at the center of the cell (Figures 6.6 and 6.5).

In order to determine the smallest computational domain size without altering the accuracy of the TMP results, the TMP for the cell and nuclear membranes in four simulations with different computational domain sizes were compared. For each simulation, the computational domain is a cube with different edge lengths (Table 6.5). The geometry was generated in Sim4life and the settings for the mesh were different for each computational domain (Table 6.5).

Computational domain dimension (μm)	**Surface Mesh**		**3-D Mesher**		**Number of meshcells in millions**
	Target Edge Length [μm]	Minimum Edge Length [μm]	Target Edge Length μm	Minimum Edge Length [μm]	
30	0.2	0.1	0.2	0.1	0.2
40	0.5	0.1	0.5	0.1	1.2
50	0.5	0.1	0.5	0.1	2.6
100	2	0.1	2	0.1	13

Table 6.5: Mesh settings used for different computational domain sizes

In Figure 6.7, the cell membrane TMPs as a function of frequency at the pole for four different computational domain sizes created in Sim4life are compared with the TMP from the model of Schwan's equation [14] and the model of Kotnik and Miklavcic [26].

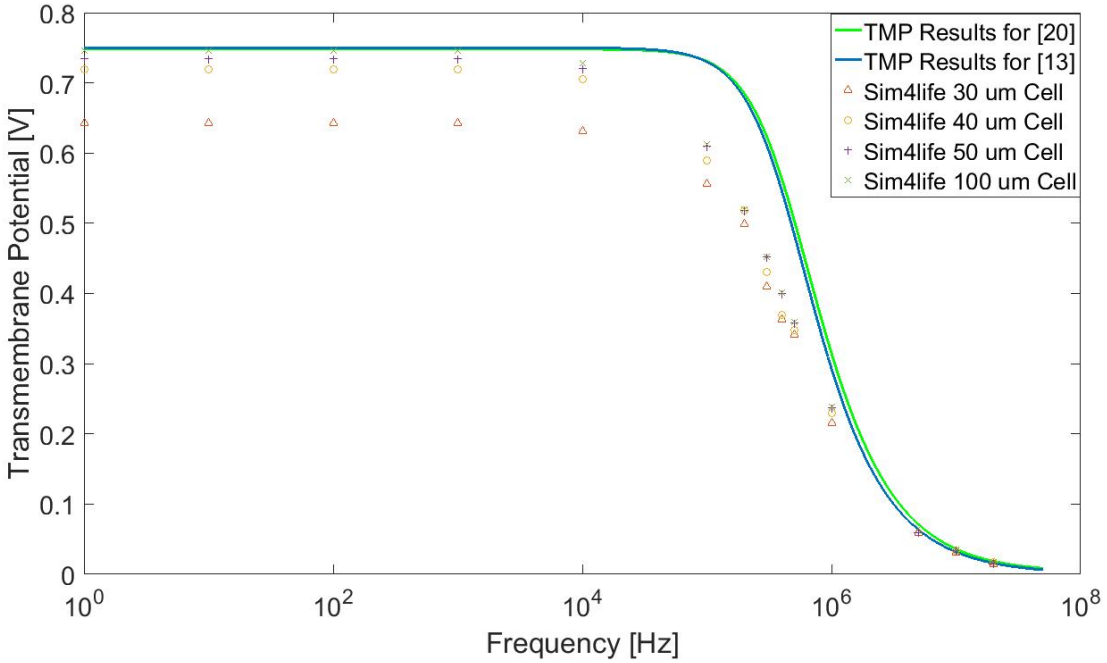

Figure 6.7: The cell membrane TMP located at the pole for the models in Sim4life, the model of Schwan [14] and the model of Kotnik and Miklavcic [26] at different frequencies are compared. The model of Schwan and Kotnik and Miklavcic agree to within 0.1%. The TMP results extracted from Sim4life agree well with Schwan and Kotnik and Miklavcic model at low frequencies (DC-500 kHz) and high frequencies (5 MHz and above). From 500 kHz to 5 MHz the Sim4life results differ from Schwan and Kotnik by 20% to 30%.

The model developed by Schwan et al. [14] and the model of Kotnik and Miklavcic [26] agree to within 0.1% (Figure 6.7). The TMP results for the different computational domain sizes (box sizes) are different. This difference in the TMP can be explained due to the varying levels of inhomogeneity in the E-field in the four cases. In order to quantify the percentage error Eq 30 was used.

$$percent\ error\ = \frac{|Sim4life_{model} - theoretical|}{|theoretical|} \tag{30}$$

where "theoretical" is the TMP result from the model of Kotnik and Miklavcic [26]. The

TMP results in the frequency range DC to and 5 MHz to 30 MHz for the 50 μm and the 100 μm computational domain sizes are similar to within 1% while the results of the other computational domain sizes (30 and 40 μm) in Sim4life simulations differ by 30% from the theoretical result. It must be pointed out that even for the 50 μm and 100 μm computational domain sizes that in the frequency range from 500 kHz to 5 MHz the TMP obtained from the Sim4life simulations has a maximum of 30% when compared to the TMP obtained from Schwan's model [14] and the model of Kotnik and Miklavcic [26].

The main reason for disagreement between the model in Sim4life (with 50 μm and 100 μm computational domain sizes) and the model developed by Kotnik and Miklavcic [26], is that the LF Stationary Currents solver of Sim4Life cannot process complex numbers and hence both the real and imaginary parts of the complex permittivity.

The next step in the validation process is to compare the TMP of the nucleus obtained from Sim4life with that obtained from the model developed by Kotnik and Miklavcic [26]. In Figure 6.8, the TMP at the pole of the nucleus vs frequency is displayed for the different geometries simulated in Sim4life (different computational domain sizes) as well as the TMP for the model developed by Kotnik and Miklavcic [26].

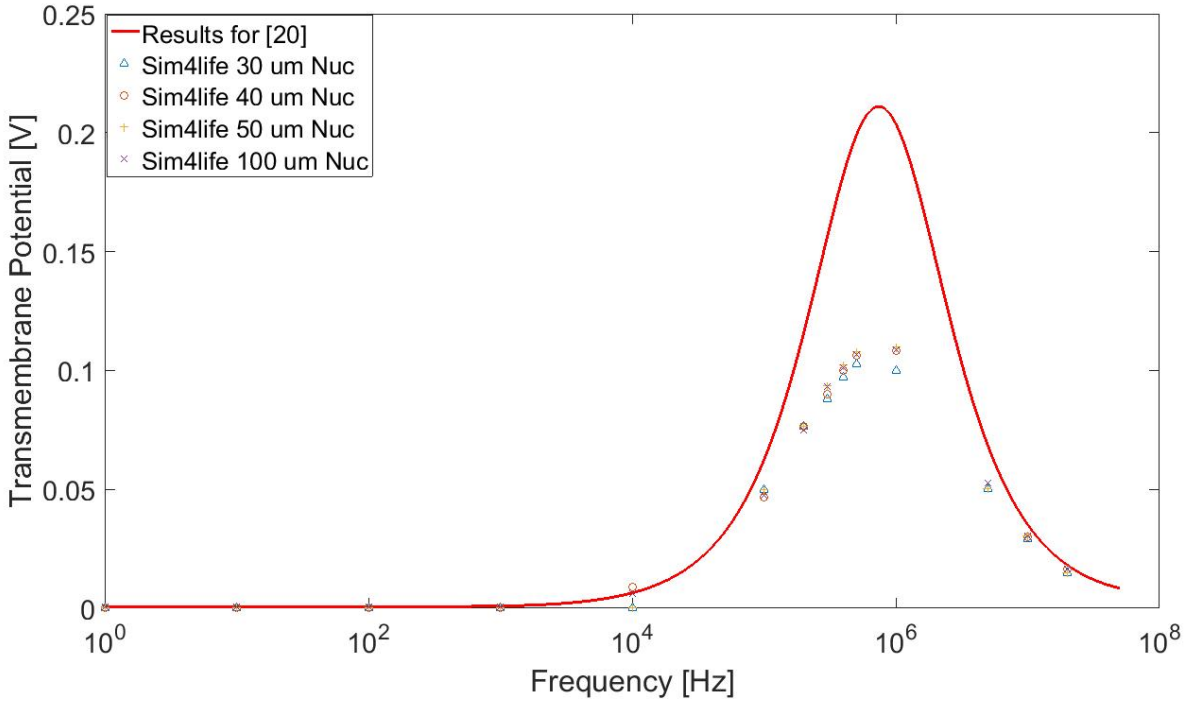

Figure 6.8: Evaluation of the TMP for the nuclear membrane for different computational domain sizes at different frequencies. As can be seen from 300 kHz to 8 MHz the error compared to the results from Kotnik and Miklavcic [26] ranges from 20% to 30%.

The computation of the TMP of the nucleus seems to be more sensitive LF solver is not capable of incorporating complex magnitudes. The maximum disagreement at 1 MHz is 37% percentage error (Calculated from Eq 30).

The frequency response of the nuclear TMP is different from the frequency response of the cell TMP. The TMP of the cell membrane remains constant up to 300 kHz where it starts decreasing and at 10 MHz has a value of 0.02 V. The TMP of the nucleus has a peak value at 760 kHz and then starts decreasing with an increase in frequency.

In Tables 6.6 and 6.7 the percentage error at various frequencies in the range displayed in Figures 6.7 and 6.8 are summarized the percentage difference for a 50 μm computational domain simulation.

Table 6.6: Percentage error between the model developed in Sim4life with a 50 μm computational domain size and the model developed by Kotnik and Miklavcic [26].

Frequency [kHz]	0	1	10	50	100	200	500
Percentage error TMP cell membrane	4.42	4.43	5.39	8.98	12.88	18.92	26.52
Percentage error TMP nuclear membrane	1.5	7.76	4.02	1.13	6.8	23.22	30.13

Table 6.7: Percentage error between the model developed in Sim4life with a 50 μm computational domain size and the model developed by Kotnik and Miklavcic [26].

Frequency [MHz]	1	2	4	5	10	16	32
Percentage error TMP cell membrane	28.07	21.20	11.57	8.98	2.25	0.3	0.2
Percentage error TMP nuclear membrane	37.97	37.08	34.93	34.59	22.00	13.92	9.16

Since the cell and nuclear TMPs for the simulations with computational domains of 100 μm and 50 μm size are similar to within 1%, the simulation with a computational domain of 50 μm size will be used for the rest of this project (Section 8) in order to optimize the computational resources.

From this chapter it can be concluded that in the Stationary Currents solver of Sim4life the effects of frequencies relevant to the NEPs used in our laboratory in experiments from DC to 500 kHz and from 8 MHz and above can be modeled accurately. In the intermediate frequency range of [500 kHz - 8 MHz] the TMP obtained from Sim4life differs from the model of Kotnik and Miklavcic [26] with an error of up to 45%. This disagreement is probably caused by the limitation of the LF FEM solver of Sim4life in processing the real and the imaginary parts of the complex permittivity simultaneously.

CHAPTER 7

A realistic model of a chromaffin cell

7.1 Introduction

In our laboratory, chromaffin cells are exposed to NEPs to evoke responses, such as increase of intracellular calcium and the release of catecholamines [8,9]. In chromaffin cells, catecholamines are stored inside secretory granules that are distributed randomly within the cytosol. When chromaffin cells are exposed to NEPs, a TMP is generated across the cell membranes and membranes of intracellular organelles like the nucleus and secretory organelles. However, experimentally it is not possible to make TMP measurements of the nucleus or secretory granules due to their extremely small size. Therefore, a realistic model of a chromaffin cell is required to gain a better understanding of how NEPs affect the intracellular organelles in terms of E-field and TMP distribution. For this project, the two main organelles of interest are the nucleus and the secretory granules.

Sim4life has the unique ability to compute the TMP and E-field distribution in thousands of membranes such as the cell membrane and the membranes of intracellular organelles. In this chapter three cell models for a chromaffin cell developed in Sim4life will be presented. Furthermore, the mesh settings and the mesh quality will be also discussed. This chapter will be divided into four sections: 1. The optimal computational domain size, 2. The structure of a chromaffin cell, 3. The three models generated in Sim4life for a chromaffin cell and 4. The mesh quality of the models.

7.2 Computational domain

As was shown in Section 6.5 a cubical computational domain generates an uniform E-field. As was discussed in Section 6.5, a 50 μm computational domain size is used in order to

minimize computational resources and obtain reliable results for the TMP. In order to create an uniform E-field of 5 MV/m parallel to the Z-axis, a voltage of 250 V is applied (Eq 19) to the upper face normal to the Z-axis and the opposite face of the cube is set to 0 V.

7.3 Structure of a chromaffin cell

Platnner et al. [20] describe the histology of a bovine chromaffin cell. The nucleus is the largest organelle and the secretory granules represent the largest group of organelles occupying approximately 30% of the intracellular volume. Chromaffin cells typically have approximately 10,000 granules with radii that can be quantified by a normal distribution N(180,60), where the average radius is 180 nm, and the variance is 60 nm (Figure **??**) [20]. The radii of the granules ranges from 50 nm to 300 nm. In Sim4life two different geometries with granule radius of 200 nm and 300 nm respectively have been generated. Smaller granules were not modeled due to the limitations of the mesher.

The granules are randomly distributed and the nucleus is typically located off-center within the cytosol [20]. The geometries created in Sim4life include 1000 granules randomly distributed. The cell, the nucleus and the granules are modeled as perfect spheres.

Both the cell and the granules have a single membrane (5 nm in thickness) while the nucleus has a double membrane consisting of two membranes each of thickness 5 nm. Due to the limitations of the mesher in stacking two membranes on top of each other, the nuclear membrane will be modeled as a single 10 nm thickness membrane. In Sim4life, the dielectric properties and the thickness of all membranes can be assigned with the thin layer feature (Section 5.3).

Other organelles such as mitochrondria and the endoplasmic reticulum were not modeled due to limitations of the mesher in generating small meshcells.

7.4 Generated geometries and mesh settings

In this section the geometries and their mesh settings will be discussed. In all simulations, the dimensions of the cell and the organelles will be the same as in a chromaffin cell [10, 20]. BSS surrounds a sphere of 8 μm radius that represents a chromaffin cell. In all simulations the radius of the nucleus is set to 2.5 μm and its location is (-2,2,-2) μm off-center (Figure 7.1). In the cytosol, 1000 granules are randomly distributed and depending on the geometry, a 200 nm or a 300 nm radius will be assigned. Multiple attempts were made to reduce the size of the granules to 180 nm but the mesher was not capable of handling such small dimension granule. In most of the geometries 200 nm is used for the radius of the granules because this was the smallest granule size that the mesher was capable of generating.

One restriction in the geometric generation of granules is that the granules must be separated by a minimum distance of 100 nm. Likewise, the nucleus and cell membrane must be separated by a minimum distance of 100 nm. The main reason for a minimum space between the various structures is the limitations of the mesher in creating small meshcells.

After this section, a mesh quality study will be performed in order to ensure the reliability of the results for electric potential and E-field obtained in Sim4life.

A Python script was written in order to create the chromaffin cell models. In this script multiple parameters can be adjusted: 1. Number of granules, 2. Minimum distance between structures 3. Radius of the cell, granules and nucleus, 4. The random parameters to determine the location of the granules, 5. Location of the granules and 6. Increased conductivity of the membranes upon pore formation. In Section 7.4.1 through Section 7.4.3, the geometries for a chromaffin cell generated with the Pyhton script will be discussed.

7.4.1 Geometry genrated to study the effect of pores and electrode position on TMP

In Figure 7.1 the geometry generated for the study of the effects of pores and electrode position is shown. In this geometry 1000 granules (radius = 200 nm) are randomly distributed within the cytosol and the nucleus is off-center.

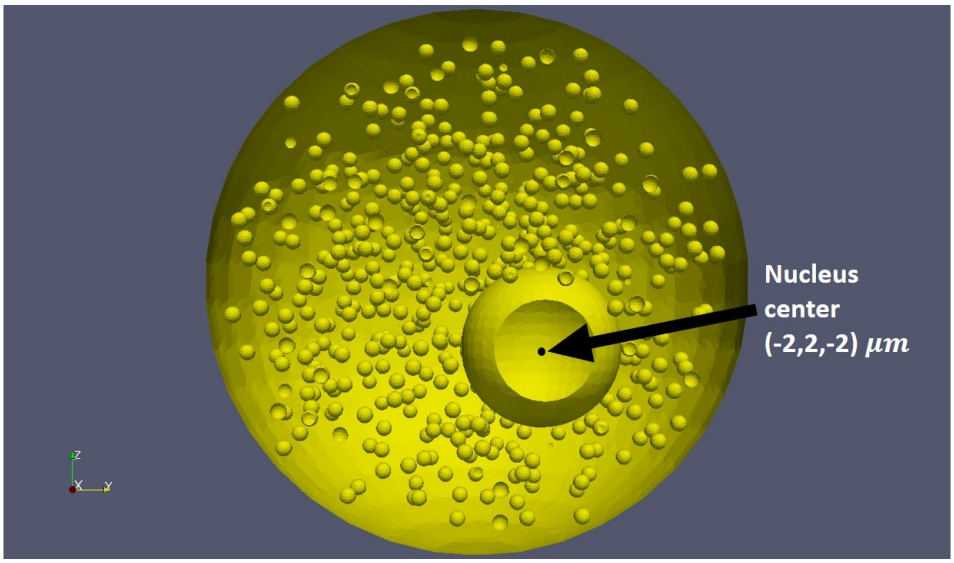

Figure 7.1: Schematic of a chromaffin cell with 1000 granules (radius = 200 nm) randomly distributed within the cytosol. The nucleus (radius = 2.5 μm) is placed off-center (-2,2,-2) μm.

In Table 9, the mesh settings for the surfaces in the computational domain (granules, nucleus and cell) are shown. The LF FEM solver of Sim4life is based on an unstructured mesh. The unstructured mesh discretizes the geometry into triangles for surfaces and tetrahedra for volumes. The user can specify the range for the size of the triangles and the tetrahedra by defining the target edge length and minimum edge length parameters. These parameters determine the desired length and the minimum length of the side of the triangles and tetrahedra (Section 5.2).

Table 7.1: Surface mesh settings used for the simulations in Chapter 9

Structure	**Surface Mesh**		**Number of triangles (per surface)**
	Target Edge Length [μm]	**Minimum Edge Length** [μm]	
Cell Membrane	0.4	0.2	12238
Nuclear Membrane	0.2	0.1	4985
Granule Membrane	0.1	0.05	170

After re-meshing all the surfaces in the computational domain, the complete 3-D geometry must be generated. The mesher in Sim4life uses tetrahedra for generating the 3-D mesh and in Table 7.2 the 3-D mesh settings are shown.

Table 7.2: 3-D Mesh settings for the simulations

3-D Mesher	
Target Edge Length [μm]	**Minimum Edge Length** [μm]
0.5	0.1

7.4.2 Geometry generated to study the effects of the nucleus on the surrounding granules

In this section, a cell geometry (Figure 7.2) to study the effect of the nucleus on the surrounding granules will be discussed. The nucleus ($2.5\mu m$ in radius) is the largest organelle inside the cell , and it may affect the TMP of the surrounding granules (200 nm in radius). To study these effects, 500 granules are placed within a region of 4.5 μm radius from the center of the nucleus (Figure 7.2). Furthermore, 500 additional granules are randomly distributed

within the rest of the cytosol to compare their TMPs to the TMPs of the granules within the region of radius 4.5 μm from the center of the nucleus.

In Figure 7.2 the geometry generated for the study of the nucleus effect is shown.

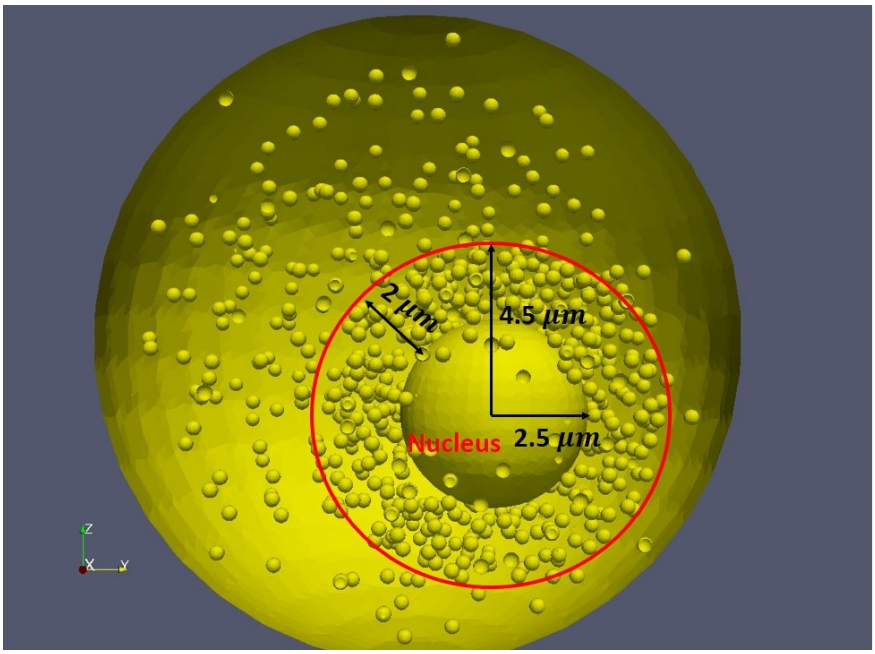

Figure 7.2: Schematic of the chromaffin cell model created using the Python script showing a higher concentration of granules (500 granules) around the nucleus within a region of radius 4.5 μm from the center of the nucleus. The radius of the nucleus is 2.5 μm and the radius of the granules is 200 nm and there are 500 granules randomly distributed within the rest of the cytosol (for a total of 1000 granules).

The mesh settings for this geometry are the same as the ones used in Section 7.4.1. In Table 7.1 the mesh settings for the surfaces are described and in Table 7.2 the mesh settings for the tetrahedra are described.

7.4.3 Geometry generated to study the effects of the radius of the granules on the TMP of the granules

In this section a geometry to determine the influence of granule radius on the TMP of the granules will be generated. Two different geometries are generated: 1. The radius of the granules is 200 nm and 2. The radius of the granules is 300 nm. The geometry with 1000

granules of radius 200 nm is the same one as the geometry used for the study of electrode position and study of pores (Figure 7.1). A new geometry was generated for the cell model with 1000 granules of radius 300 nm (Figure 7.3).

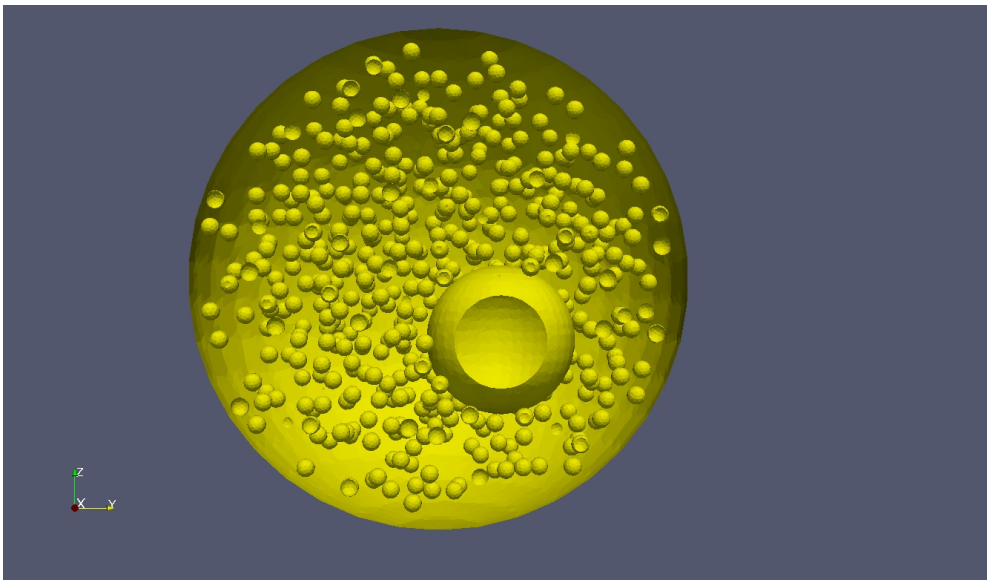

Figure 7.3: Schematic of a chromaffin cell with 1000 granules (radius = 300 nm) randomly distributed within the cytosol. The nucleus(radius = 2.5 μm) is placed off-center at (-2,2,-2) μm

Two different mesh settings are required because the number of triangles in the surface mesh was too large for the granules of radius 300 nm granules (Section 5.2). A large number of triangles can cause very long simulations. In Table 7.3, the mesh settings for granules with radius 200 and 300 nm are shown.

Table 7.3: Mesh settings for the simulations with granules of radius 200 and 300 nm.

Structure	**Surface Mesh**		**Number of triangles (per surface)**
	Target Edge Length [μm]	**Minimum Edge Length** [μm]	
Cell Membrane	0.4	0.2	12238
Nuclear Membrane	0.2	0.1	4985
Granule Membrane 200 nm	0.1	0.05	170
Granule Membrane 300 nm	0.2	0.1	220

After re-meshing all the membranes in the computational domain, the tetrahedra were generated and the same mesh settings as in Table 7.3 were used (Table 7.4).

Table 7.4: 3-D Mesh settings for the study of the effect of granule radius

3-D Mesher	
Target Edge Length [μm]	**Minimum Edge Length** [μm]
0.5	0.1

7.5 Mesh quality analysis

In this section, the quality of the mesh in all the generated geometries in Sim4life will be analyzed. To do so, the tool "Mesh quality" of Paraview will be used. This tool in Paraview allows the user to detect any poorly designed tetrahedra created by the mesher [41]. In Figure 7.4 various examples of tetrahedra considered to create good and unreliable results are shown. A poor quality mesh is considered to produce inaccuracies in the results and a good quality mesh is considered to generate reliable results.

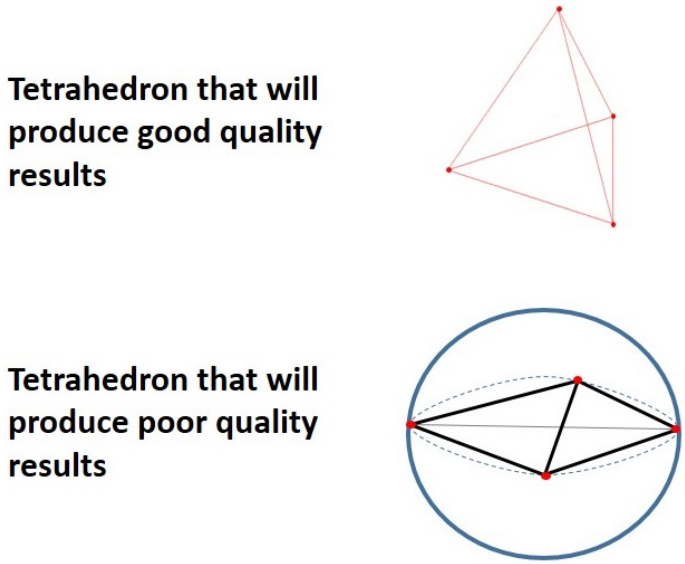

Figure 7.4: Various examples of tetrahedra. The upper tetrahedra will generate reliable results while the tetrahedra at the bottom generate unreliable results.

Paraview evaluates all the tetrahedra in a mesh and detects the tetrahedra that could produce poor results [41]. For this project, the region where the computations of the electric potential is critical is located in the membranes. These are important regions because the E-field is not homogeneous and there can be large fluctuations in the magnitude of the E-field.

The "Mesh quality" filter has been applied in all the geometries and the tetrahedra in the cytosol have a good quality. Quality is based on the aspect ratio. "The aspect ratio is the ratio between the longest edge to the shortest normal dropped from a vertex to the opposite face, normalized with respect to the shortest normal dropped from a vertex to the opposite face of a perfect tetrahedral element" [42] (Figure 7.5)

The aspect ratio of the tetrahedron also lies between 0 and 1, and a larger aspect ratio implies a better quality of the tetrahedron. For a tetrahedron with zero volume, the aspect ratio is 0 [41]. For an equilateral tetrahedron, the aspect ratio is 1 (Figure 7.5).

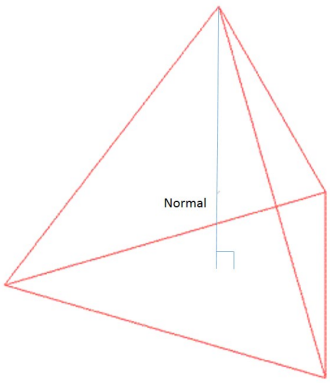

Figure 7.5: Definition of the aspect ratio of a tetrahedron. The line shown is the shortest normal dropped from the upper vertex to the opposite face. The aspect ratio of this tetrahedron is 1.

All the generated meshes in Sim4life were analyzed to ensure the quality of the results. The aspect ratio of most of the tetrahedra (90%) was above 0.707, which is an acceptable value for obtaining accurate results in the computations of electric potential and E-field. In this chapter the geometries generated for studying the effects of NEPs in chromaffin cells were presented. In the next chapter, these geometries will be exposed to a homogenous E-field (5 MV/m as in our laboratory [8, 9]) at single frequencies.

CHAPTER 8

Results

8.1 Introduction

As stated in Chapter 1, the goal of this study is to determine the TMP and E-field distribution in the cell membrane and membranes of intracellular organelles of chromaffin cells, specifically the nucleus and secretory granules of chromaffin cells exposed to NEPs. To achieve this goal, multiple cell geometries have been generated in Sim4life to evaluate the interaction of the applied E-field with the membranes of the intracellular organelles and the cell (Chapter 7). This study explores the effect of varying the following parameters: 1. Orientation of the applied E-field, 2. The radius of the granules (200 and 300 nm) and 3. the effect of the nucleus on the granules located in the vicinity of the nucleus. The last parameter that will be explored is the effect of pore formation in the cell, nuclear and granular membranes. In the experiments conducted in our laboratory [8–10] the formation of pores upon exposure of chromaffin cells to NEPs is inferred [5]. Pore formation will be modeled in this project as an instantaneous change in electrical conductivity of the membranes since pores open within 1 ns (Section 8.7) [16]. This chapter is divided into seven sections. In Section 8.2, the TMP extraction for all the membranes from the results obtained from Sim4life will be explained. In Section 8.3, the effects of the applied E-field orientation on the TMP will be discussed. In Section 8.4, the effects of the nucleus on the TMP of the secretory granules in the vicinity of the nucleus will be analyzed. In Section 8.5, the effect of granule radius on the TMP will be analyzed. In Section 8.6, the effects of frequency on the granular TMP will be analyzed. In Section 8.7, it will be shown that the poration of biological cells exposed to NEPs occurs within 1 ns, i.e. poration is an instantaneous phenomenon. In Section 8.8, the effects of membrane poration on the granular, nuclear and cellular TMP will be discussed.

8.2 Extraction of the TMP from Sim4life

From Sim4life the detailed distribution of the electric potential and the E-field in all regions of the chromaffin cell and its surrounding BSS can be extracted. For example, the cell model described in Section 7.4 in which the nucleus is off-center and 1000 granules are distributed within the cytosol, is excited with a homogeneous E-field in the Z direction, magnitude of 5 MV/m and a frequency of 300 kHz. After running the simulation, the electric potential distribution is extracted from Sim4life and processed with Paraview and shown over a two dimensional plane (normal to Y plane) through the center of the chromaffin cell model (Figure 8.1).

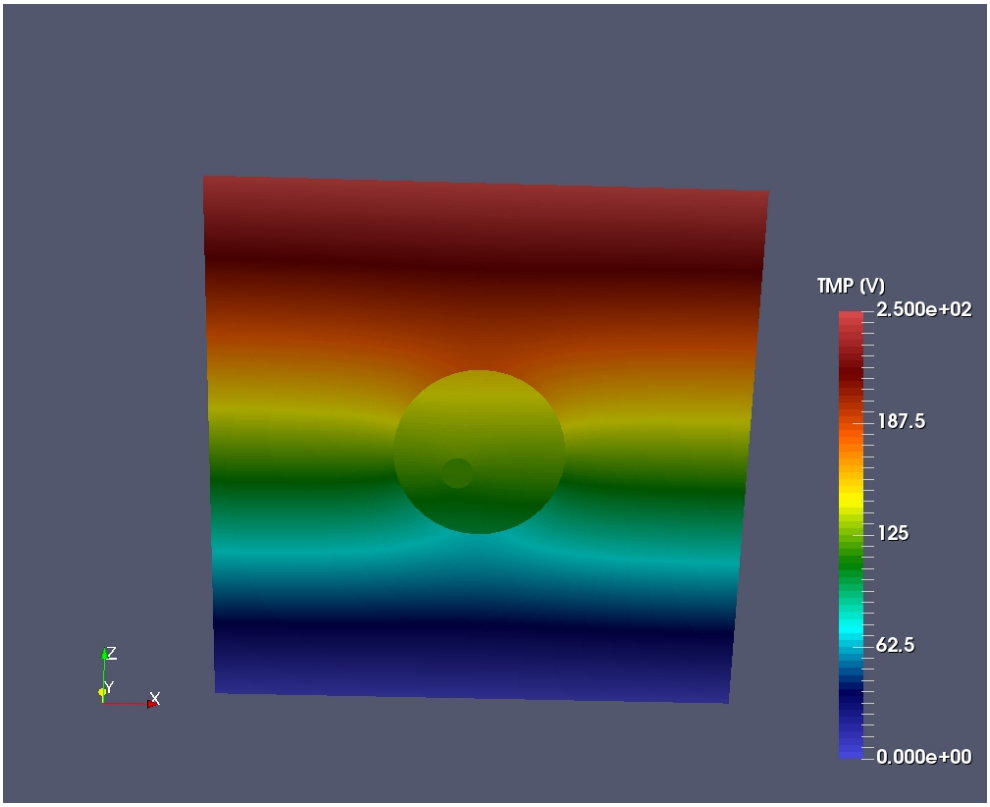

Figure 8.1: Electric potential distribution extracted from Sim4life. In this chromaffin cell geometry the nucleus and 1000 granules with membranes are included. The cell membrane is also modeled. Frequency = 300 kHz. The upper boundary is set to 250 V and lower boundary to 0 V. These boundaries create an E-field of 5 MV/m in the region between them. With these results and a custom Python script the TMP for every membrane was computed.

Since the TMP is a key quantity of interest for the study of electroporation, a Python script was written in order to extract the TMP from the electric potential results in Sim4life. This custom Python script extracts the TMPs of each membrane in the geometry. The Python script creates a hollow geometry in which the TMP is computed (Figure 7.1); this geometry is processed with the Visualization Toolkit (VTK) library and exported as a VTK file. The VTK library is an excellent tool for data processing with 3-D objects. After generating the VTK file, the VTK file is imported into Paraview in order to visualize the data. Paraview is a program developed for visualizing files containing complex geometries (such as VTK files (Figure 8.2)) associated with data (such as EM fields). The Paraview interface allows the user to extract the TMP of specific granules.

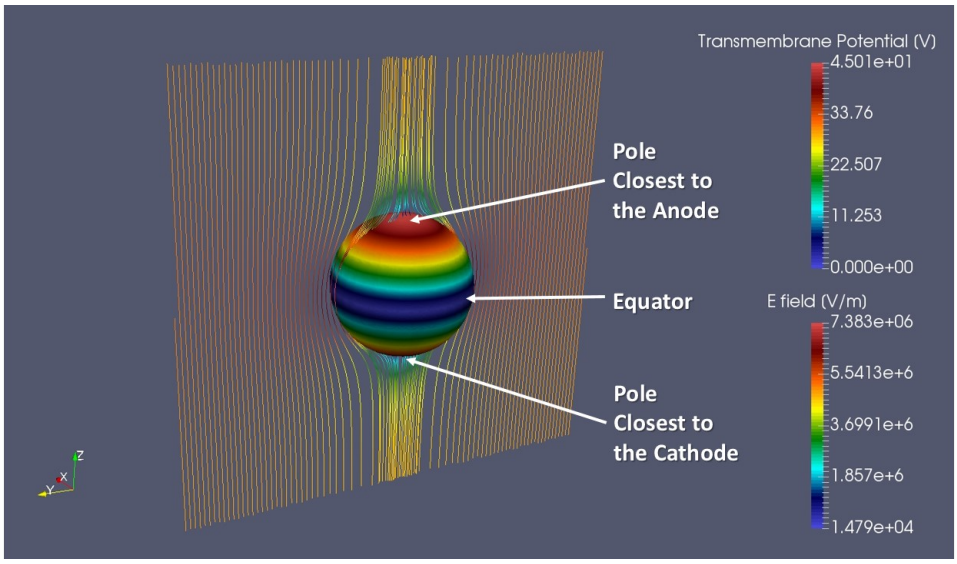

Figure 8.2: 3-D view of the E-field distribution (colored contour lines) in the BSS surrounding the chromaffin cell and the TMP (surface contours) across the cell membrane. The maxima for the E-field occur at the equator and the minima at the poles. For the TMP, the maxima occur at the poles and minima occur at the equator. Applied E-field magnitude = 5 MV/m. Frequency = 300 kHz. These results agree well with those found in the literature for biological cells [6, 26]

The value of the TMP is maximum at the poles and minimum at the equator a result that agrees with those in the literature [6, 10, 14, 26].

For the chromaffin cell model, the dielectric properties used in the simulations are

tabulated in Table 8.1. It must be pointed out that the conductivity of the nucleus is much less conductivite than the value used in [10, 12].

Table 8.1: Dielectric properties used in Sim4life simulations to model chromaffin cells

Material	**Epsilon [F/m]**	**Conductivity [S/m]**
External Medium (BSS)	80	1.3
Cellular Internal Medium	80	0.5
Nuclear Internal Medium	80	0.5
Granule Internal Medium	80	0.5
Cell Membrane	5.5	$8.3 \cdot 10^{-10}$
Nuclear Membrane	5.5	$8.3 \cdot 10^{-10}$
Granule Membrane	5.5	$8.3 \cdot 10^{-10}$

In this chapter only the TMP and E-field results will be shown since the electric potential results do not give any additional information. In Chapter 9, the TMP and E-field results will be discussed. Furthermore in Chapter 9, the results for the TMP of multiple granules will be compared and discussed

8.3 Effect of the applied E-field orientation on the TMP of the cell and granule membranes

In this section, the direction of the applied E-field is changed from along the Z-axis to 1. Along the X-axis and, 2. Along the Y-axis. The aim of these simulations is to study the effect of applied E-field orientation on the E-field and TMP distribution of the granules. In Figure 8.3 the results for the TMP and E-field distribution in a chromaffin cell exposed to a 5 MV/m applied E-field in the X direction are shown. The E-field is shown as contour lines and the TMP distribution is shown as surface contours.

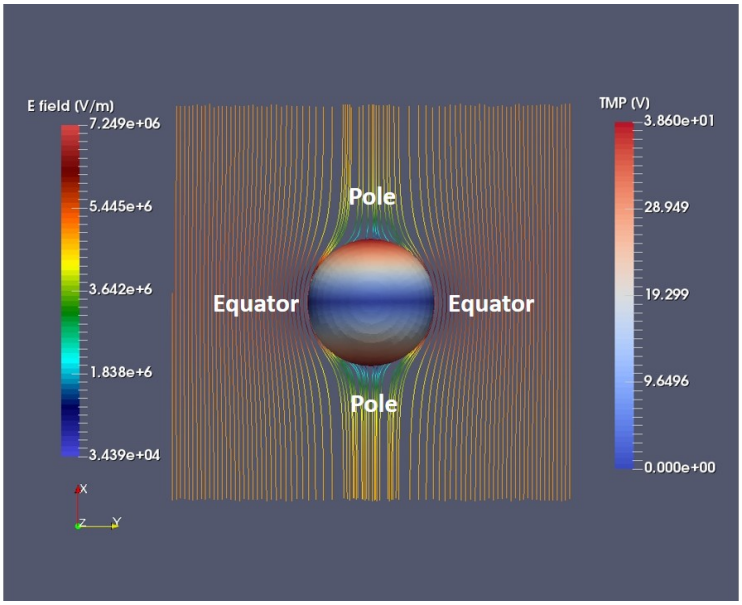

Figure 8.3: E-field and TMP distribution in a chromaffin cell with an applied E-field in the X direction. The contour lines represent the E-field and the surface contours represent the cell membrane TMP. Applied E-field magnitude = 5 MV/m. Frequency = 500 kHz

The maximum E-field occurs at the equator of the cell and the minimum at the poles. The results for the cell membrane are now hidden in order to better visualize the interior of the cell, i.e. the nucleus and the granules (Figure 8.4).

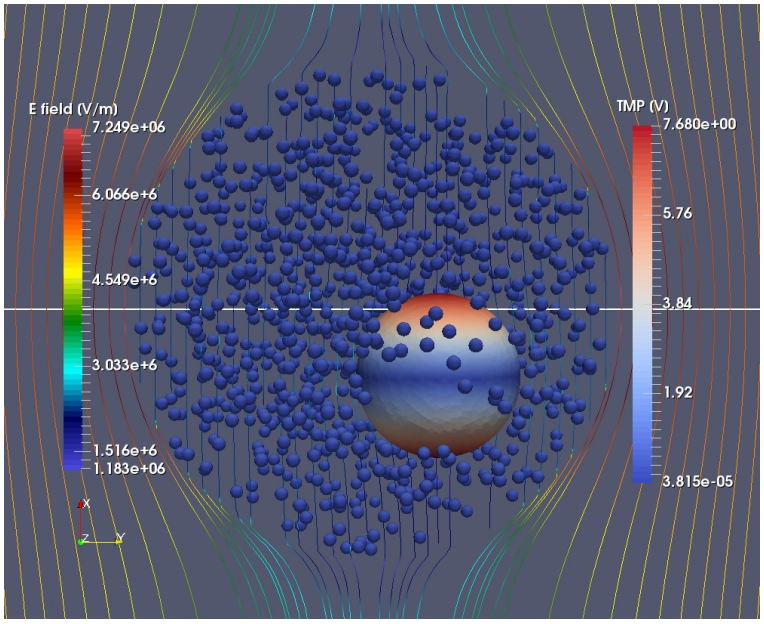

Figure 8.4: E-field and TMP distribution inside a chromaffin cell with an applied E-field in the X direction. The contour lines show the E-field and the surface contours show the nuclear and granular TMP. Applied E-field magnitude = 5 MV/m, Frequency = 500 kHz

As expected, the change in the direction of the applied E-field shifts the maxima in the TMP to the Y-direction. In Figures 8.5 and 8.6, the E-field is parallel to the Y-axis and it can be seen that the TMP maxima has been shifted 90 degrees compared to Figures 8.3 and 8.4 respectively. In Figure 8.5, the E-field is maximum at the equatorial side of the cell and minimum at the poles.

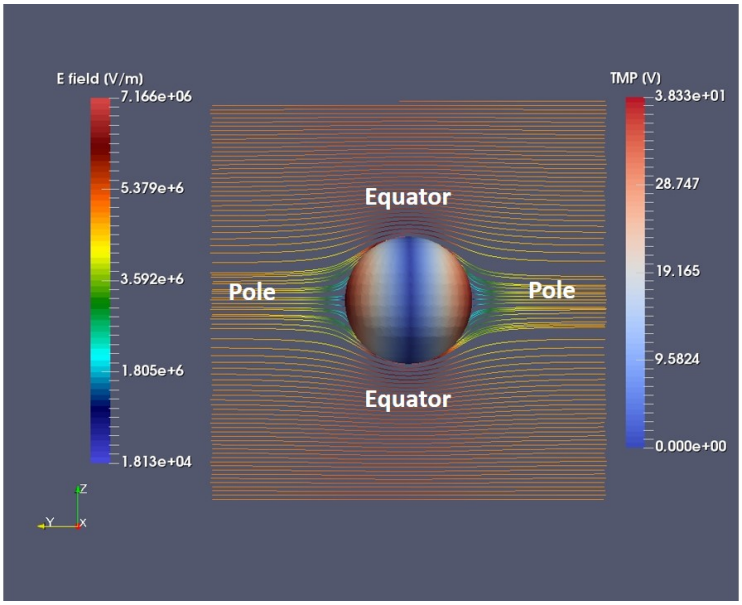

Figure 8.5: In this simulation the E-field is applied in the Y direction. The E-field distribution (contour lines) and the TMP (surface contours) for the cell membrane are shown. Frequency = 500 kHz, Applied E-field magnitude = 5 MV/m.

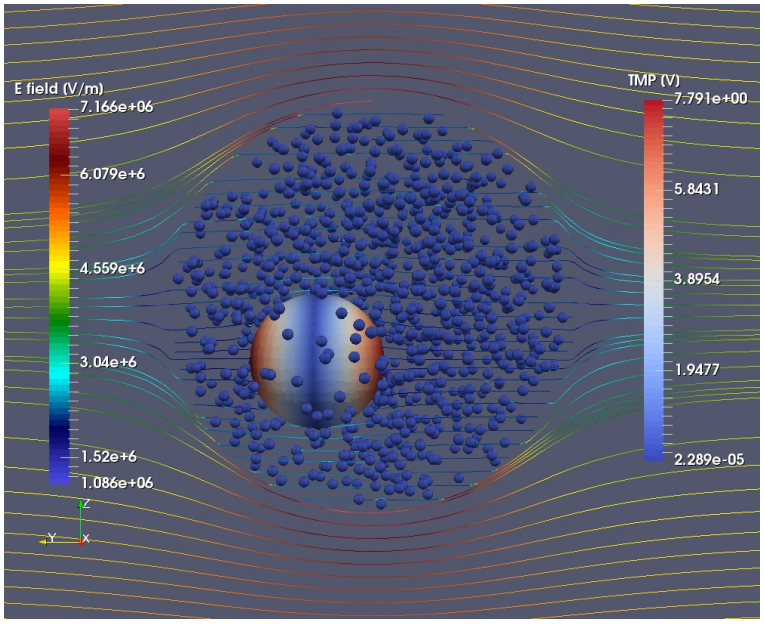

Figure 8.6: In this simulation the E-field is applied in the Y direction. The E-field distribution (contour lines) and the TMP (surface contours) for the nuclear and granular are shown. Frequency = 500 kHz, Applied E-field magnitude = 5 MV/m.

From Figures 8.3-8.6 it can be concluded that the TMP distribution in the granules is

determined by the direction of the E-field. The results also indicate that the TMP magnitude is not altered by the direction of the applied E-field.

8.4 Effect of the nucleus on the E-field and TMP of the granules at the vicinity of the nucleus

In this section, the effect of the nucleus on the surrounding granules will be analyzed. The nucleus is the largest organelle inside the cell (2.5 μm in radius), and it may affect the TMP of the surrounding granules (200 nm in radius). The cell geometry explained in Section 7.4 will be used. In this section the TMP of all the membranes in a chromaffin cell exposed to a homogeneous E-field of 5 MV/m at a frequency of 300 kHz will be analyzed.

To visualize better the TMP for the nucleus and granules, the results for the cell membrane in Figure 8.3 are hidden. The large red sphere in Figure 8.7 represents the TMP of the nucleus and the smaller spheres represent the TMP of the granules. The TMP scale was adjusted in order to better visualize the TMP of the granules.

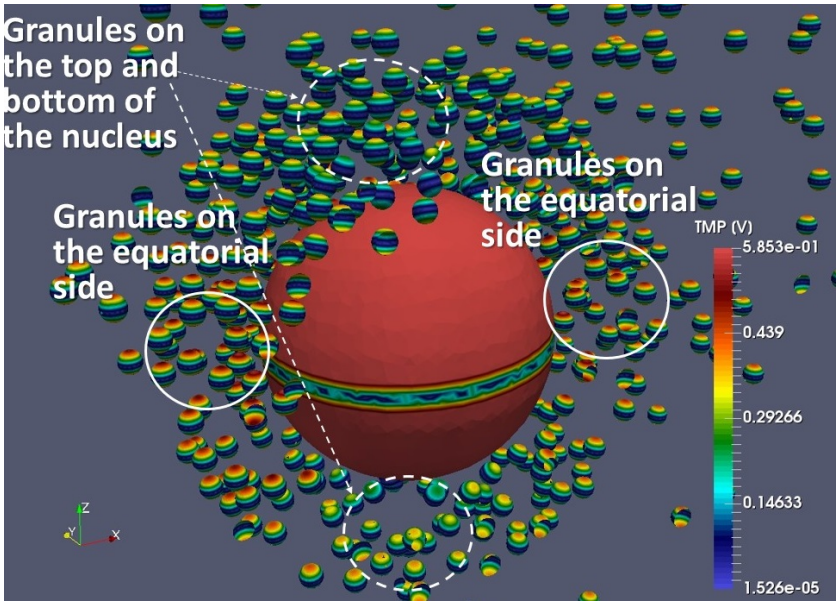

Figure 8.7: Zoomed-in view of the TMP of the nucleus and granules in the proximity of the nucleus. It is seen that the granules in the vicinity of the equatorial side of the nucleus (granules within the solid white circles) have a higher TMP than the rest of the granules. The granules on the nuclear pole sides (granules within the dashed circles), have a lower TMP than the rest of granules. Applied E-field magnitude = 5 MV/m

Furthermore, in order to visualize better the TMP for the granules in the close vicinity of the nucleus shown in Figure 8.7, the nucleus is hidden (Figure 8.8).

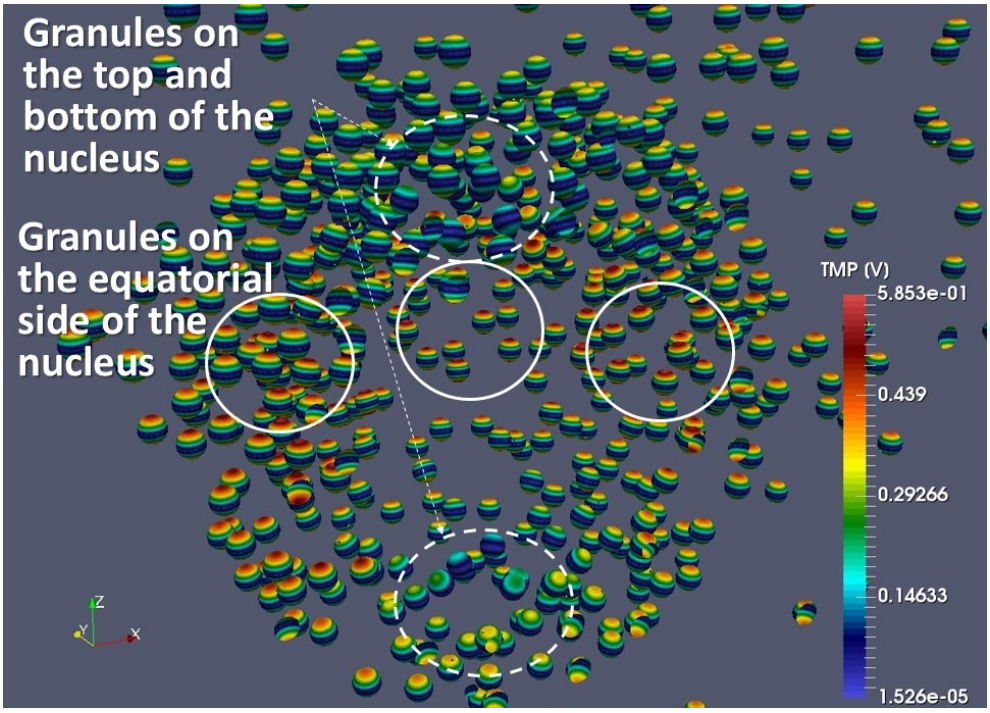

Figure 8.8: Zoomed-in view of the granules in close vicinity of the nucleus. The nucleus has been hidden. The granules within the solid white circles (located on the equatorial side of the nucleus) have a higher TMP than the rest of granules. The granules within the dashed circles (located on the pole side of the nucleus) have a lower TMP. Applied E-field magnitude = 5 MV/m. Frequency = 300 kHz

Figures 8.7 through 8.8 show the results at a frequency of 300 kHz. The E-field distribution in the vicinity of the chromaffin cell is depicted by contour lines and the TMP across the cell membrane is depicted by contour surfaces in Figure 8.7.

In the next section four specific granules shown in Figure 8.9 will be analyzed in further detail. Due to the large number of granules (1000), the results for only four granules at specific locations of interest will be examined and discussed in detail (Chapter 9). In the following sections the results for the effect of the nucleus on the TMP of the neighboring granules will be shown.

8.4.1 Comparison of the TMP of four specific granules at different locations within the cytosol

In this section, four granules are selected from different regions of interest within the cytosol: the first two granules (# 1 and # 4) are located below the nucleus (distance from the nucleus = 150 nm), granule # 3 is located on the equatorial side of the nucleus (distance from the nucleus = 150 nm), and granule # 2 is selected in a region of the cytosol beyond the 'influence' of the nucleus (distance from the nucleus = 4 μm) (Figure 8.9). The 'range of influence' will be discussed further in Section 8.4.2. Each of these granules has a different TMP distribution and TMP magnitude. For example, granule # 3 has the highest TMP magnitude of the four granules.

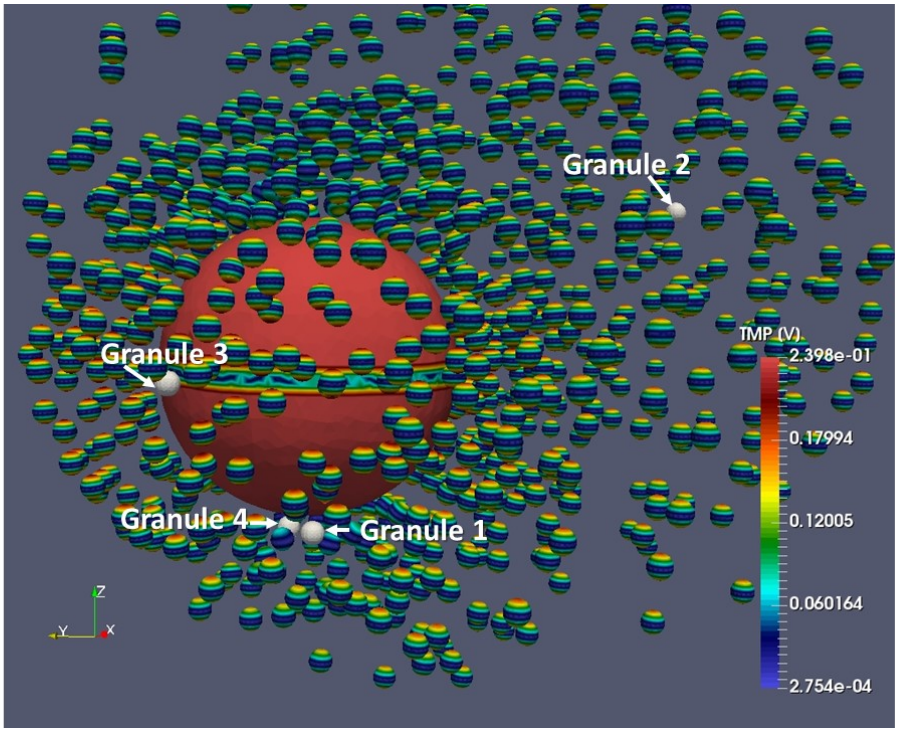

Figure 8.9: The location of the four granules (granules shown as white spheres) to be further analyzed. Granules # 1 and # 4 are below the nucleus, granule # 3 is located on the equatorial side of the nucleus and granule # 2 is located in the upper part of the cell beyond the influence of the nucleus. Applied E-field magnitude = 5 MV/m. Frequency = 300 kHz

The process of isolating a granule and extracting the spatial distribution of the TMP can be performed in Paraview with the tool "Select Cell". With this tool,

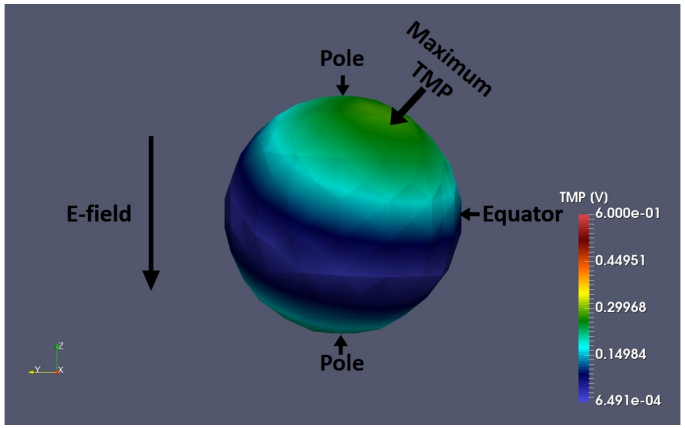

(a) TMP of granule # 1. The maximum value for the TMP is 0.23 V and has been shifted approximately 40 degrees from the pole.

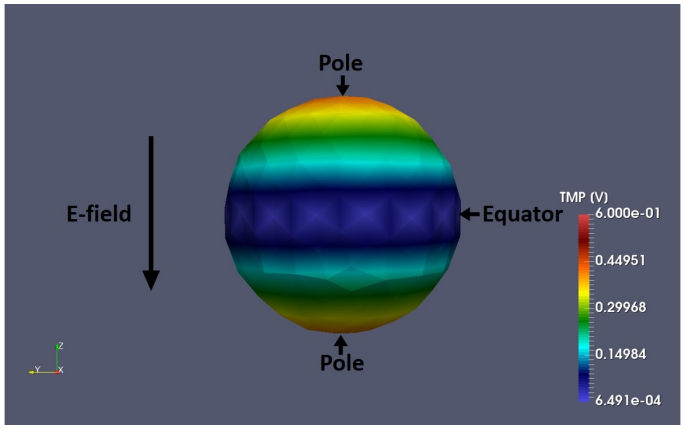

(b) TMP of granule # 2. The maximum value for the TMP is 0.35 V and occurs at the pole.

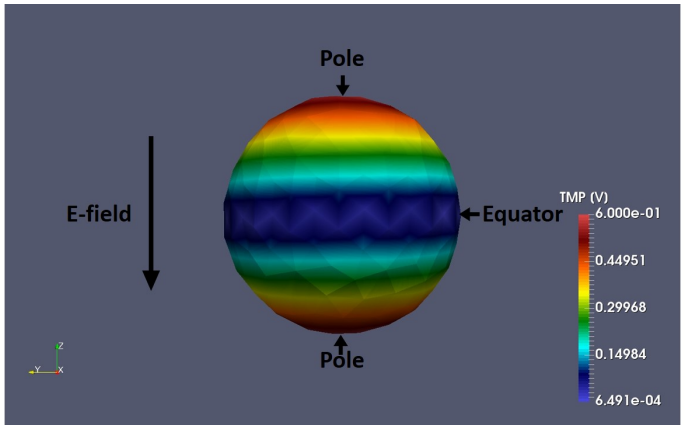

(c) TMP of granule # 3. The maximum value for the TMP is 0.58 V and occurs at the pole.

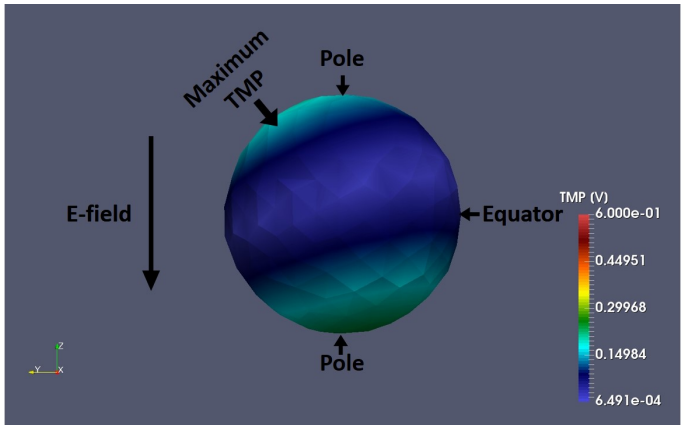

(d) TMP of granule # 4. The maximum value for the TMP is 0.15 V and has been shifted approximately 40 degrees from the pole

Figure 8.10: TMP distribution for the four specific granules shown in Figure 8.9. Applied E-field magnitude = 5 MV/m. Frequency = 300 kHz. The different locations of the granules can lead to different TMP distributions and magnitudes. The location of the granules can be seen in Figure 8.9.

the user can specify the exact meshcells that comprise a granule and isolate the granule from the rest of the geometry. The TMP of the four granules are shown in Figure 8.10. As can be seen from Figures 8.10 (a) and (b), the TMP pattern is tilted for granules # 1 and # 4. The reasons for these differences in the TMP distribution will be discussed in 9.

8.4.2 Effect of the nucleus on the E-field within the cell

In this section, in order to understand the different TMP distributions and magnitudes seen in the previous section (Figure 8.10) (specifically the granules within the vicinity of the nucleus) the E-field distribution inside the cell will be explored. This will determine the effective "range of influence" within which the E-field and TMP distribution of the granules are altered by the nucleus (Figure 8.11).

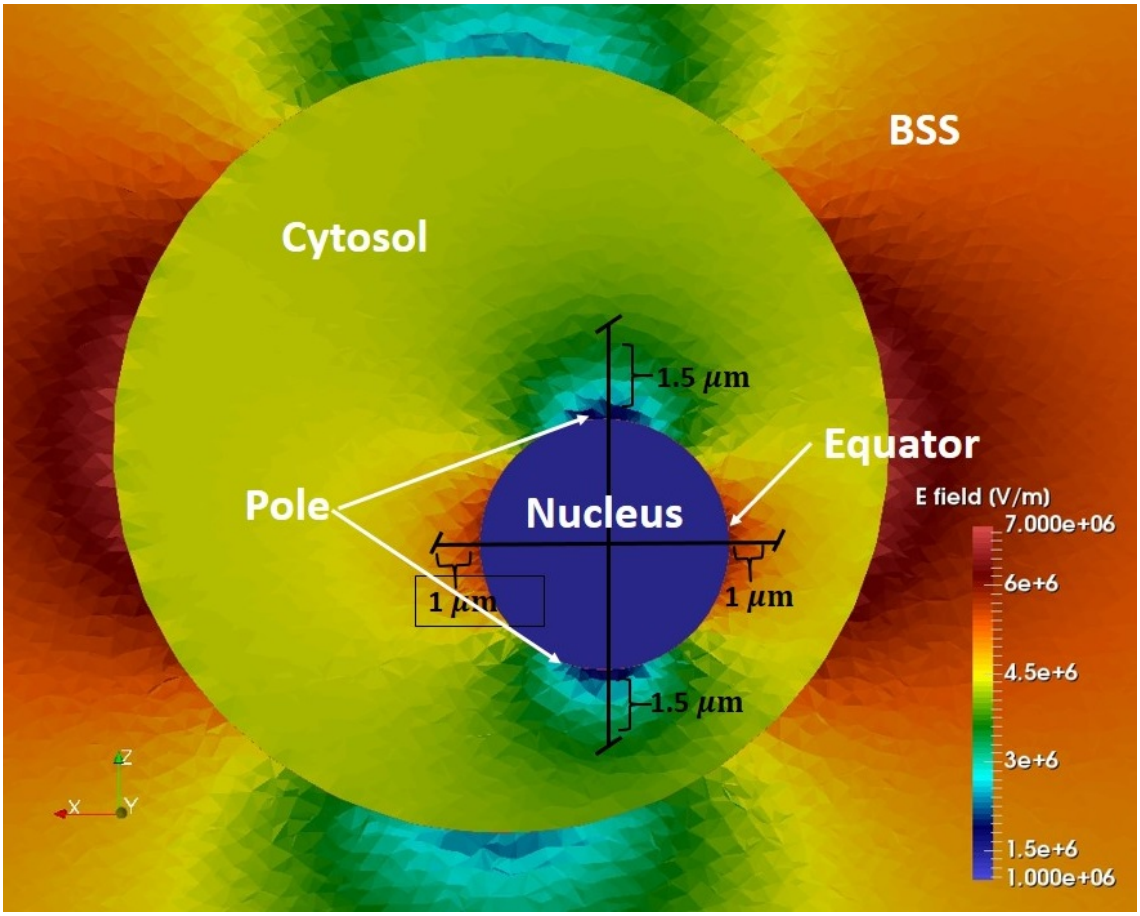

Figure 8.11: E-field distribution in the chromaffin cell model. Maximum E-field occurs at the equator of the nucleus. Minimum E-field occurs at the bottom and top of the nucleus (poles). The E-field is homogeneous to within 10% over the rest of the cell cytosol (i.e. region beyond the maxima and minima. Applied E-field magnitude = 5 MV/m. Frequency = 300 kHz.

Figure 8.11 shows the E-field distribution in the chromaffin cell model. Maximum E-field occurs at the equator of the nucleus. Minimum E-field occurs at the bottom and top (poles) of the nucleus. The E-field is homogeneous to within 10% over the rest of the cell cytosol region i.e. in the region not including the maxima and minima (Figure 8.11).

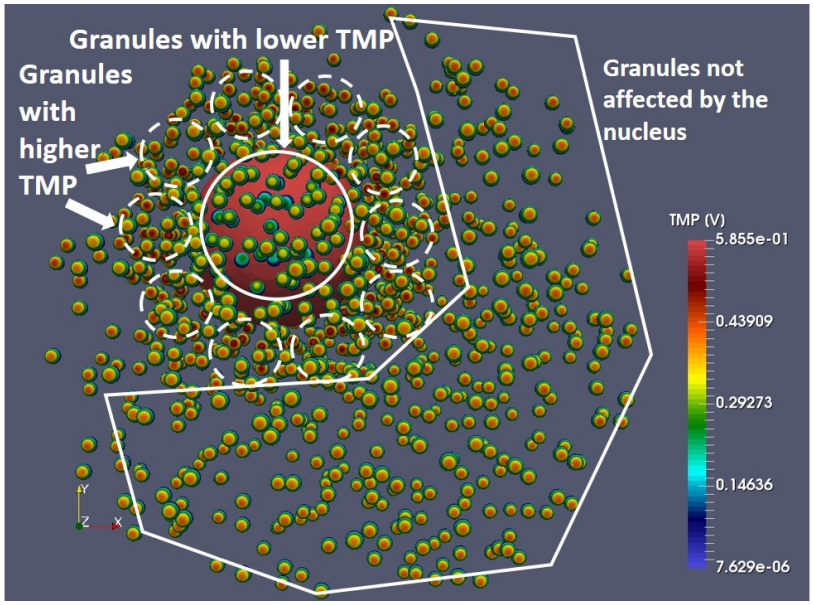

Figure 8.12: Zoomed-in top view of the TMP distribution of the nucleus and granules in its vicinity. The granules within the white circle have a lower TMP than the rest of the granules; their maximum TMP magnitude is approximately 0.2 V. The granules that are around the equator of the nucleus (shown by the dashed circles) have a higher TMP than the rest of the granules. The granules enclosed within the white polygon all have the same TMP distribution and magnitude. Applied E-field magnitude = 5 MV/m. Frequency = 300 kHz

Figure 8.12 shows a zoomed-in view of the TMP distribution for the nucleus and granules in its vicinity. The granules located within the white circle have a higher TMP than the rest of the granules and their maximum TMP is approximately 0.2 V. In addition, the granules located around the equator (dashed circles) have a higher TMP than the rest of the granules. The granules located within the white polygon all have the same TMP distribution and magnitude (Further discussion in Chapter 9).

8.5 Effect of the radius of the granules on the TMP

In this section, the effects of different granule radii will be explored. Regardless of the granule location, the granules far enough from the nucleus (i.e. outside the "range of influence") have a similar TMP distribution and magnitude to within 1% (Section 8.4.2).

The radii of granules in chromaffin cells can be represented as a normal distribution

N(180,60) [20], i.e they can range from 50 nm to 300 nm. Two chromaffin cell geometries with different granule radii (200 and 300 nm respectively) were generated in Sim4life and the results for TMP distribution for these two cases were compared at a frequency of 500 kHz (Figures 8.13 and 8.14). The mesher in Sim4life was not able to mesh granules with smaller radii due to the extremely small meshcell size required.

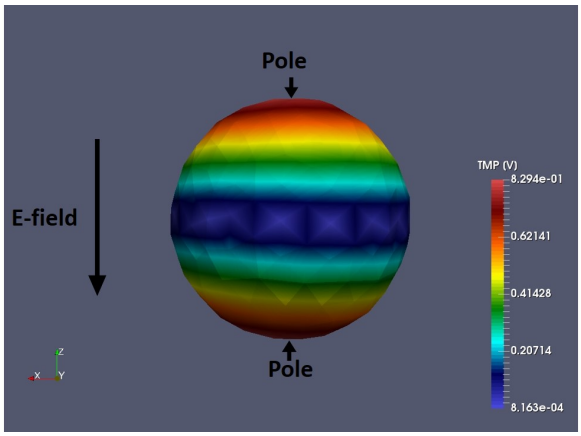

Figure 8.13: TMP distribution in a granule with radius 200 nm. Frequency = 500 kHz, applied E-field magnitude = 5 MV/m. The location of the granule is 4 μm from the nucleus. The maximum TMP value is 0.81 V and is located at the pole.

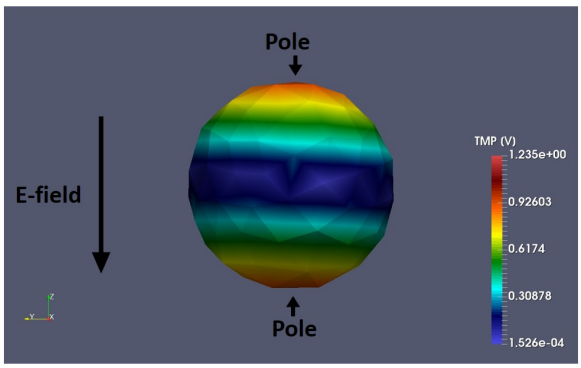

Figure 8.14: TMP distribution for a granule with radius 300 nm. Frequency = 500 kHz, applied E-field magnitude = 5 MV/m. The location of the granule is 4 μm from the nucleus. The maximum TMP value is 1.21 V and is located at the pole.

As can be seen from Figures 8.13 and 8.14 the TMP at the pole for the granule with a radius of 200 nm is 0.824 V at 500 kHz and the TMP at the pole for the granule with a radius of 300 nm is 1.23 V at 500 kHz. From these results it can be concluded that the larger the radius of the granules, the higher is the TMP (Discussion in Chapter 9). In the next section the effects of frequency on the TMP of the granules will be discussed.

8.6 Frequency effects on the TMP of the granules

In this section, the TMP of granule # 2 (a granule which is outside the "range of influence" of the nucleus, Figure 8.9) at four different different frequencies in the range DC to 10 MHz computed in Sim4life is shown.

As seen in Figure 8.15 at different frequencies the magnitude of the TMP varies. The TMP at the pole for granule # 2 at 100 kHz is 0.17 V, 500 kHz is 0.823 V, 1 MHz is 1.16 V and 10 MHz is 1.33V. The TMP peak occurs at 5 MHz (Results not shown). Above 30 MHz the TMP becomes zero and at DC the TMP is also zero (Results not shown). In Section 9.3 the magnitudes of the TMP at the pole for different frequencies will be discussed. From these results it can be concluded that the TMP varies as a function of frequency. Also as was stated in Chapter 6, the membranes become electrically transparent above 30 MHz, i.e. the TMP becomes zero.

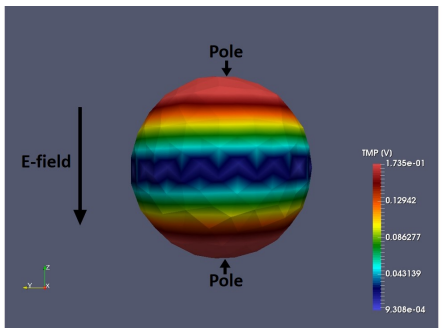

(a) TMP distribution for granule # 2 at 100 kHz. The maximum TMP value is 0.17 V and is located at the poles.

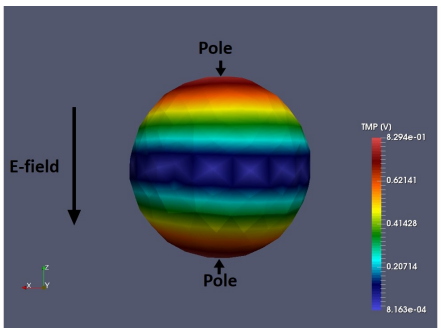

(b) TMP distribution for granule # 2 at 500 kHz. The maximum TMP value is 0.8 V and is located at the poles.

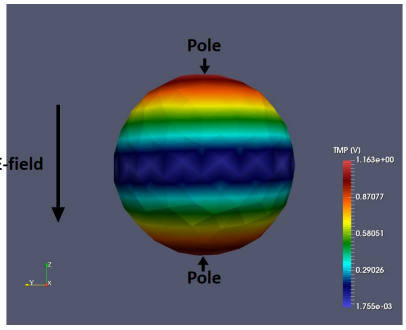

(c) TMP distribution for granule # 2 at 1 MHz. The maximum TMP value is 1.16 V and is located at the poles.

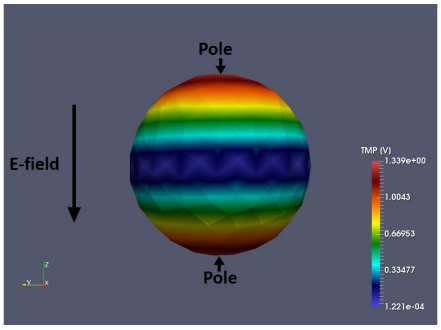

(d) TMP distribution for granule # 2 at 10 MHz. The maximum TMP value is 1.33 V and is located at the poles.

Figure 8.15: TMP distribution for granule # 2 at 100 kHz, 500 kHz, 1 MHz and 10 MHz. respectively. Applied E-field magnitude = 5 MV/m

Experiments with chromaffin cells in our laboratory exposed to NEPs have shown pore formation in the cell membrane [5]. In the next section a simplified model to take into account the formation of pores within the membranes (both intracellular and plasma membrane) will be discussed.

8.7 Simplified model of poration in a chromaffin cell exposed to NEPs

NEPs are known to create pores in biological membranes and the effects of porated vs non-porated membranes on the TMP will be explored. In this section a simplified model for the formation of pores in multiple membranes (cell, nuclear and granular membranes) of

a chromaffin cell exposed to high intensity NEPs will be implemented. Debruin et al. [18] describe a model for pore formation within a membrane. In this model the radius of the pores is assumed to remain constant. Since the pores created by NEPs do not grow in size [12], the mathematical model for poration in [18] is adequate for the study of electroporation in biological cells exposed to NEPs. Pore formation results in an increase in electrical conductivity of the membrane and hence can be modeled in Sim4life as an increase in the conductivity of the membrane [12]. In this project, this approach is implemented for modeling pore formation in membranes. The pores are created within a time frame of 1 ns after the NEP is applied. As explained in Section 3.3, non-linearities of electrical properties cannot be incorporated in Sim4life. However, due to the speed of pore formation, the formation of pores in the membranes can be modeled as an instantaneous change in the membrane conductivity [12]. A model of a chromaffin cell with 1000 granules and a nucleus has been built in Sim4life to study the effect of the change in electrical conductivity of the membranes due to pore formation.

The conductivity of the various membranes (cell, nucleus and granules) will be increased in a certain order. Three different schemes will be analyzed in order to study how pore formation affects the TMP of the membranes: 1. Only the cell membrane is porated, 2. The cell and nuclear membranes are both porated and, 3. The cell, nuclear and granule membranes are porated. These three schemes are based on the temporal evolution of pore formation within the membranes [1, 12]. Smith et al. [6] and Retlej et al. [12] show that first the cell membrane gets porated, then the nuclear membrane and finally the membranes of the intracellular organelles, all within a timeframe of a few nanoseconds. In Section 8.7.1 it is shown that poration takes place within this timeframe.

8.7.1 1-D model of an electroporated chromaffin cell

To prove that poration is an instantaneous phenomenon (that happens within 1 ns time duration), a 1-D model of the NEP exposure system including the BSS, a cell membrane

and a cytosol was built in Python. This model is based on the circuit shown in Figure 8.16. However, in order to include the formation of pores upon exposure of the cell to NEPs, the poration model developed by DeBruin and Krassowska [18] was included in the part of the circuit representing the cell membrane.

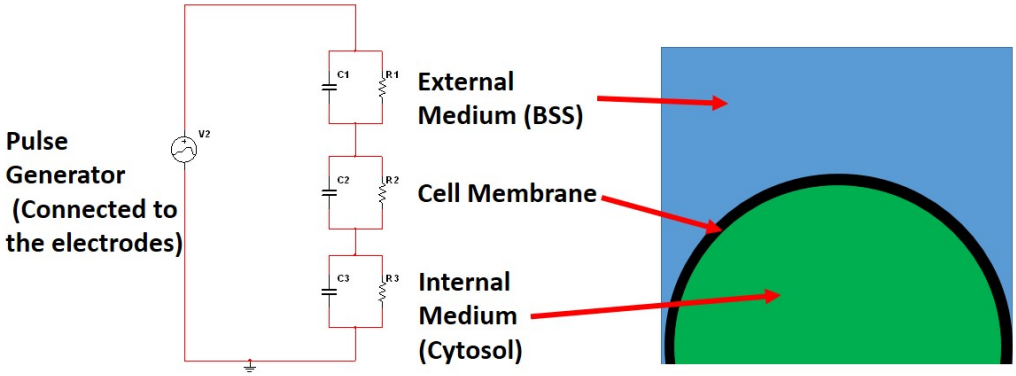

Figure 8.16: A simplified equivalent circuit of an exposure system for stimulation of biological cells. The pulse generator is modeled as a voltage source. The external medium (BSS), the cell membrane and the cytosol (the intracellular medium) are each represented a resistor and a capacitor in parallel. The three sets of resistors and capacitors are connected in series. The poration model developed by DeBruin and Krassowska [18] was incorporated in the cell membrane.

As stated previously, the pore density N is dependent on the TMP and can be calculated from equation 31

$$\frac{dN}{dt} = \alpha e^{(\frac{ITV}{Vep})^2} * (1 - \frac{N}{N_0} * e^{(-q*\frac{ITV}{Vep})^2}) \tag{31}$$

where N is the pore density, ITV is the TMP across the cell membrane, N_0 is the initial pore density (set to $1.5 \cdot 10^9$), α, V_{ep} and q are electroporation constant (set to 10^9, 0.258 and 2.46 respectively) [18].

The TMP and pore density are calculated for each time step. In order to model the effects of pores, the conductivity of the cell membrane is updated for every time step [12]

and given by:

$$\sigma_{ep} = \pi r^2 \sigma_{pore} N \frac{e^{V_m} - 1}{\frac{\omega e^{\omega - nV_m} - nV_m}{\omega - nV_m} e^{V_m} - \frac{\omega e^{\omega + nV_m} + nV_m}{\omega + nV_m}} \tag{32}$$

where r is the radius of a pore, σ_{pore} its conductivity, N is the pore density and the rest of parameters are shown in Table 8.2.

Table 8.2: Description of the parameters in Eq 32

Parameter	**Value**	**Description**
ω	2.65	energy cost for moving an ion from a region of high dielectric constant (water) to a small pore in the lipid bilayer
r_{pore}	0.76	radius of a single pore
σ_{pore}	1	Conductivity of a single pore
n	0.15	length of pore entrance area

The excitation source is a square pulse, and the E-field is set to 5 MV/m as in the experimental setup [5, 10]. The time step for the simulation is set to 2 ps. In Figure 8.17 the time evolution of the cell membrane conductivity as pores form as calculated by the Python script is shown. In other similar models of electroporation, the formation of pores also takes place within nanoseconds [6, 10, 12] which agrees with the obtained results. Figure 8.17b shows that the pores are formed within of a few nanoseconds. The results in Figure 8.17a show that the conductivity of the cell membrane increases from $8.3 \cdot 10^{-10}$ S/m to 0.01 S/m in a time period of a few nanoseconds This conductivity value will be used in Sim4life simulations to model a porated membrane.

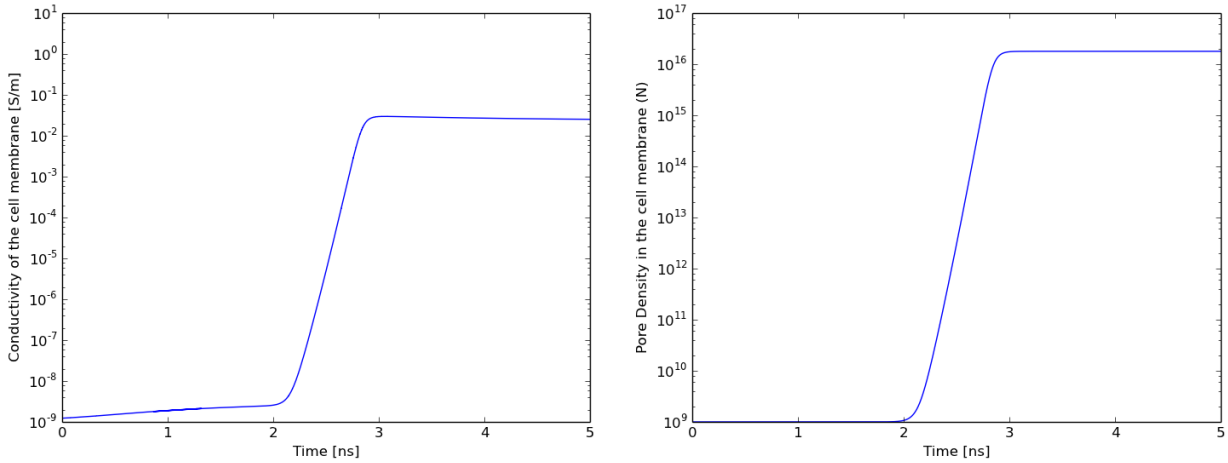

(a) Time evolution of the conductivity of the cell membrane.

(b) Time evolution of the pore density of the cell membrane.

Figure 8.17: Time evolution of the pore density and conductivity value in the cell membrane as obtained using DeBruins model [18]. The formation of pores can be modeled as an increase in the conductivity of a membrane. When a chromaffin cell is exposed to NEPs, pores are created within a few nanoseconds [6, 10, 12]

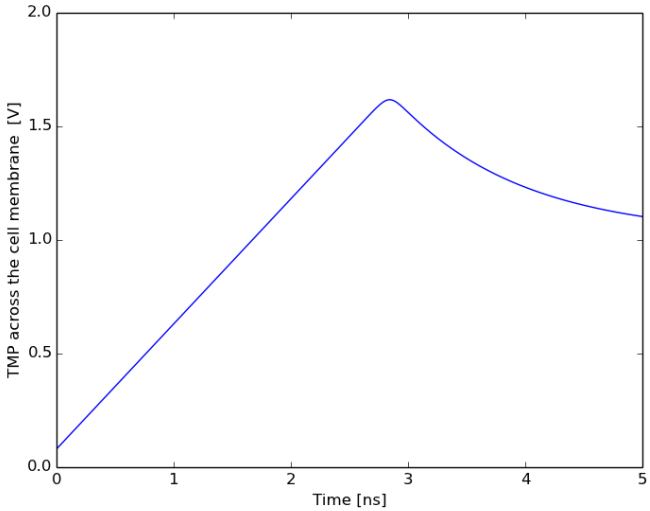

Figure 8.18: Time evolution of the TMP across the cell membrane

In Figure 8.18 the corresponding TMP evolution in time across the cell membrane is shown and it is seen that the maximum TMP value is 1.6 V. This is the maximum TMP that the cell membrane reaches before the cell membrane becomes conductive. Thus, from

these results obtained from the simplified cell model incorporating poration and, as shown in Figure 8.17, it can be assumed that the poration of a membrane is an instantaneous phenomenon in which the conductivity of the cell membrane goes from almost zero to 0.01 S/m within a few nanoseconds. In the next section, a geometry with 1000 granules will be exposed to a homogeneous E-field in which the effects on the TMP of three different poration schemes will be analyzed. The goal is to analyze the effects on the TMP (cell membrane, nuclear membrane and granule membranes) as a result of these different poration schemes.

8.8 Analysis of different pore formation schemes

In the previous section it was shown that the time to fully porate a biological membrane is approximately a few nanoseconds. A cell model of a chromaffin cell described in Section 7.4.2 is exposed to a 5 MV/m E-field. To evaluate the effects of poration of different membranes in a chromaffin cell, as stated before, three different poration schemes are evaluated: 1. Only the cell membrane is porated, 2. The cell and nuclear membrane are porated and 3. The cell, nuclear and granule membranes are porated. The choice of these schemes is based on work by Smith et al. [6] and Retlej et al. [12]. Also, four granules located in different regions of a chromaffin cell are examined since depending on their location, they will have different TMP distributions and magnitudes. In Figure 8.19, the specific granules to be analyzed are shown.

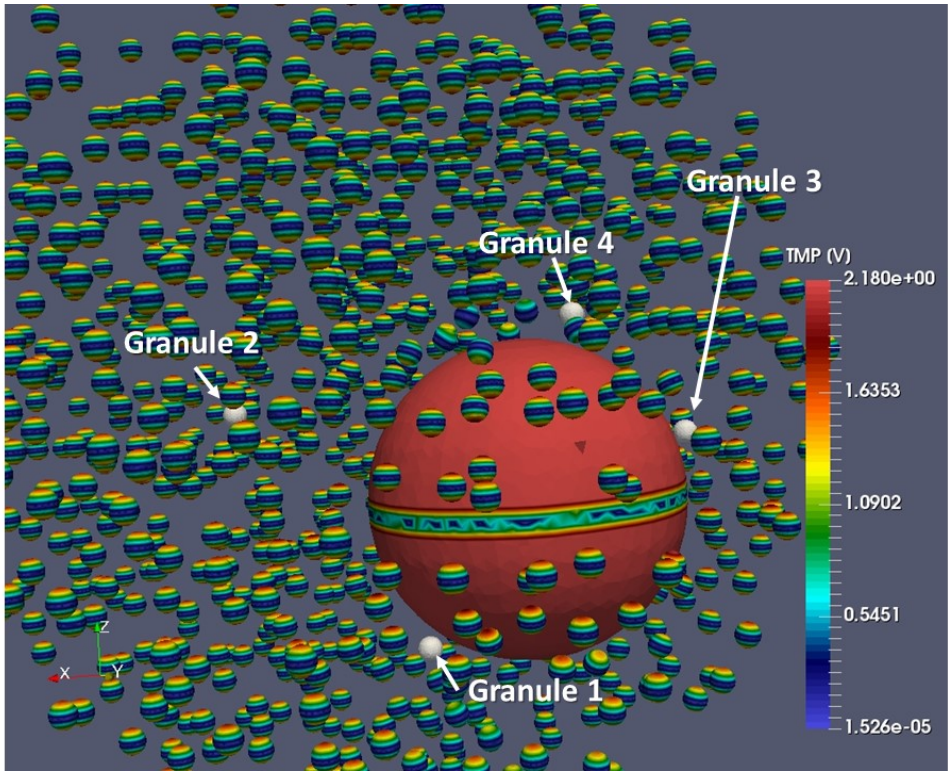

Figure 8.19: Location of the granules to be analyzed with different poration schemes.

The TMP in these four granules will be analyzed in detail to study the effects of the four different pore schemes. The TMP values will be compared quantitatively in Chapter 9.

8.8.1 Scheme 1: Pore formation only in the cell membrane

The first scheme examines a fully porated cell membrane with a conductivity value set to $\sigma = 0.01$ S/m (Figure 8.17a). The conductivity of the nuclear and granule membranes is set to $\sigma = 8.3 \cdot 10^{-10} S/m$ i.e. they are not porated. The applied E-field is set to 5 MV/m. The resulting TMP distribution of the cell membrane is shown in Figure 8.20.

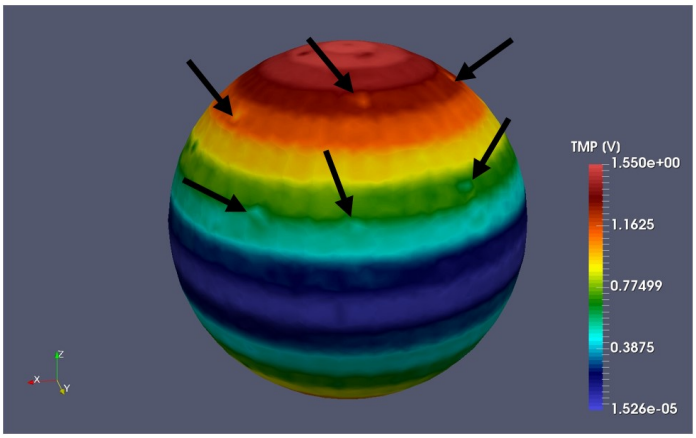

Figure 8.20: View of the TMP of a fully porated cell membrane (σ = 0.01 S/m). TMP alterations (indicated by black arrows)) can be seen in some regions of the cell membrane. These TMP alterations are caused by the presence of granules closest to the cell membrane. Magnitude of the applied E-field = 5 MV/m

In Figure 8.20, alterations in the TMP of the fully porated cell membrane indicated by black arrows are visible. These alterations in the TMP are caused by the presence of granules in the proximity of the cell membrane. These alterations are attributed to the non-conductive granule membranes that modify the E-field in their immediate vicinity. In Figure 8.21, the TMP of the four specific granules depicted in Figure 8.21 is shown. As was shown in Section 8.4.2, the nucleus causes an inhomogeneous E-field in its vicinity and the TMP distribution and magnitude of some granules have been altered. There are certain granules that are docked in the cell membrane and therefore can influence the TMP of the cell membrane much more. Furthermore, these alterations in the TMP of the cell membrane could influence the exocytosis of the granules.

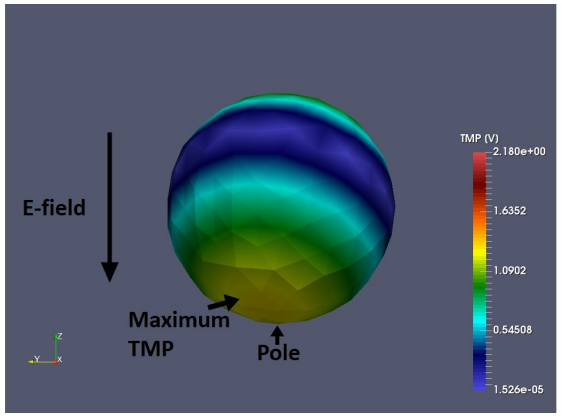

(a) Granule # 1. The maximum value for the TMP is 1.15 V and is not at the pole but has been shifted approximately -30 degrees from the pole.

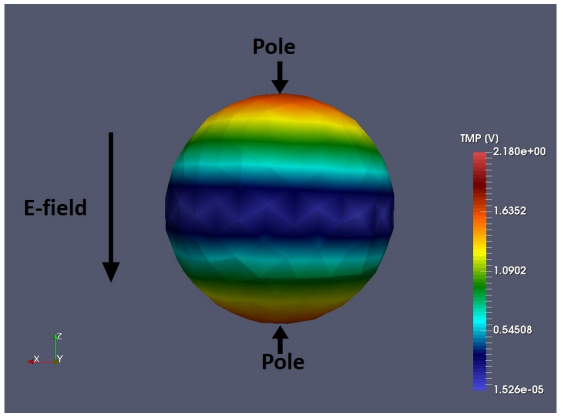

(b) Granule # 2. The maximum value for the TMP is 1.85 V and occurs at the pole.

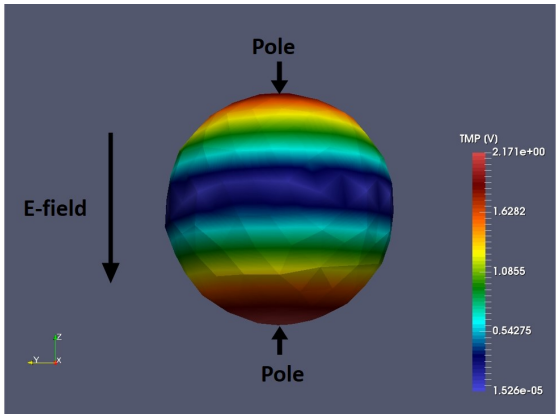

(c) Granule # 3. The maximum value for the TMP is 2.17 V and occurs at the pole.

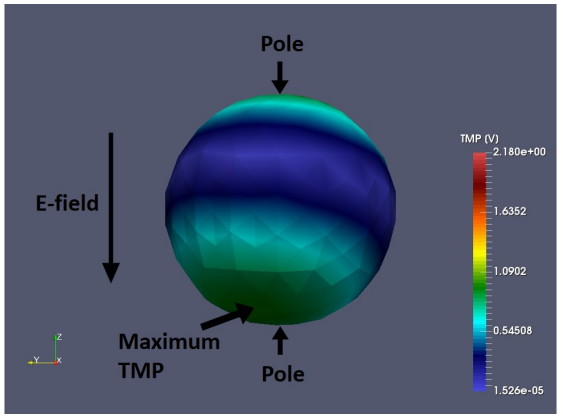

(d) Granule # 4. The maximum value for the TMP is 1.05 V and is not at the pole but has been shifted approximately 40 degrees from the pole.

Figure 8.21: View of the 4 specific granules shown in Figure 8.20. The granules have different TMP distributions and magnitudes due to the inhomogeneity of the E-field caused by the presence of the nucleus.

8.8.2 Scheme 2: Pore formation in both the cell and nuclear membrane

In this poration scheme, the nuclear and cell membranes are porated ($\sigma = 0.01\ S/m$). The granules have a non conducting membrane ($\sigma = 8.3 \cdot 10^{-10}\ S/m$) as they are not porated.

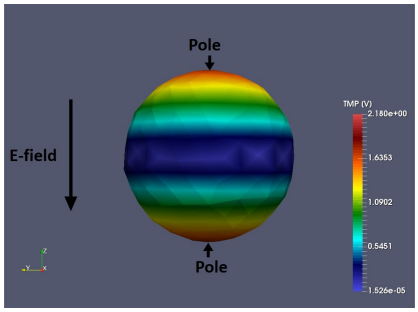

(a) Granule # 1. The maximum value for the TMP is 2.05 V and occurs at the pole.

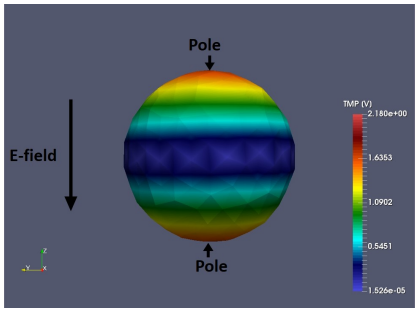

(b) Granule # 2. The maximum value for the TMP is 2.05 V and occurs at the pole.

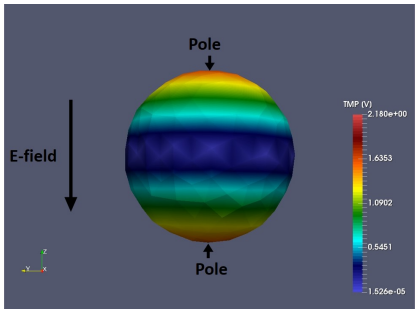

(c) Granule # 3. The maximum value for the TMP is 2.05 V and occurs at the pole.

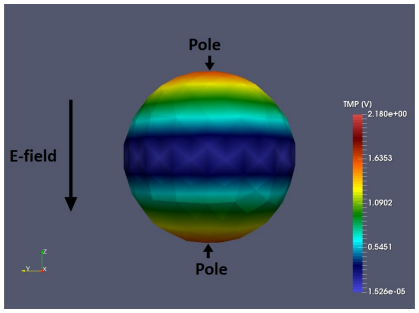

(d) Granule # 4. The maximum value for the TMP is 2.05 V and occurs at the pole.

Figure 8.22: TMP distribution of the 4 specific granules shown in Figure 8.19. The granules have the same TMP distribution and magnitude because the nuclear membrane does not alter the E-field in its surroundings due to the high conductivity of the nuclear membrane ($\sigma = 0.01\ S/m$). Applied E-field magnitude = 5MV/m

In Figure 8.22 it can be seen that all granules have the same TMP distribution and magnitude. The maximum TMP occurs at the pole with a value of 2.05 V. In this scheme the nuclear membrane is conductive and the E-field is homogeneous in the vicinity of the nucleus. As a consequence, the TMP distribution and magnitude of all the granules is the same.

The TMP of the cell membrane in this scheme is similar to the poration scheme 1 where

only the cell membrane was porated (Results not shown). The granules closest to the cell membrane affect the cell membrane TMP due to the alterations in the E-field produced by the low conductive granule membranes. Therefore, if the granules are not porated, they can influence on the cell membrane TMP and as a consequence have an impact on exocytosis. However, when the granules are porated (poration scheme 3), the cell membrane TMP is not altered.

8.8.3 Scheme 3: Pore formation in the cell, nuclear and granule membrane

In this poration scheme, all the membranes in the chromaffin cell are assumed to be porated. The conductivity for each membrane is set to $\sigma = 0.01\ S/m$

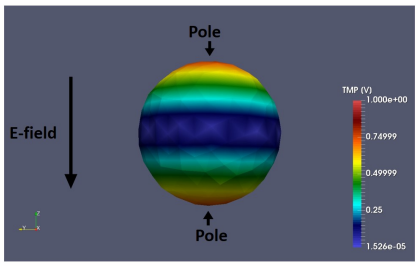

(a) TMP results for granule # 1. The maximum value for the TMP is 0.83 V and occurs at the pole.

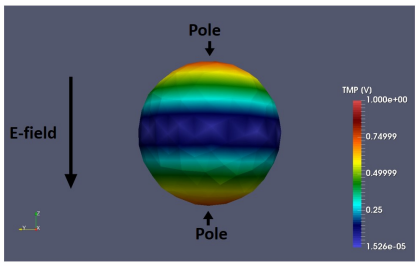

(b) TMP results for granule # 2. The maximum value for the TMP is 0.83 V and occurs at the pole.

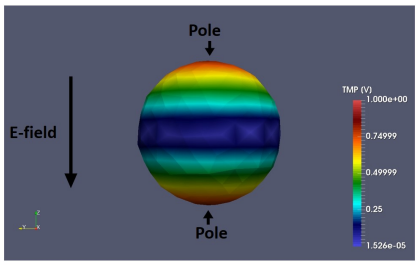

(c) TMP results for granule # 3. The maximum value for the TMP is 0.83 V and occurs at the pole.

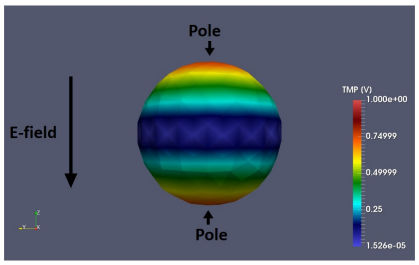

(d) TMP results for granule # 4. The maximum value for the TMP is 0.83 V and occurs at the pole.

Figure 8.23: View of the TMP distribution in the 4 specific granules shown in Figure 8.19. The TMP distribution is exactly the same as that in Figure 8.22 but has a lower magnitude.

The TMP of the granules is lower than in Figure 8.22; the TMP magnitude and distribution

are the same for all the granules (TMP maximum is located at the poles and minimum at the equator) but in this poration scheme the TMP magnitudes are lower than in poration scheme 2 (Section 8.8.2). This lower TMP is due to the higher conductivity of the granular membranes, i.e. when the membrane conductivity is higher, the TMP lower.

In this poration scheme the TMP of the cell membrane was not altered due to the high conductivity (0.01 S/m) of the granule membrane.

From the results presented in this chapter four main points that will be discussed in Chapter 9 are: 1. The effects of the nucleus on the TMP of the granules in the vicinity of the nucleus, 2. The effects of a porated membrane vs a non-porated membrane on the TMP, 3. The effects of the frequency on the TMP and 4. The effect of the size of the granules.

CHAPTER 9

Discussion

This chapter, which is divided into four section an analysis and discussion of the results shown in Chapter 8 will be presented. In Section 9.1, the process by which the TMP is extracted from a 3-D distribution in order to simultaneously compare the TMP vs theta (θ) of multiple granules is outlined. In Section 9.2, specific granules in close vicinity to the nucleus will be compared to visualize differences in the TMP distribution and magnitude. Also, the effects on TMP of a porated membrane vs a non-porated membrane will be discussed. In Section 9.3, the effects of frequency on the TMP of granules and in Section 9.4, the effects of the radius of the granules on the TMP will be discussed.

9.1 Extraction process from a 3-D distribution of TMP to a 2-D plot

In this section the TMP of the granules will be compared quantitavely. For the chromaffin cell geometry shown in Figure 7.1, the detailed distribution of the TMP and E-field inside the cell have been computed at ten different frequencies in the range DC to 10 MHz. In all simulations the applied E-field was set to 5 MV/m as in experiments being conducted in our laboratory [8, 9]. In order to extract the TMP in a plane from the 3-D results shown in Figure 9.1a and to compare the TMP of the four granules, (shown in Figure 8.19), for each granule a plane cut in the ZY plane was made (Figure 9.1).

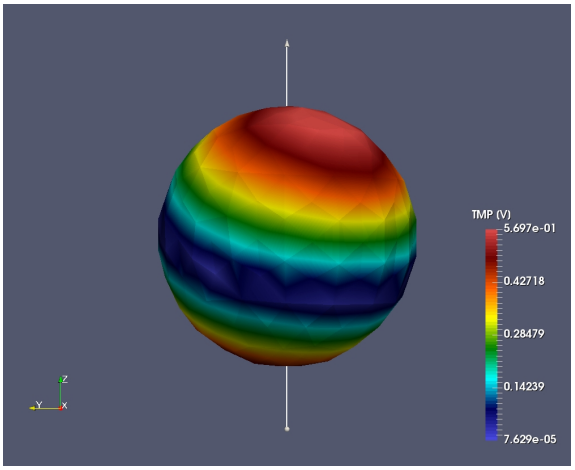

(a) 3-D view of TMP distribution for a granule. The TMP distribution is tilted due to the effect of the nucleus.

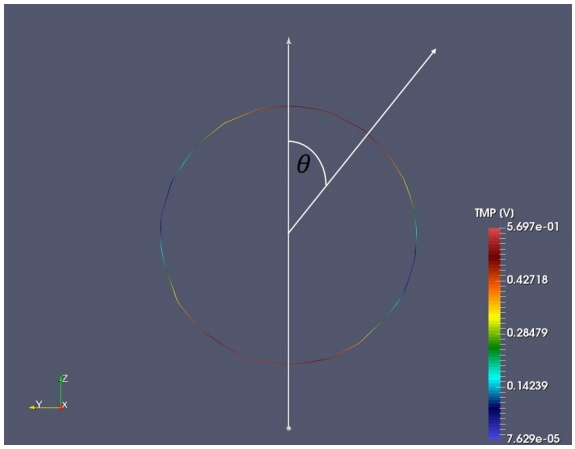

(b) Plane cut of the 3-D TMP distribution in the ZY plane. Angle θ is shown

Figure 9.1: Procedure for extracting the TMP in a plane from the 3-D results in Figure (a) to a 2-D plane shown in (b). From the 3-D geometry, a plane cut in the ZY plane of a granule is made for ease of quantitative comparisons. Applied E-field magnitude = 5 MV/m, Frequency = 300 kHz.

By transforming Cartesian coordinates into cylindrical coordinates, the TMP vs θ will be plotted in the following sections. The angle theta (θ) is represented in Figure 9.1b and as can be seen the TMP is not maximum at the pole. The TMP of the granule shown in Figure 9.1a has a "tilted" TMP distribution because the granule is being affected by the nucleus.

In order to generate linear plots of TMP vs theta, the data in Figure 9.1 must be sampled. The size of the granules is small (radius = 200 nm) and the number of sampling data points for the plots of TMP per granule membrane is 170. This is not an optimal number of sampling points and as a result the extracted TMP does not have optimum resolution. To improve the resolution of the TMP, a Matlab script was written to calculate the most adequate polynomial fit to the results. Figure 9.2 shows the TMP sampling procedure for the linear plots. In the following sections the TMP of the granules will be compared using this sampling technique in order to see the differences in TMP magnitude and distribution. Granules influenced by the nucleus will have the maximum TMP shifted from the pole and their magnitude will be lower or higher depending on their location: granule # 3 which is located on the equator of the nucleus will have the highest TMP magnitude and granule #

1 and granule # 4 will have the lowest TMP magnitude.

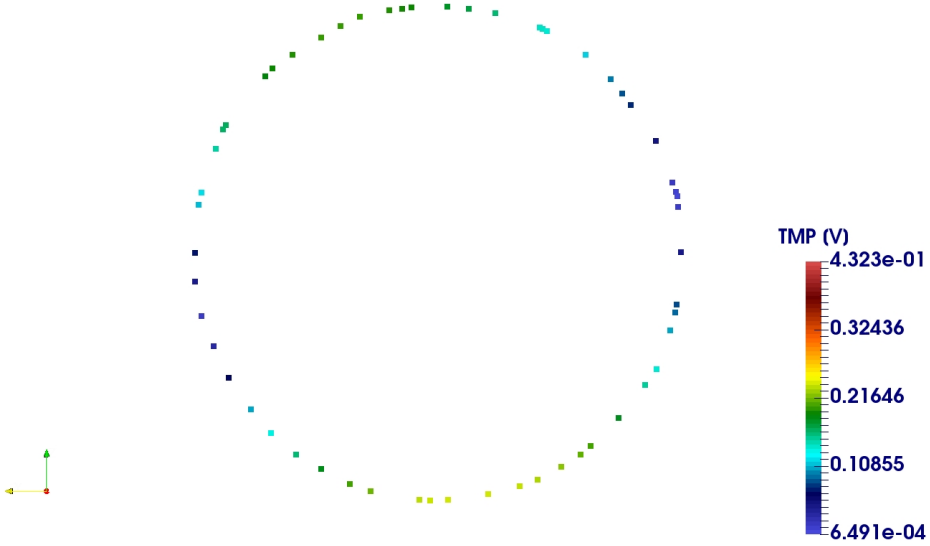

Figure 9.2: Example of the extracted TMP values in the ZY plane of a granule (Figure 9.1b) using Paraview. Due to the low number of sampling points, the TMP values needed to be interpolated in order to increase the resolution of the plots. Applied E-field magnitude = 5 MV/m, Frequency = 300 kHz.

9.2 Influence of the nucleus on the TMP of neighboring granules

In Chapter 8 it was shown that the nucleus created inhomogeinities in the E-field and as a consequence granules close to the nucleus had their TMP affected. For example, the granules below the nucleus had a lower TMP compared to the rest of the granules and their TMP distribution was tilted from 30 to 40 degrees from the poles. The reason for these differences in TMP is due to an inhomogenous E-field. In this section, the influence of the nucleus on neighboring granules has been quantified by comparing the TMP of specific granules vs θ using the procedure outlined in Section 9.1.

For the analysis, four specific granules within the cytosol location shown in Figure 8.19 were exposed to an applied E-field of 5 MV/m at 300 kHz. Figure 9.3 is a plot of the TMP vs θ for the four specific granules (qualitative TMP distribution shown in Figure 8.10).

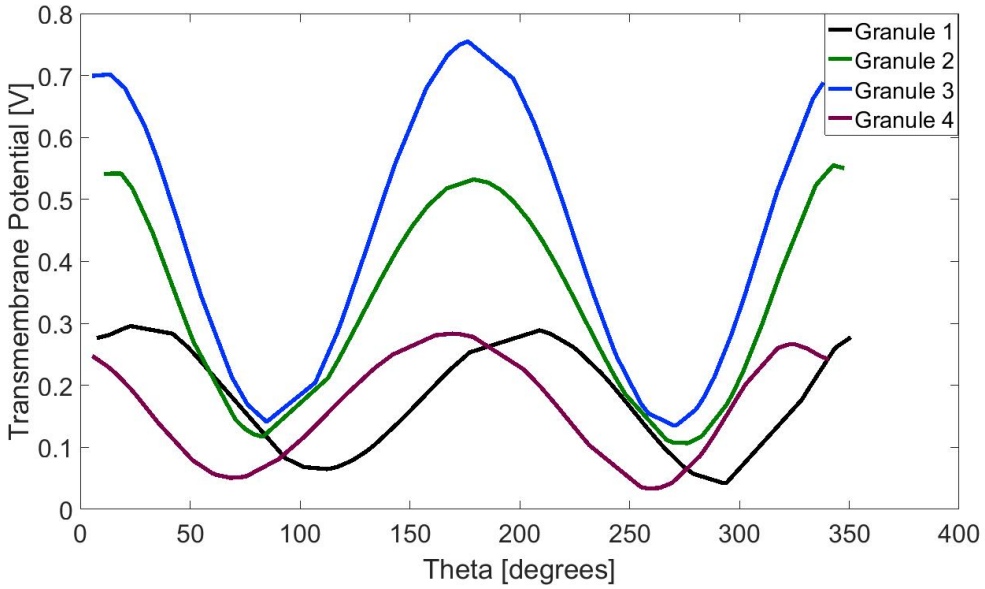

Figure 9.3: Comparison of TMP vs θ of the four selected granules at 300 kHz. Granule # 1 and # 4 are located on top the nucleus, granule # 3 is in the equatorial side and granule # 2 is outside the effective range of the nucleus.

The results show (Figure 9.3) shows that the granules closest to the nucleus have a different TMP distribution from those further away. For example, granules # 1 and # 4 (Figures 8.10a and 8.10d) have a tilted TMP distribution compared to granules # 2 and # 3 (Figure 8.10b and 8.10c). The nucleus appears to be altering the E-field distribution in its immediate vicinity: the E-field is minimum at the poles of the nucleus and maximum on the equatorial side. The granules above and below the nucleus (such as granules # 1 and # 4), have a lower TMP than the rest of the granules (such as granule # 2) because the E-field in the regions above and below the nucleus is lower. The granules located on the equatorial side of the nucleus (such as granule # 3) has a higher TMP than the rest of granules because the E-field is higher in this region.

In order to demonstrate that the E-field in the cytosol is being altered by the presence of the nucleus, the results for the E-field distribution within the cell model shown in Figure 9.4a) in the case of two poration schemes are presented. In the first scheme the cell membrane is porated and the nuclear membrane is not porated (Figure 9.4b) and in the second scheme

both the cell membrane and the nuclear membrane are porated (Figure 9.4b). In Figure 9.4a the E-field within the cytosol is rendered inhomogeneous by the presence of

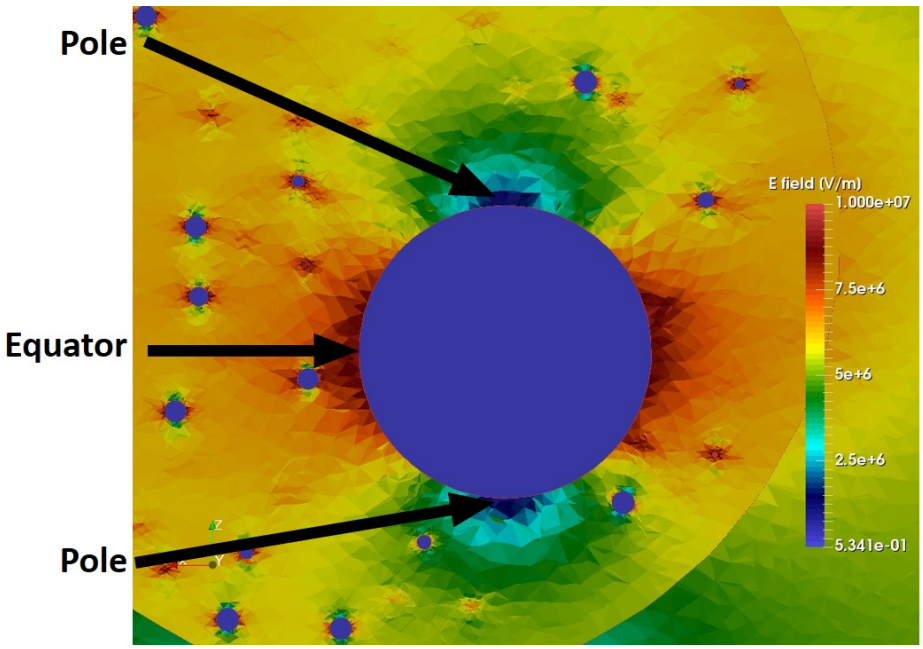

(a) E-field distribution for the first poration scheme in which only the cell membrane is porated (nuclear and granule membrane is not porated). The presence of the non-conductive nuclear membrane causes inhomogeneity in the E-field within the cytosol. The E-field is minimum at the poles and maximum at the equatorial side.

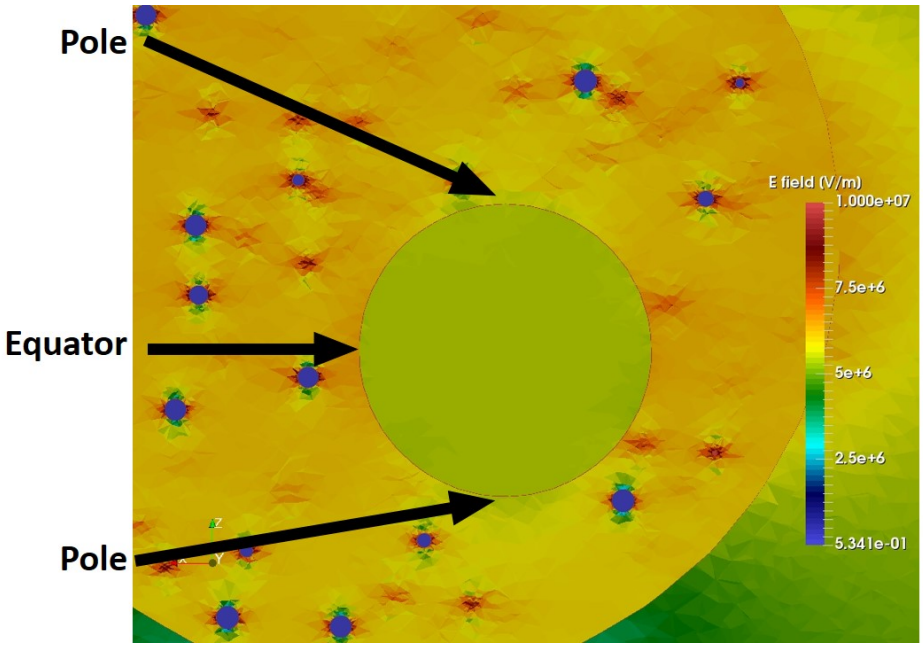

(b) E-field distribution for the second poration scheme of a porated nuclear and cell membrane; the granule membranes are not porated. The E-field homogeneity is not altered due to the higher conductivity value of the nuclear membrane ($\sigma = 0.01\ S/m$).

Figure 9.4: E-field distribution in the vicinity of the nucleus as a function of the conductivity of the nuclear membrane. The E-field distribution in the vicinity of the nucleus is not homogeneous when the nuclear membrane is non-conductive ($\sigma = 8.3 \cdot 10^{-10}\ S/m$). The E-field distribution in the vicinity of the nucleus is homogeneous for a conductive nuclear membrane ($\sigma = 0.01\ S/m$).

the non-conductive membrane ($\sigma = 8.3 \cdot 10^{-10}\ S/m$) of the nucleus with a minimum in the E-field at the poles and maximum on the equatorial side. When the nuclear membrane becomes porated ($\sigma = 0.01\ S/m$), the E-field in the cytosol retains its homogeneity (Figure 9.4b).

In Figure 8.21 the TMP vs θ is plotted for the four specific granules selected as their location is shown in Figure 8.9. In this scheme only the cell membrane is porated ($\sigma = 0.01$ S/m) and the other membranes (granular and nuclear) are not porated ($\sigma = 8.3 \cdot 10^{-10}$ S/m).

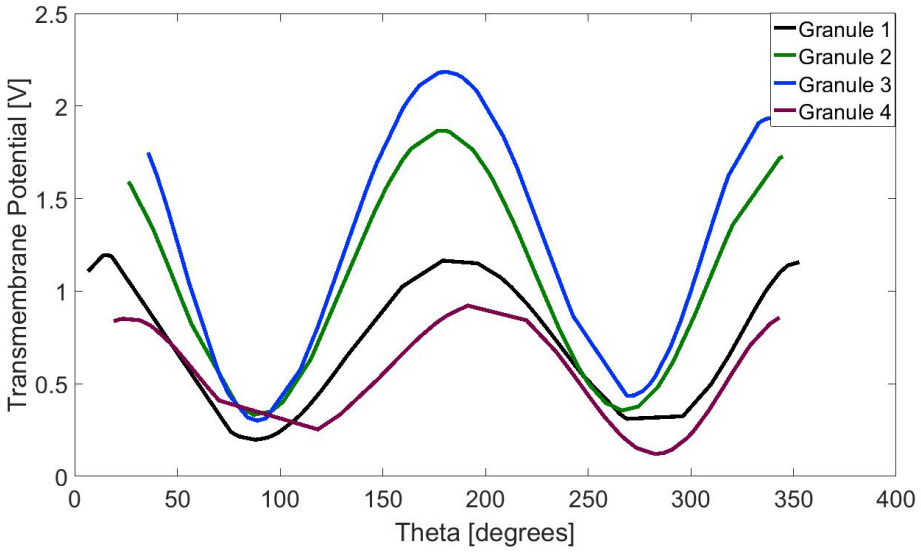

Figure 9.5: Comparison of the TMP vs theta for the four specific granules in the scheme where only the cell membrane has been porated ($\sigma = 0.01$ S/m). Granule # 1 and # 4 are located on top the nucleus, granule # 3 is in the equatorial side and granule # 2 is outside the effective range of the nucleus.

As was seen in Section 8.4, the TMP of the granules in the vicinity of the nucleus is affected by the presence of the nucleus. As expected, granule # 3 (granule in the vicinity of the nucleus on the equatorial side) has the highest TMP compared to the other three granules. Granule # 2, located 4 μm away from the nucleus and therefore out of the "range of influence" of the nucleus, has a lower TMP than granule # 3. The maximum TMP of granule # 3 is 2.2 V and the maximum TMP of granule # 1 is 1.1 V (Figure 9.5). Granule # 1 (located below the nucleus) and granule # 4 (located below the nucleus) have a much

lower TMP than granules # 2 and # 3 (approximately half the TMP of granule # 3) due to the presence of the nucleus.

In Figure 9.6 the TMP of the four specific granules shown in Figure 8.9 are compared for the scheme where the cell membrane and the nuclear membrane are porated $\sigma = 0.01 S/m$ and the granule membranes are not porated ($\sigma = 8.3 \cdot 10^{-10}$ S/m).

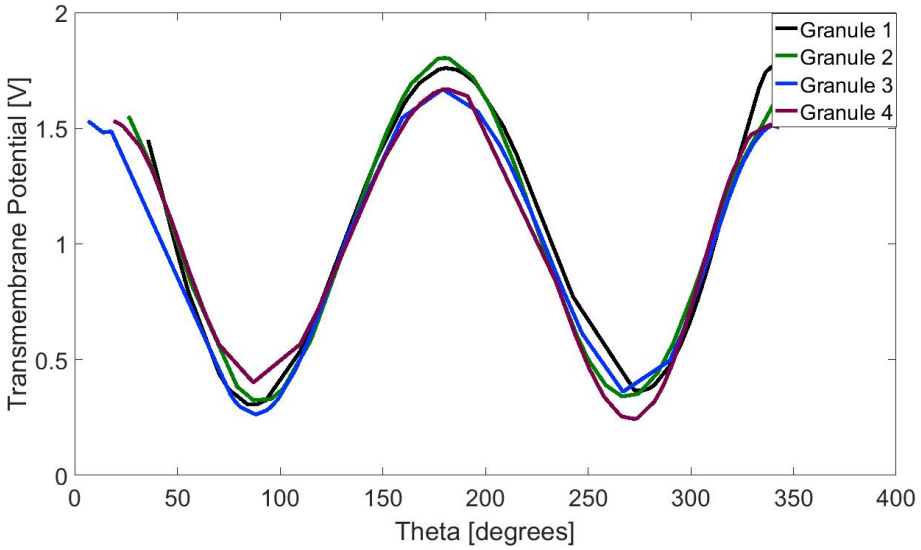

Figure 9.6: Comparison of the TMP vs theta (θ) of the four specific granules for the poration scheme where the cell and the nuclear membrane have been porated ($\sigma = 0.01\ S/m$) and the granular membranes are not porated ($\sigma = 8.3 \cdot 10^{-10}$ S/m). Granule # 1 and # 4 are located on top the nucleus, granule # 3 is in the equatorial side and granule # 2 is outside the effective range of the nucleus.

Due to the high conductivity of the nuclear membrane when it is fully porated, the E-field is not altered in the vicinity of the nucleus and as a consequence the granules around the nucleus have the same TMP distributions. In Figure 9.7 the TMP vs θ for the four specific granules shown in Figure 8.9 are compared for the poration shcme where all membranes (cell, nucleus and granules) are porated (0.01 μm). In this scheme since all the membranes are fully porated, the TMP of the granules is lower than the other two poration schemes.

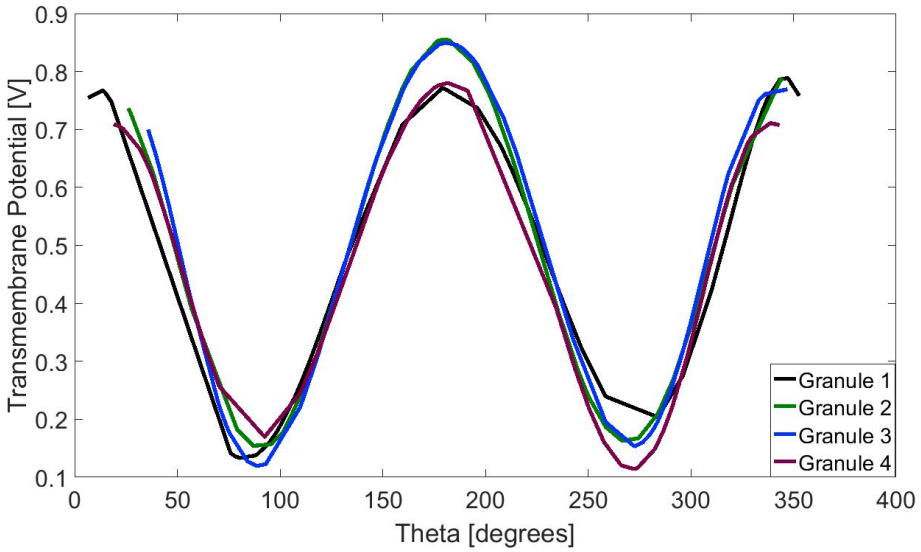

Figure 9.7: Comparison of the TMP vs θ for the four specific granules for the poration scheme where the cell, the nuclear and the granule membranes have been fully porated ($\sigma = 0.01$ S/m). Granule # 1 and # 4 are located on top the nucleus, granule # 3 is in the equatorial side and granule # 2 is outside the effective range of the nucleus.

From these results, it can be concluded that a non-conductive nuclear membrane can create inhomogeneities in the E-field and as a consequence it can alter the TMP magnitude and distribution of the neighboring granules. However, when the membrane of the nucleus gets fully porated the TMP of the granule membranes remains unaltered.

9.3 Frequency analysis of a granule outside the effective range of the nucleus

In this section the effects of frequency on the TMP of a granule # 2 that is outside the effective range of the nucleus (granule # 2) will be discussed (Figure 8.9). As stated in Section 6.5 different frequencies have different effects on membranes, i.e. different frequencies create different TMP. The maximum TMP value is located at the poles, i.e. at $\theta = 0$ and 180 degrees (Figure 8.15). The TMP of granule #2 vs θ at different frequencies is plotted in Figure 9.8.

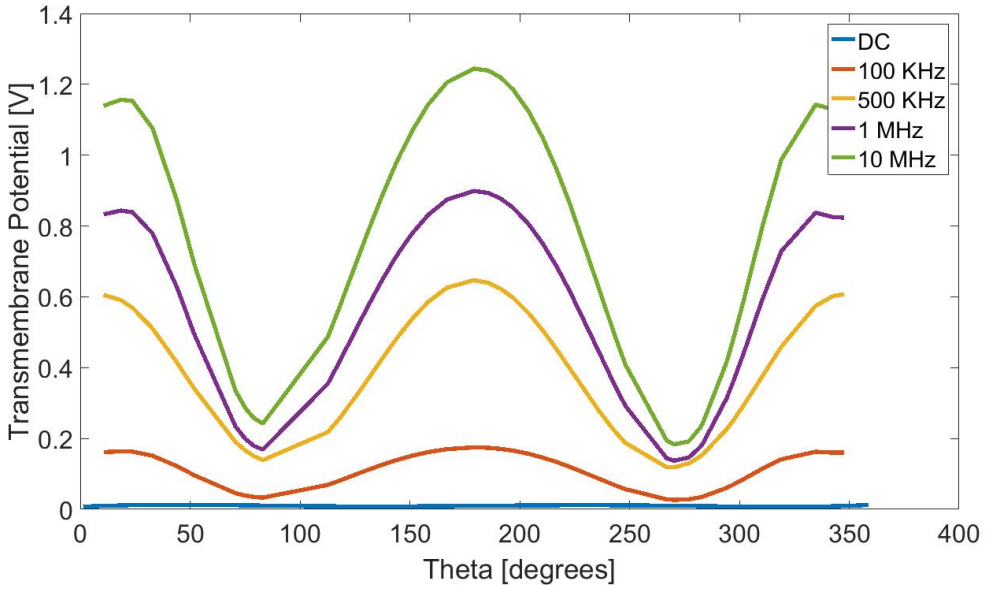

Figure 9.8: Comparison of the TMP vs θ of granule # 2 at different frequencies

At DC, the TMP is of the order of 10^{-5} V for every θ value and at 10 MHz the TMP reaches a maximum value (at $\theta = 180$ degrees) of 1.35 V. From these results it can be concluded that the TMP of granule #2 varies with frequency. In the next section the effect of the radius on the TMP of the granules will be discussed.

9.4 Analysis of the effect of granule radius

The radius of the granules can influence the TMP of the granules and in this section two specific granules within the cytosol (located 4 μm from the nucleus, i.e. outside the effective range of the nucleus) examined in Section 8.5 will be analyzed. Two cell models with different granule sizes (200 and 300 nm) were created in order to evaluate the effect of granule radius on the TMP. The granules were placed at the same exact location within the cytosol. However, in Section 8.4 it was shown that all granules located at a distance of 1.5 μm or greater from the nucleus have the same TMP distribution and magnitude. The TMP of the granules with the two radii is plotted vs θ to quantify the effect of granule radius (Figure 9.9).

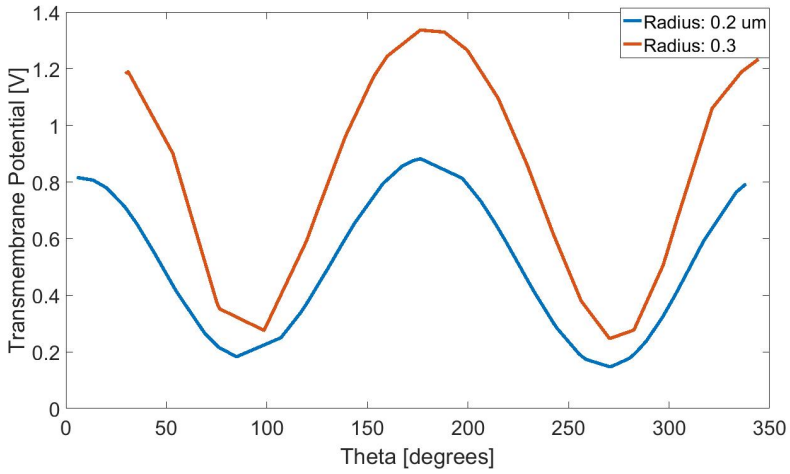

Figure 9.9: Comparison of TMP vs theta (θ) for two granules of radii 200 nm and 300 nm. Frequency = 500 kHz. The larger granule (300 nm in radius) has a higher TMP than the smaller one (200 nm in radius).

From Schwans equation [14] shown below (same equation shown in Eq 29) the TMP (ΔV) for a spherical cell models it is seen that ΔV is directly proportional top the radius R.

$$\Delta V = 1.5 \cdot E \cdot R \; cos(\theta) \tag{33}$$

where E is the magnitude of the applied E-field, R is the radius of the cell and θ is the angle measured from the center of the cell with respect to the direction of the E-field. The results in Figure 9.9 agree with this dependence of TMP on radius, i.e. higher TMP for larger granule radius.

CHAPTER 10

Conclusions

From the single frequency results for TMP and E-field distributions for a chromaffin cell model presented and discussed in this thesis, it can be concluded that the TMP of the granules, and the cell membrane can be influenced by the presence of the off-center nucleus of the chromaffin cell. If a low conductivity for the nuclear membrane is assumed ($\sigma = 8.3 \cdot 10^{-10}\ S/m$), the non-conductive nature of the nuclear membrane is the main factor that influences the E-field and TMP distribution of the neighboring granules, creating for example a tilted TMP distribution and a change in the TMP magnitudes. It was shown using the LF Solver in Sim4life that when the nuclear membrane became fully porated (implemented by making the nuclear membrane more conductive ($\sigma = 0.01\ S/m$)), the TMP distribution and magnitude of all granules in the cytosol were the same. Furthermore, both the nuclear and cell membrane TMP distributions were symmetrical (Section 5.4). The consequences of inhomogeneity in the E-field and hence the TMP could be that different granules within the cytosol, depending on their location could have membranes that become non-uniformly permeable to certain ions. From these results, it can be concluded that the nucleus is capable of altering the E-field distribution within the cytosol and hence modifying the TMP of the granules in its close vicinity. Also, granules with a radii of 200 nm or 300 nm modeled in this thesis are too small in size to alter the E-field distribution in their surroundings and hence they do not influence the TMP of neighboring granules. This could have implications on determining the value of applied E-fields when using NEPs for certain applications.

Another important finding in this project is that there were certain alterations in the TMP of a porated cell membrane (Section 8.8). These were caused by the presence of the granules closest to the cell membrane. These TMP irregularities on the cell membrane could have implications on exocytosis since there is always a small population of granules are

docked on the cell membrane.

CHAPTER 11

Future Work

In this project single frequency simulations with a detailed geometry of chromaffin cell were computed. The major findings is that the non porated (which are non conductive) intracellular membranes can influence the TMP of the surrounding organelles as well as the cell membrane.

11.1 Processing complex permittivity in Sim4life

In Section 3.3.1, the limitation of the LF solver in Sim4life to accept as input the complex permittivity of materials was discussed. This limitation causes a high percentage error in the computation of the electric potential and hence E-field in the chromaffin cell in the intermediate frequency [500 kHz - 5 MHz] (Chapter 6). In the cell membrane the maximum percentage error in the TMP is 30% at 700 KHz when compared to the results from well accepted models of Schwan's equation [14] and Kotnik et Miklavcic [26]. For the nucleus, the percentage error is of the order of 45% (Discussed in Section 6.5). If the LF solver in Sim4life could process both real and imaginary parts of the complex permittivity, it is expected these errors would be reduced to 1% or lower. In this chapter the limitations in the LF FEM solver of Sim4life such as the inability of processing the complex permittivity will be discussed: 1. Procedure to compute TMP for an actual NEP, 2. Addition of mitochrondria and endoplasmic reticulum to the chromaffin cell model and 3. Decreasing the distance between granules in the cytosol.

11.2 Procedure to compute TMP for an actual NEP

In this section a process for computing the E-fields and TMPs for an actual NEP is suggested. Poration can be modeled as an increase in the conductivity of the membranes in biological cells [12]. The Stationary Currents solver in Sim4life is a quasi-static solver. The equation solved by this solver is given by

$$\nabla \cdot \sigma \nabla V = 0 \tag{34}$$

where σ is the electrical conductivity and V is the electric potential. The idea proposed to compute the E-field and TMP distribution in a detailed model of a chromaffin cell incorporating poration of the membranes and using the Stationary Current solver in Sim4life, is to concatenate hundreds of LF simulations at various time samples of an actual NEP and incorporate the increasing conductivity in the membranes as pores are formed within the membranes. With a large enough number of LF simulations, a signal in the time domain could be sampled and with multiple Python scripts the TMP of each membrane could be extracted and the pore density and conductivity of the membranes computed (with the model in [18]). These computed quantities would serve as inputs for the next LF simulation until the entire NEP was sampled.

Thus, the suggested procedure is as follows: Step 1: The σ value for non-porated membranes ($\sigma = 8.3 \cdot 10^{-10} S/m$) is used and the LF simulation is run. Step 2: The TMP is extracted, the pore density is computed and a new value for the membrane conductivity $\sigma_{porated}$ is estimated. Step 3: In the next simulation the value of $\sigma_{porated}$ obtained in Step 2 is input into the LF solver and the simulation is run. This iterative process is continued until the entire NEPs sampled (Figure 11.1).

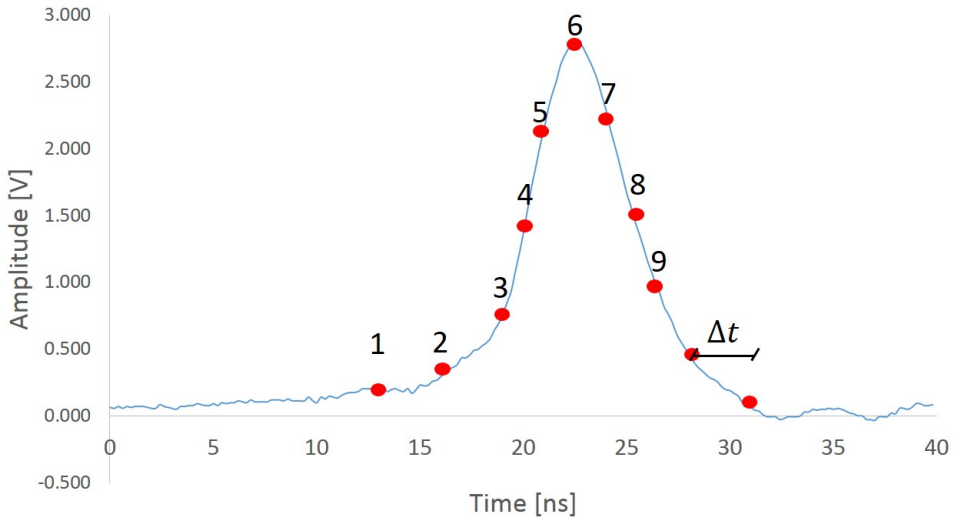

Figure 11.1: Average of ten NEPs used in our laboratory [8, 9] (Averaging performed to lower the noise level). The red dots represent the sampling points for the pulse. All points are separated by a sampling rate (Δt). For each sampling point a LF simulation is run and the σ of the membranes for the following simulation is calculated. For clarity, the sampling rate in this figure is rather large; however, in the suggested simulations the sampling rate will be set to as low as 50 ps.

11.3 Addition of structures representing an endoplasmic reticulum and mitochrondria

Chromaffin cells have other intracellular organelles like mitochondria, and the endoplamic reticulum (ER) in addition to thousands of granules. The ER does not have regular shapes as shown in Figure 11.2.

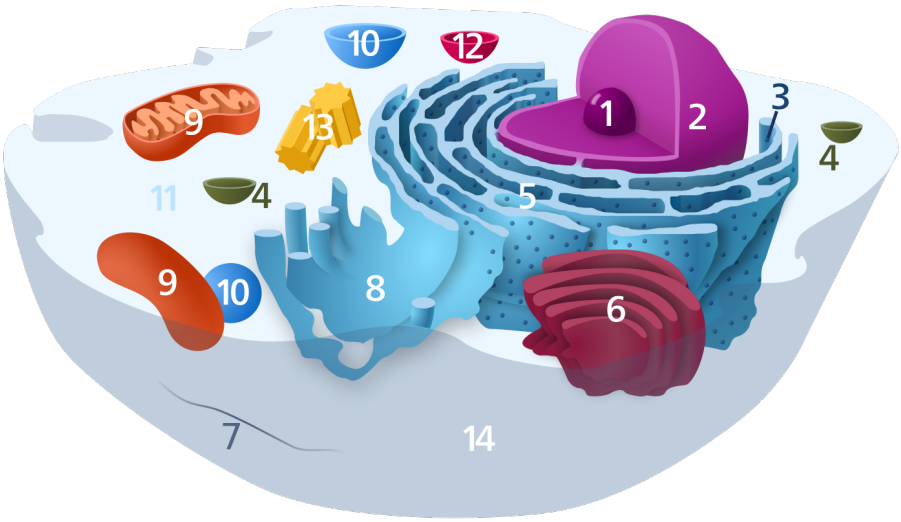

Figure 11.2: Suggested model for an ER (number 5). The rough ER is usually located within the proximity of the nucleus (number 2). In Sim4life the geometry of the ER can be built. Image created by Kelvinsong [43]

Due to limitations of the currently available computational resources in our laboratory, these organelles were omitted from the cell models considered in this thesis. Incorporating them into the chromaffin cell model would increase tremendously the number of meshcells and as a consequence computational time way beyond the capacity of currently available computer resources in our laboratory. In the future these organelles could be modeled as regular shapes. For example, the mitochondria could be approximated by ellipsoids and the ER as multiple irregular rings.

The addition of these organelles in the cell model could cause new inhomogeneities in the E-field and affect the TMP distribution and magnitude of the granules.

11.4 Reduction of the distance between granules to verify the possible influence of granules on another one

The distance between organelles in an actual chromaffin cell has not been determined. In this project, the granules had to be separated by a distance of 100 nm due to geometrical limitations of the mesher. However, with more RAM, the meshcell dimension could be

reduced to 25 nm, hence accommodating inter-granule spacings of much less than 100 nm. The Sim4life simulations with inter-granule spacings of the order of 25 nm could potentially be able to predict effects on the TMP and E-field distribution of the granules on each other. Therefore, it would be ideal if in the cytosol the meshcell size could be set to 25 nm in order to place the granules closer to each other.

References

[1] T. R. Gowrishankar, A. T. Esser, Z. Vasilkoski, K. C. Smith, and J. C. Weaver, "Microdosimetry for conventional and supra-electroporation in cells with organelles," *Biochemical and Biophysical Research Communications*, vol. 341, no. 4, pp. 1266–1276, 2006.

[2] J. F. Kolb, S. Kono, and K. H. Schoenbach, "Nanosecond pulsed electric field generators for the study of subcellular effects," *Bioelectromagnetics*, vol. 27, no. 3, pp. 172–187, 2006.

[3] A. G. Pakhomov, R. Shevin, J. A. White, J. F. Kolb, O. N. Pakhomova, R. P. Joshi, and K. H. Schoenbach, "Membrane permeabilization and cell damage by ultrashort electric field shocks," 2007.

[4] F. Dehez, L. Delemotte, P. Kramar, D. Miklavčič, and M. Tarek, "Evidence of conducting hydrophobic nanopores across membranes in response to an electric field," *Journal of Physical Chemistry C*, vol. 118, no. 13, pp. 6752–6757, 2014.

[5] J. Yoon, N. Leblanc, J. Zaklit, P. T. Vernier, I. Chatterjee, and G. L. Craviso, "Enhanced Monitoring of Nanosecond Electric Pulse-Evoked Membrane Conductance Changes in Whole-Cell Patch Clamp Experiments," *The Journal of Membrane Biology*, vol. 249, no. 5, pp. 633–644, 2016.

[6] K. C. Smith and J. C. Weaver, "Active mechanisms are needed to describe cell responses to submicrosecond, megavolt-per-meter pulses: cell models for ultrashort pulses," *Biophysical journal*, vol. 95, no. 4, pp. 1547–1563, 2008.

[7] A. G. Pakhomov, D. Miklavcic, and M. M. S. Markov, *Advanced electroporation techniques in biology and Medicine*. CRC Press, 2010.

[8] G. L. Craviso, P. Chatterjee, G. Maalouf, A. Cerjanic, J. Yoon, I. Chatterjee, and P. T. Vernier, "Nanosecond electric pulse-induced increase in intracellular calcium in adrenal chromaffin cells triggers calcium-dependent catecholamine release," *IEEE Transactions on Dielectrics and Electrical Insulation*, vol. 16, no. 5, pp. 1294–1301, 2009.

[9] G. L. Craviso, S. Choe, P. Chatterjee, I. Chatterjee, and b. P. T. Vernier, "Nanosecond Electric Pulses: A Novel Stimulus for Triggering Ca 2+ Influx into Chromaffin Cells Via Voltage-Gated Ca 2+ Channels," *Cellular and Molecular Neurobiology*, vol. 30, no. 8, pp. 1259–1265, 2010.

[10] J. E. Zaklit, *Electroporation of Intracellular Membranes of Adrenal Chromaffin Cell with High Intensity, 5-ns Electric Pulses: an Experimental and Modeling Study.* Phd. dissertation, University of Nevada, Reno, 2016.

[11] C. Merla, A. Denzi, A. Paffi, M. Casciola, G. Dinzeo, F. Apollonio, and M. Liberti, "Novel passive element circuits for microdosimetry of nanosecond pulsed electric fields," *IEEE Transactions on Biomedical Engineering*, vol. 59, no. 8, pp. 2302–2311, 2012.

[12] L. Retelj, G. Pucihar, and D. Miklavcic, "Electroporation of intracellular liposomes using nanosecond electric pulses-a theoretical study," *IEEE Transactions on Biomedical Engineering*, vol. 60, no. 9, pp. 2624–2635, 2013.

[13] P. T. V. Josette Zaklit, Gale L. Craviso, Normand Leblanc, Lisha Yang and I. Chatterjee, "Adrenal chromaffin cells exposed to 5-ns pulses require higher electric fields to porate intracellular membranes than the plasma membrane: an experimental and modeling study," *J. Membrane Biology, Manual Submitted*, 2017.

[14] H. P. Schwan, "Dielectric properties of biological tissue and cells at RF and MW-frequencies," *Biological and Dosimetry of Nonionizing Radiation*, pp. 195–211, 1983.

[15] R. Joshi, Q. Hu, and K. Schoenbach, "Modeling Studies of Cell Response to Ultrashort, High-Intensity Electric FieldsImplications for Intracellular Manipulation," *IEEE Transactions on Plasma Science*, vol. 32, pp. 1677–1686, aug 2004.

[16] W. Krassowska and P. D. Filev, "Modeling Electroporation in a Single Cell," *Biophysical Journal*, vol. 92, no. 2, pp. 404–417, 2007.

[17] K. C. Smith, "Modeling cell and tissue electroporation," Master's thesis, MIT, 2006.

[18] K. A. DeBruin and W. Krassowska, "Modeling Electroporation in a Single Cell. I. Effects of Field Strength and Rest Potential," *Biophysical journal*, vol. 77, no. 3, pp. 1213–1224, 1999.

[19] G. Saulis and R. Saule, "Size of the pores created by an electric pulse: Microsecond vs millisecond pulses," *Biochimica et Biophysica Acta - Biomembranes*, vol. 1818, no. 12, pp. 3032–3039, 2012.

[20] H. Plattner, A. R. Artalejo, and E. Neher, "Ultrastructural organization of bovine chromaffin cell cortex - Analysis by cryofixation and morphometry of aspects pertinent to exocytosis," *Journal of Cell Biology*, vol. 139, no. 7, pp. 1709–1717, 1997.

[21] E. Sequoia, S. A. Lausanne, A. Barnett, and J. C. Weaver, "Electroporation: a unified, quantitative theory of reversible electrical breakdown and mechanical rupture in artificial planar bilayer membranes *," *Bioelectrochemistry and Bioenergetics. J. Efectruanol. Chem.. and constituting*, vol. 25, no. 320, 1991.

[22] *Sim4life Manual*. SPEAG, 2016.

[23] E. Neufeld, A. M. Cassará, H. Montanaro, N. Kuster, and W. Kainz, "Functionalized anatomical models for EM-neuron Interaction modeling.," *Physics in medicine and biology*, vol. 61, no. 12, pp. 4390–401, 2016.

[24] R. Borges, N. Domínguez, J. Estévez-Herrera, D. Pereda, and J. D. Machado, "Vesicular Ca2+ mediates granule motion and exocytosis," *Cell Calcium*, vol. 51, pp. 338–341, mar 2012.

[25] J. SantoDomingo, L. Vay, M. Camacho, E. Hernández-SanMiguel, R. I. Fonteriz, C. D. Lobatón, M. Montero, A. Moreno, and J. Alvarez, "Calcium dynamics in bovine adrenal medulla chromaffin cell secretory granules," *European Journal of Neuroscience*, vol. 28, pp. 1265–1274, oct 2008.

[26] T. Kotnik and D. Miklavcic, "Theoretical evaluation of voltage inducement on internal membranes of biological cells exposed to electric fields.," *Biophysical journal*, vol. 90, no. 2, pp. 480–491, 2006.

[27] K. H. Schoenbach, B. Hargrave, R. P. Joshi, J. F. Kolb, R. Nuccitelli, C. Osgood, A. Pakhomov, M. Stacey, R. J. Swanson, J. A. White, S. Xiao, J. Zhang, S. J. Beebe, P. F. Blackmore, and E. S. Buescher, "Bioelectric effects of intense nanosecond pulses," *IEEE Transactions on Dielectrics and Electrical Insulation*, vol. 14, no. 5, pp. 1088–1107, 2007.

[28] J. M. Chalovich and E. Eisenberg, "NIH Public Access," *Biophysical Chemistry*, vol. 257, no. 5, pp. 2432–2437, 2005.

[29] M. Vetterli, J. Kovacevic, and V. K. Goyal, *Foundations of signal processing*. Cambridge University Press, 2014.

[30] *Semcad Manual*. SPEAG, 2014.

[31] M. N. O. Sadiku, *Numerical techniques in electromagnetics*. CRC Press, 2001.

[32] K. S. Kunz and R. J. Luebbers, *The finite difference time domain method for electromagnetics*. CRC Press, 1993.

[33] A. Taflove and S. Hagness, *Computational Electrodynamics: The Finite-difference Time-domain Method*. Artech House antennas and propagation library, Artech House, 2005.

[34] A.C. Sabuncu, M. Stacey, G.L. Craviso, N. Semenova, P.T. Vernier, N.Leblanc, I. Chatterjee and J. Zaklit., "Dielectric properties of isolated adrenal chromaffin cells determined by microfluidic impedance spectroscopy.," *Manual under review*.

[35] N. Kuster and F. Schonborn, "Recommended minimal requirements and development guidelines for exposure setups of bio-experiments addressing the health risk concern of wireless communications," *Bioelectromagnetics*, vol. 21, pp. 508–514, oct 2000.

[36] D. A. Stewart, T. R. Gowrishankar, K. C. Smith, and J. C. Weaver, "Cylindrical cell membranes in uniform applied electric fields: Validation of a transport lattice method," *IEEE Transactions on Biomedical Engineering*, vol. 52, no. 10, pp. 1643–1653, 2005.

[37] H. Si and J. R. Shewchuk, "Incrementally constructing and updating constrained delaunay tetrahedralizations with finite precision coordinates," *Proceedings of the 21st International Meshing Roundtable, IMR 2012*, pp. 173–190, 2013.

[38] A. Eaton, "Course notes, Chapter 7: Analysis of the Finite Element Method,"

[39] O. de Weck Il Yong Kim, "Finite Element Method," 2004.

[40] "Detailed Explanation of the Finite Element Method (FEM), Comsol Manual," 2016.

[41] L. S. Avila and I. Kitware, *The VTK user's guide : install, use and extend the visualization toolkit*.

[42] V. N. Parthasarathy, C. M. Graichen, and A. F. Hathaway, "A comparison of tetrahedron quality measures," *Finite Elements in Analysis and Design*, vol. 15, no. 3, pp. 255–261, 1994.

[43] Kelvinsong, “File:Animal Cell.svg - Wikimedia Commons.”